NTNU

Norwegian University of
Science and Technology

Synthetic Inertia from a Converter-Fed Synchronous Machine in a Hydro-Electric Power Plant

Modeling, Control and Analysis

Mathias Gallefoss

Master of Energy and Environmental Engineering
Submission date: June 2018
Supervisor: Trond Toftevaag, IEL

Norwegian University of Science and Technology
Department of Electric Power Engineering

Problem Description

Increasing integration of variable renewable energy sources in the electric power system raises the demand for balancing technologies to compensate for fluctuations in production. Of all the balancing technologies available, pumped-storage hydroelectricity is by far the most mature technology. In recent years, the interest for adjustable speed drives has increased due to the ability to adjust power consumption in pumping mode. However, decoupling generators from the grid using power electronic converters reduces the total inertia of the power system. In grids with high penetration of power electronic controlled production, this can reduce the overall system stability.

This work is a continuation of a specialization project carried out during fall 2017. The thesis focus on deriving and analyzing control methods which emulate inertia for a convert-fed synchronous machine in a hydro-electric power plant. Two separate methods are to be derived; classical torque control with supplementary inertia controllers and virtual synchronous machine control which emulates the dynamic operation of a synchronous machine. These methods should be tested and compared in a system consisting of a converter-fed hydro-electric machine connected to a simplified power grid using simulation software.

Project start: January 2018
Supervisor: Trond Toftevaag

Abstract

As the share of variable renewable energy in the power system rises, the demand for balancing technologies to compensate for fluctuation in production increases. Pumped-storage hydropower has significant potential globally and is seen as the most mature storage technology available. Modern pump-storage plants utilize a power electronic interface between the machine and power system to control power consumption in pump mode. Introducing power electronic converters between the machine and grid causes the rotating mass of the machine to be independent of the frequency in the power grid. Therefore, the machine loses its ability to contribute to the inertia in the power system. To solve this, the converters can be controlled such that the effect of inertia is synthesized, often termed synthetic inertia.

A number of methods to emulate inertia exist, with a broad span in complexity and design. The most straightforward solutions release stored kinetic energy based on the frequency derivative or deviation. Other more complex solutions mimic the behavior of a synchronous machine, often referred to as virtual synchronous machine (VSM). The VSM method enables the converter to operate as a grid-connected synchronous machine with a speed governor and excitation system.

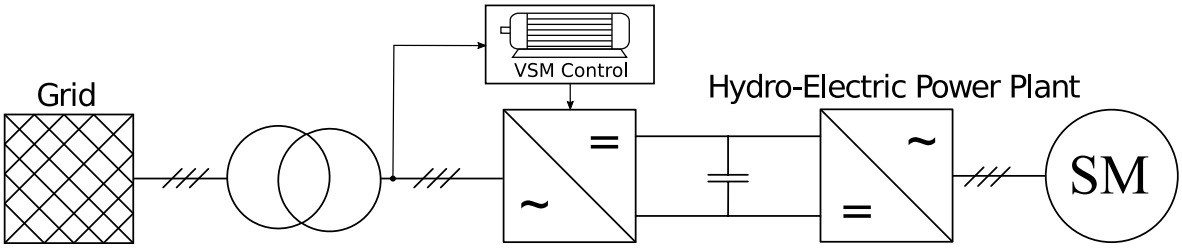

In this thesis two methods are developed; classical torque control with supplementary inertia controllers and virtual synchronous machine control. The methods are tested in a simulation model consisting of a converter-fed hydro-electric power plant connected to a simplified grid. It is shown that both methods performed as intended, emulating the effect of inertia during a power imbalance event. The classical torque control and VSM control improve the frequency nadir by 36.4% and 54.5% respectively based on the steady-state frequency for

a given test case. The VSM method is found superior in the context of inertia support due to fast power control. Also, the VSM inherits a number of other advantages such as the possibility for dynamic inertia support. Dynamic inertia support allows the VSM to change the amount of synthetic inertia in the grid during operation, which can improve small-signal stability.

Sammendrag

Økende innslag av uregulerbar kraftproduksjon, som vindkraft og solkraft, stiller større krav til tilgjengelig fleksibilitet i kraftsystemet. Pumpekraftverk har et betydelig potensiale for å levere nødvendig fleksibilitet, og kan hevdes å være den mest modne lagringsteknologien tilgjengelig. Moderne pumpekraftverk er integrert i kraftsystemet ved hjelp av kraftelektronikkomformere, for å øke fleksibiliteten til kraftverket. Dette fører derimot til at den roterende massen til maskinen er uavhengig av frekvensen til kraftnettet, og derav vil den ikke bidra til treghet i systemet. Dette kan løses ved at omformerne styres slik at virkningen av treghet syntetiseres, ofte betegnet syntetisk treghet.

En rekke metoder for å etterligne treghet eksisterer, med et bredt spekter av kompleksitet og design. De enkleste løsningene frigjør lagret kinetisk energi basert på frekvensderivatet eller frekvensavviket. Andre og mer kompliserte løsninger etterligner oppførselen til en synkronmaskin, ofte referert til som virtuell synkronmaskin (VSM). VSM-metoden gjør at omformeren oppfører seg som en synkronmaskin som er direkte koblet til kraftnettet.

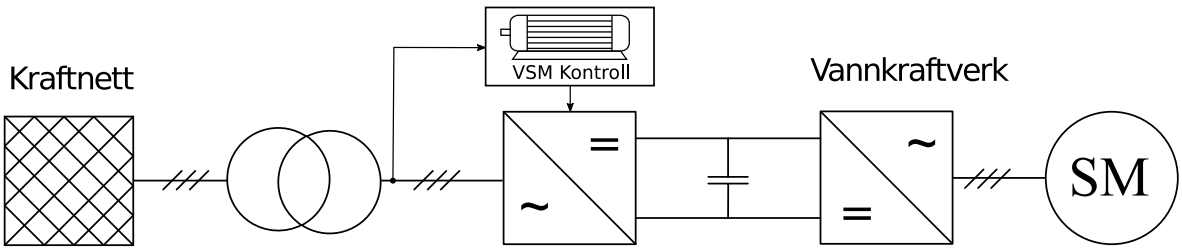

Denne avhandlingen foreslår to metoder for å etterligne treghet for en omformermatet maskin i et vannkraftverk; klassisk dreiemomentkontroll med tilleggsregulatorer for treghetsstøtte og virtuell synkronmaskinkontroll. Metodene blir testet i en simuleringsmodell, bestående av en omformermatet vannkraftmaskin koblet til et forenklet kraftnett. Resultatene viser at begge metodene har en gunstig innvirkning på frekvensresponsen til kraftsystemet. Klassisk dreiemomentkontroll og VSM-kontroll forbedrer bunnpunktet til frekvensen med henholdsvis 36,4 % og 54,5 %, sammenlignet med frekvensen uten støtte fra treghetskontrollerne. VSM-metoden viste seg å være overlegen frekvensregulering på grunn av rask effektrespons.

Dessuten har VSM-metoden en rekke andre fordeler, som muligheten for dynamisk treghetsstøtte. Dynamisk treghetsstøtte gjør at omformeren kan endre mengden av syntetisk treghet i kraftnettet, noe som kan være gunstig for å dempe svingninger.

Preface

This Master's Thesis is submitted to the Department of Electric Power Engineering at the Norwegian University of Science and Technology (NTNU) and concludes my Master of Science (MSc) degree in Energy and Environmental Engineering.

The thesis represents a follow-up of a specialization project carried out during fall 2017. The work is related to research interest at the Norwegian Research Centre for Hydropower Technology (HydroCen) and Norwegian Hydropower Centre (NVKS).

I wish to thank my supervisor Trond Toftvaag for guidance and motivation. I greatly appreciate his support and encouragement in letting me find my own way, pursuing what I found interesting. A special thanks go to Abel Assegid Taffese for his out of this world abilities in Simulink and valuable guidance. I would also like to thank Salvatore D'Arco for sharing his knowledge and advice.

Finally, I would like to thank my fellow students for many exciting discussions and motivational support.

Trondheim, June 2018
Mathias Gallefoss

Contents

Nomenclature

δ_g	Grid rotor angular position with respect to a synchronously rotating reference
δ_T	VSM terminal rotor angular position with respect to a synchronously rotating reference
λ_{sd}	Stator d-axis flux linkage
λ_{sq}	Stator q-axis flux linkage
ω	Angular velocity in electrical rad/s
ω_b	Base angular velocity in electrical rad/s
ω_m	Angular velocity in mechanical rad/s
ω_T	VSM angular velocity in electrical rad/s
θ_g	Grid rotor angular position with respect to a stationary axis
θ_T	VSM terminal rotor angular position with respect to a stationary axis
C_{dc}	DC link capacitance
e_f	Field voltage
$e_{g,abc}$	Three-phase grid voltage
e_{gd}	d-axis grid voltage
e_{gq}	q-axis grid voltage
$e_{s,abc}$	Three-phase stator terminal voltage
e_{sd}	Stator d-axis voltage
e_{sq}	Stator q-axis voltage
f	Grid frequency
f_{sw}	Switching frequency
G_{max}	Maximum gate limit (governor)
G_{min}	Minimum gate limit (governor)
H	Inertia time constant
i_f	Field current
i_{fd}	Equivalent field-winding current

$i_{g,abc}$	Three-phase grid current
i_{gd}	d-axis grid current
i_{gq}	q-axis grid current
i_{sd}	Stator d-axis current
i_{sq}	Stator q-axis current
J	Moment of inertia
K_D	Damping coefficient in the swing equation
k_T	Constant representing the relation between i_{sq} and T_{em}
K_s	Servo gain (governor)
$L_{g,eq}$	Sum of line and converter inductance on the grid-side
L_{ls}	Leakage inductance
L_{md}	d-axis magnetizing inductance
L_{mq}	q-axis magnetizing inductance
L_{sd}	Sum of leakage and magnetizing inductance in the d-axis
L_{sq}	Sum of leakage and magnetizing inductance in the q-axis
P_{em}	Electromagnetic power
P_m	Mechanical power
R_p	Permanent Droop (governor)
R_t	Temporary Droop (governor)
$R_{g,eq}$	Sum of line and converter resistance on the grid-side
T_a	Mechanical time constant ($T_a = 2H$)
T_f	Pilot valve and servomotor time constant (governor)
T_g	Servo Time Constant (governor)
T_r	Governor Time Constant (governor)
T_w	Water Time Constant (governor)
T_{em}	Electromagnetic torque
T_{eq}	Equivalent time delay in the current loop
T_m	Mechanical torque
v_T	VSM terminal voltage
v_t	Stator terminal voltage
V_{dc}	DC link voltage
$v_{g,abc}$	Three-phase converter terminal voltage (GSC)

v_{gd} d-axis converter terminal voltage (GSC)

v_{gq} q-axis converter terminal voltage (GSC)

$v_{m,abc}$ Three-phase converter terminal voltage (MSC)

$Z_{g,C}$ Grid-side converter impedance

$Z_{g,L}$ Grid-side line impedance

$Z_{m,C}$ Machine-side converter impedance

Abbreviations

AC Alternating current.

AVR Automatic voltage regulator.

CFSM Converter-fed synchronous machine.

CSC Current source converter.

d-axis Direct-axis.

DC Direct current.

DFIM Doubly-fed induction machine.

FACTS Flexible alternating current transmission system.

GSC Grid-side converter.

IGCT Integrated gate-commutated thyristor.

LCI Load-commutated inverters.

MMC Modular multi-level converter.

MPPT Maximum power point tracking.

MSC Machine-side converter.

PI-controller Proportional–integral controller.

PLL Phase locked loop.

PWM Pulse-width modulation.

q-axis Quadrature-axis.

ROCOF Rate of change of frequency.

SG Synchronous generator.

SM Synchronous machine.

SRF Synchronous reference frame.

STATCOM Static synchronous compensator.

SV-PWM Space vector pulse-width modulation.

VSC Voltage source converter.

Chapter 1

Introduction

1.1 Background

Penetration of power generated from variable renewable energy sources has increased rapidly in recent years and is expected to continue to grow in the future [1]. This is energy sources that are non-dispatchable due to their fluctuating nature, like photovoltaics and wind generation, as opposed to controllable energy sources such as hydroelectricity and biomass. Power grids are also undergoing a transformation from centralized power production to distributed generation. This transformation towards distributed and unpredictable power production is the primary motivation behind the transition towards a new power system architecture with more flexibility between generation and load, often termed "Smart Grid" [2].

In this new power system, energy storage is often considered an essential factor to ensure a reliable supply of power [3]. Today, hydroelectricity amounts to around 16% of global electricity production, which in turn constitutes most of the renewable energy production in the world [4]. According to [4], storage hydropower represents 99% of electricity storage globally. With the implementation of more pumped-storage facilities, hydropower could play an essential role in ensuring a reliable supply of electricity in the future power system.

The principle of pumped-storage hydroelectricity is to pump water back to the reservoir when there is a surplus of power in the grid. However, traditional pumped-storage plants lack the flexibility and controllability necessary to compensate for rapid fluctuations in power production. To solve this modern pump storage plants are often equipped with an adjustable speed unit where the machine is decoupled from the grid through a power electronic converter. This enables the plant to follow the surplus in power production with high precision, contributing to frequency stability [5]. However, decoupling a machine using a converter reduces the total inertia in the power system.

The use of power electronic converters in power production is not unique for pump storage plants and is becoming increasingly common for other energy sources. In 2000, the portion of electrical energy controlled by power electronic converters was around 40%, while ECPE/EPE estimated in 2007 that this number would increase to 80% by 2015 [6]. This number represents the percentage of power which passes at least one converter from primary energy conversion to consumption. Even though the development was slightly lower than estimated, the number is still significant and is expected to increase in the future [7].

In recent years, a number of solutions to contribute to inertia from converter controlled generation have been suggested. Most solutions take advantage of the dynamic operation of modern voltage source converters to emulate the effect of inertia. The solutions are many, with a wide range of complexity and design. The most straightforward solutions focus on adding supplementary inertia controllers to classical control schemes. Other more complex solutions mimic the behavior of grid-connected synchronous machines with speed governor and excitation system. The latter solution enables the VSC to contribute to inertia, primary frequency regulation and voltage control similar to a synchronous machine, often termed virtual synchronous machine (VSM) [7].

1.2 Objectives

This thesis includes a thorough review of two control strategies to enable inertia support from a converter control synchronous generator; classical torque control with supplementary inertia controllers and virtual synchronous machine control. The control strategies are developed and analyzed separately, then compared using simulation tools. A brief overview of the motivation and technology behind adjustable speed drives will also be presented, along with challenges related to frequency stability due to loss of inertia.

1.3 Scope of Work

Based on the objectives described in Section 1.2 above, the scope of work can be summarized as:

- Investigate the main benefits and challenges related to adjustable speed drives in hydroelectric power plants.
- Investigate available technologies for enabling adjustable speed operation.
- Develop a dynamic model for a converter-fed synchronous machine using classical torque control, including supplementary inertia controllers which aim to emulate inertia.

- Develop a dynamic model for a converter-fed synchronous machine using virtual synchronous machine control.
- Analyze and compare the two methods with a focus on synthetic inertia using simulation software.

1.4 Limitations

This thesis is limited only to consider technical aspects related to inertia support from converter-fed synchronous machines in hydro-electric power plants. The focus is on deriving the control systems and testing these in a simulation model. For the power system stability analysis, only frequency stability is considered. The theoretical study focuses mainly on the controllers, i.e., no in-depth mathematical analysis of power system stability is performed.

1.5 Software

MATLAB®/Simulink is the main simulation tool chosen in this project. The mechanical and electrical system is simulated using predefined Simscape models, while the control system is simulated with Simulink blocks. In addition, PowerFactory® is used for some simulations where MATLAB®/Simulink is unsuitable.

1.6 Report Structure

Chapter 1 - *Introduction*: Provides the background for the thesis work and an overview of objectives, limitations and report structure.

Chapter 2 - *Adjustable Speed Hydro*: Reviews the development and state-of-the-art technologies available to enable adjustable speed operation in hydroelectric power plants. In addition, the chapter gives a brief overview of benefits and challenges using the technology, and an example of a large-scale project.

Chapter 3 - *Frequency Stability*: Gives the underlying reason for the importance of frequency stability in a power grid, and how it can be maintained. In the last part of the chapter, the concept of synthetic inertia is presented.

Chapter 4 - *System Description*: Introduces the system which will be investigated in this thesis. The most critical parameter values are presented along with essential characteristics and structure.

Chapter 5 - *Classical Torque Control*: Derives the first control system presented in this thesis. The chapter gives a thorough review of the modeling and control which leads to the final control system with inertia emulation.

Chapter 6 - *Virtual Synchronous Machine Control*: Derives a second control system for the system presented in the system description. At the end of the chapter, the method from this chapter is compared to technique from the previous chapter.

Chapter 7 - *Results and Discussion*: Presentation, analysis and discussion of the results of simulations for both control methods. The control methods are tested individually, and then compared based on the simulation results.

Chapter 8 - *Conclusion*: Sums up the results with some concluding remarks. In the final part of this chapter, suggestions for further work is included.

Chapter 2

Adjustable Speed Hydro

As of 2012, approximately 270 pumped-storage plants were operating or under construction worldwide. These units represent a generating capacity of 127 GW combined. 36 of the 270 plants consist of adjustable speed units, 17 of which are in operation as of 2012 [8]. The first adjustable speed pumped-storage plants were installed in Japan in the early 1990s. In Japan, the goal was to reduce the number of thermal plants operating as reserves during the night [9].

2.1 Available Technologies

To realize adjustable speed operation of an electric generator, a power electronic converter is often used. Other solutions exist, such as a pole changing mechanism to enable different speed modes. However, this is often unpractical and only enables two modes of speed [10]. Using converters, two main topologies exist; doubly-fed induction machine (DFIM) and converter-fed synchronous machine (CFSM). As seen in Fig. 2.1a, a DFIM is directly connected to the grid through the stator windings, while a power electronic converter feeds the rotor. By adjusting the rotor frequency, the machine can operate at different speeds even though the stator is directly connected to the grid. An advantage of this topology is that the converter only needs to be rated at 15-30% of the rated machine power [9]. However, this results in a complicated rotor structure which limits the speed of the machine, making it unsuitable for locations with high heads [11].

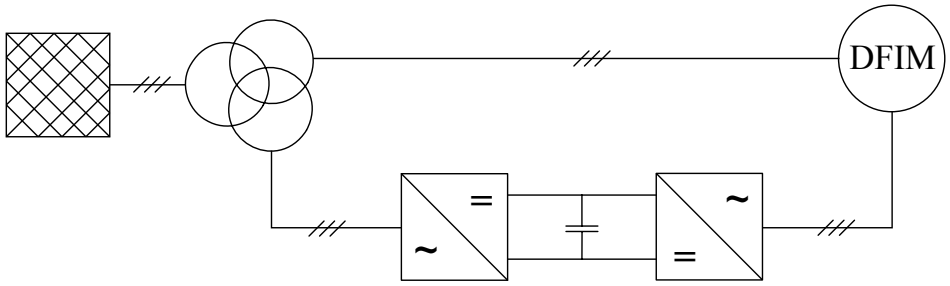

(a) DFIM

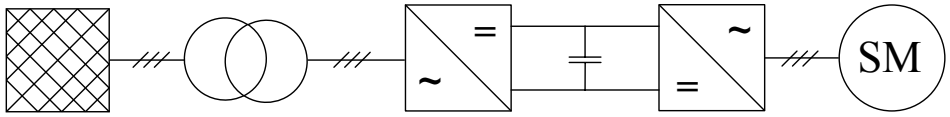

(b) CFSM

Figure 2.1: CFSM and DFIM topology

As seen in Fig. 2.1b, a CFSM is fed by a back-to-back converter without any direct connection to the grid. Compared to the DFIM, the converter needs to be rated equally to the machine as all power needs to pass the converter. However, the machine itself is a standard synchronous machine, which is much less complicated than a doubly-fed machine. Besides, the CFSM offers superior technical performance compared to the DFIM. This is due to less complicated machine design, and the machine is entirely decoupled from the grid. Some of the technical advantages include the possibility for black start, high starting torque and the option to bypass the converter [9]. Even though DFIM is the current industry standard, CFSM is expected to be the preferred choice in the future with advancements in power electronic converters [9].

A comparison by Voith shows that synchronous machines have higher efficiency (98.8%) compared to the doubly-fed induction machines (98.3%). However, CFSM has a lower efficiency overall (97.3%) compared to DFIM (97.9%) due to more losses in the converter [12].

Modern plants are often equipped with a back-to-back voltage source converter (VSC). In the past, cycloconverters (converters without an intermediate DC link) and other current source converters (CSC) has been widespread. Modular multi-level converter (MMC) is an emerging technology which can offer even higher power rating and efficiency [11]. MMC is receiving much attention for use in HVDC systems, though it has many other applications such as high power adjustable speed drives.

2.2 Benefits and Challenges

The ability to control power consumption in pumping mode is the primary motivation for installing adjustable speed drives in pumped-storage plants. Adjustable speed drives offer high controllability and fast response. This enables the power plant to improve frequency stability by following the surplus in electrical power, which is an increasingly more important ability as the power system is penetrated with more renewable energy sources. For small power system, such as on islands, research shows that by implementing adjustable speed pumped-storage units the share of variable renewable energy can increase while still maintaining grid stability [13][5]. The same principles apply to larger grids with high penetration of renewable energy. The value of having adjustable speed units became evident during the Hanshin earthquake in Japan in 1995. Measurements from the event shows that the adjustable speed machine of Ohkawachi hydropower plant functioned satisfactory, absorbing disturbances and spikes in the power grid [14].

Since a VSC is often used for modern plants, the converter can function as a FACTS-device. The converter can function as a STATCOM, delivering and absorbing reactive power, even though the machine is not operating [11]. As can be seen in Fig. 2.2, the system can absorb and deliver a substantial amount of reactive power under normal grid operation.

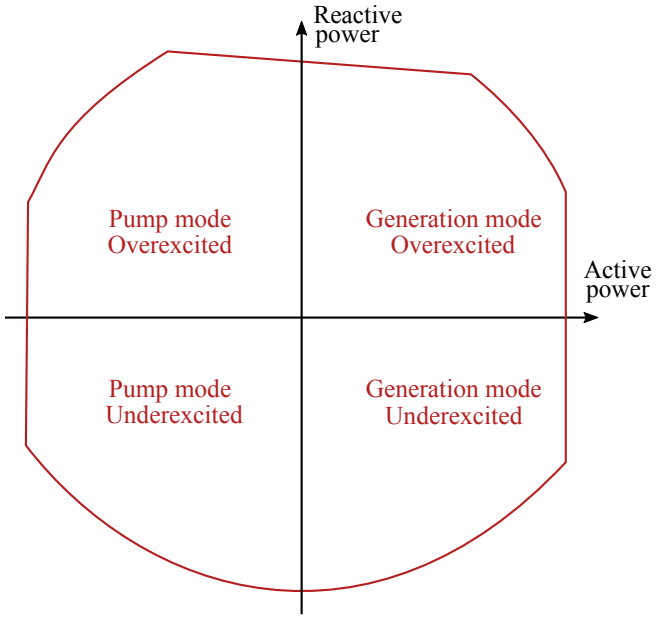

Figure 2.2: Typical PQ-diagram of a CFSM [1]

[1] Based on [11]

In generating mode, the plant also benefits from the same accurate and fast response as in pump mode. In addition, the efficiency of the turbine can increase by tracking the optimal point of operation using a maximum power point tracking (MMPT) algorithm. The plant can experience reduced vibration and cavitation due to adjustable speed operation, increasing the lifespan and reducing service costs [15]. However, to justify the use of the adjustable speed drive in generation mode the reduced stress on equipment and improved efficiency needs to compensate for increased losses due to the converter.

The most significant challenge with installing adjustable speed drives is profitability. To justify the investment, it has to be a sufficient difference between peak and off-peak electricity price. In the profitability calculation, losses associated with the pumping process needs to be accounted. In addition to profiting from the price difference, ancillary services can also provide a possible profit [9]. The increase of unpredictable production such as wind and solar might raise both the price difference between peak and off-peak and the need for ancillary services. This might make it more profitable to install adjustable speed drives in the future.

The challenge which will be investigated in the coming chapters is related to grid stability. Decoupling synchronous generators from the grid reduces the total inertia of the power system. However, the fast and dynamic performance of VSC can be taken advantage of to emulate the effect of inertia.

2.3 Example: Grimsel 2

A 100 MW full-size converter was installed at the Grimsel 2 pumped storage power plant in Switzerland in 2013. This became the largest operating drive converter at the time. The plant consists of four synchronous machines, each rated at 80/90 MW (turbine/pump operation) [16]. Before the drive converter was installed, the machine could only pump in steps of power consumption. To reach intermediate levels of power consumption, one machine needed to run in generator mode. Pumping and generating at the same time reduce the pumping capability of the plant and is an inefficient solution [16].

When the plant was built, the largest existing frequency converter for synchronous machines available was 100 MW, which was based on load-commutated inverters (LCI). However, it was found unsuitable due to high harmonic distortion and the voltage curve of the LCI would severely overload the existing machine [17]. For these reasons, it was found that a VSC would be a better option. The converter that was installed consists of two back-to-back VSC, each rated at 50 MVA, based on integrated gate-commutated thyristor (IGCT) [16].

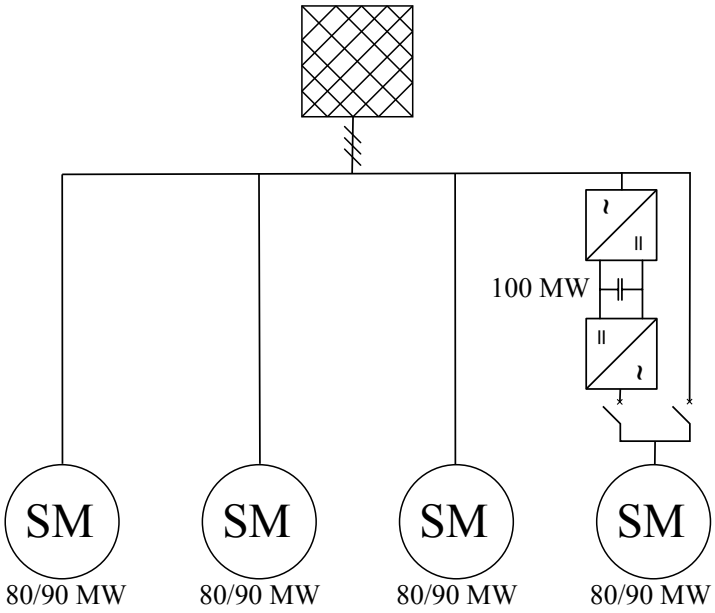

Figure 2.3: Schematic overview of Grimsel 2 pumped-storage plant

The plant has four modes of operation: pumping at adjustable speed (converter), pumping at a constant speed (direct grid-connected), generating at a constant speed (direct grid-connected) and phase angle correction. Since adjusting the Francis turbine speed to the small head range gave little increase in efficiency compared to converter losses, generating at adjustable speed was not considered [16]. Therefore, the plant was equipped with a bypass-switch as can be observed in Fig. 2.3. The pump unit can be operated in a power range of 60 MW to 100 MW, where cavitation defines the lower limit, and the converter power rating determines the maximum limit [17].

The experience at Grimsel 2 has been promising, setting a new standard for high powered pump storage plants [9]. In the first year of operation, the plant provided 3500 hours of controlled pumping and 850 hours of phase-synchronous condenser operation [16].

Chapter 3

Frequency Stability

Power system stability is the ability for a power system to regain initial operation after being subjected to a disturbance. This stability can be categorized into frequency stability, voltage stability and rotor angle stability [18]. Each of these categories can again be divided into different subcategories of stability. Voltage stability is the ability to maintain steady voltage, which is related to flow of reactive power in the system. Rotor angle stability is dependent on the system's ability to remain in synchronism during a disturbance. Finally, frequency stability is related to active power balance in the system and the ability to maintain a steady frequency. Even though power system stability is classified into different categories, they are not independent of each other. For instance, a collapse in frequency leads to changes in voltage magnitude and rotor angle. In this report, frequency stability will be the main investigation and will be thoroughly investigated in this chapter.

IEEE/CIGRE defines frequency stability as the ability for a power system to maintain steady frequency following a severe imbalance between generation and load [19]. This means that the stability will depend on the system's ability to oppose frequency deviation and restore the frequency after an imbalance has occurred. There are three main factors important to ensure frequency stability [20]:

- **Inertia**, which is the power system's ability to withstand changes in frequency. This ability emanates mainly from stored kinetic energy in rotating synchronous generators directly connected to the gird. The importance of inertia in the power system will be thoroughly reviewed in Section 3.2.
- **Dimensioning incident**, which is the highest instantaneously occurring imbalance of active power expected in the system. The dimensioning incident is often termed as the largest power unit which can be subject to an outage while the system still manages to operate within the requirements. As an example, the Nordic power system has a

dimensioning incident of 1400 MW, which means that the power system would be able to handle an unbalance of 1400 MW while maintaining an operation within the defined requirements [21].

- **Reserves**, which is active power reserves available to restore system frequency. Restoring frequency after an imbalance is in the Nordic power grid ensured by three reserves; primary, secondary and tertiary reserves [22]. Primary control changes the power output on a generator according to a speed-power characteristic in the governor, which will be explained in the next section. If the primary control fails to restore the frequency within a few minutes, the secondary control is triggered [23]. The secondary control changes the set point of generation units to restore the frequency. When the secondary control is activated, the primary control is freed to handle new imbalances. The last reserve is the tertiary reserve, which in the Nordic power grid is controlled by central regulators [22]. Tertiary control includes a wide range of possibilities, such as connect/disconnect generators, loads or pumped-storage hydro stations.

3.1 Synchronous Machines

Synchronous generators are the workhorse in the process of converting mechanical energy to electrical energy. Nearly all of the electric power in the world is generated by synchronous generators driven by steam turbines, combustion engines or hydro turbines [24]. Synchronous machines have some important advantages compared to other alternatives, such as [25][26]:

- Power output can be proportional to grid frequency.
- Excitation system can accurately control terminal voltage.
- Short-term frequency regulation from inertia response.
- Stable parallel operation with other generators and load sharing.
- High short-circuit current.

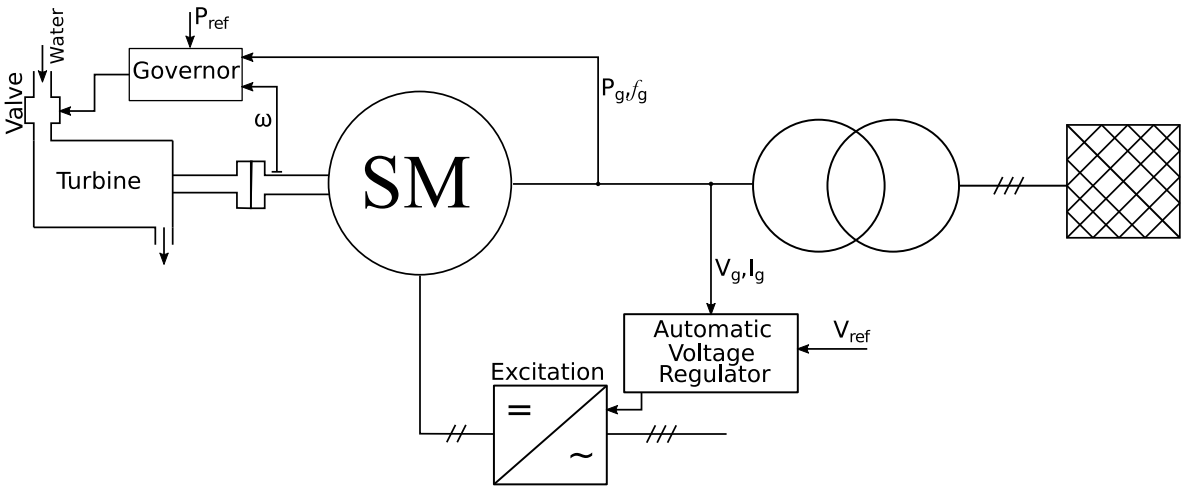

Figure 3.1: Typical control scheme for a gird-connected synchronous generator

Two main control structures control grid-connected synchronous generators. The first is the governor controlling active power by for instance changing the flow of water into the turbine. The governor is often automatically regulated according to a power-speed characteristic, often referred to as droop speed control. Fig. 3.2 show a typical droop speed control curve. From the figure, it is evident that a deviation from nominal frequency will result in a change in output power. Similarly, the reactive power flow from a synchronous generator can be controlled by the rotor excitation. This is often referred to as an automatic voltage regulator (AVR), which regulates the field current to change the terminal voltage. Also, the excitation system enhances the power system stability using a power system stabilizer, which provides damping in power system oscillations [27]. A simplified representation of these control structures is shown in Fig. 3.1.

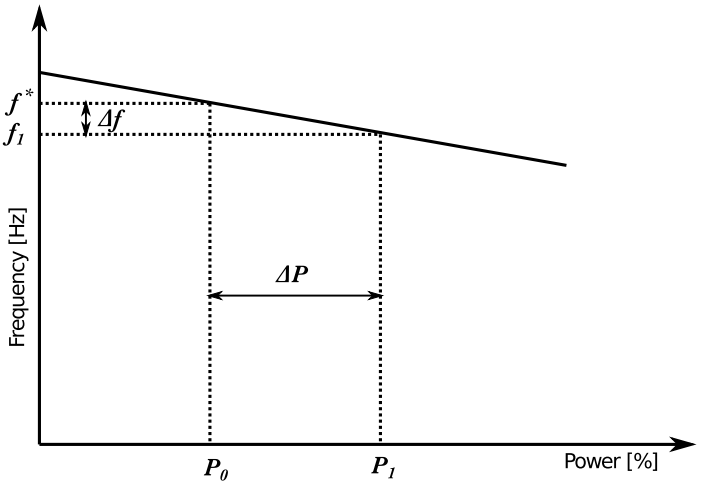

Figure 3.2: Speed–droop characteristics

3.2 Inertia

As mentioned in the previous section, synchronous generators inherits many characteristics that are desirable for the power grid. One of these is the ability to contribute to inertia response during a frequency event. Inertia is defined as an object's resistance to change its state of motion. In the context of power system stability, inertia is used as the power system's ability to withstand changes in frequency [27]. The moment of inertia, J, of a synchronous machine is dependent on the rotor mass and radius. In a power system, the total inertia is given by the sum of the inertia of every individual unit [23]. It is common to use the inertia time constant to the describe machine inertia, often termed H, which is the kinetic energy stored in the rotating mass divided by the rated machine power. This constant can be interpreted as the amount of time the machine can deliver full rated power using solely the kinetic energy stored in the rotation.

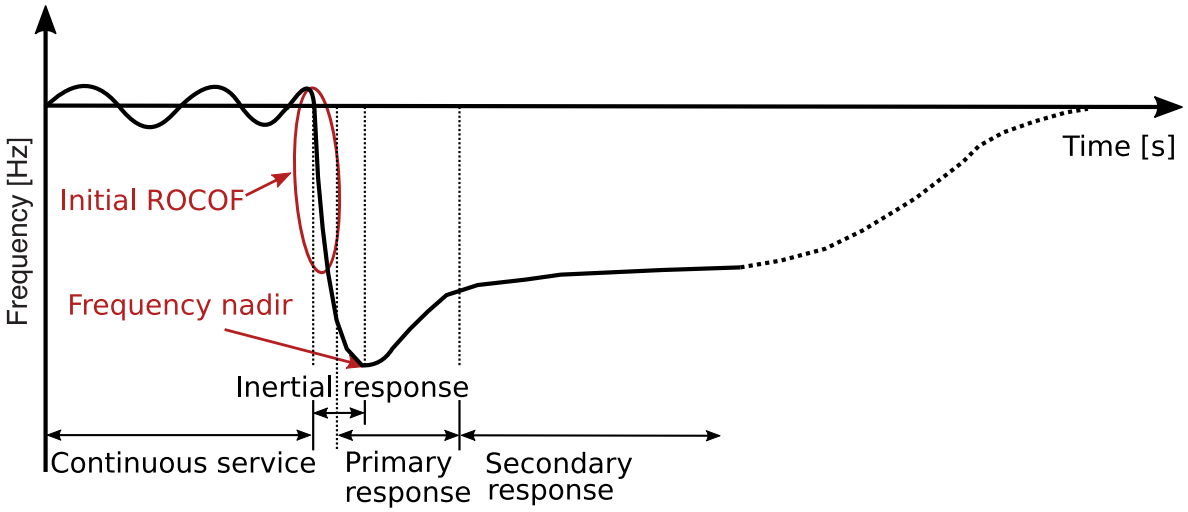

Figure 3.3: Typical frequency event following a power imbalance

When a power imbalance occurs in a network, the electromagnetic torque output (T_{em}) changes instantaneously on the generators in the system [27]. The swing equation can be written in a simplified form as [28]:

$$T_m - T_{em} = J\frac{d\omega_m}{dt} \tag{3.2.1}$$

The change in the electromagnetic torque causes a mismatch between electromagnetic and mechanical torque (T_m). From the equation above, this mismatch will result in a change in speed for generators connected to the grid. If the load increases, the generators will decelerate and vice versa for a decrease in load.

In the case of a sudden increase in load, the generators in the system will decelerate. This causes a release of kinetic energy stored in the rotating masses to electrical energy in the grid. As the generators decelerate, the frequency drops, since the frequency is dependent on the rotational speed of the generators in the systems [29]. Fig. 3.3 illustrate such a situation. In a short period of time after the imbalance has occurred, the balance of electrical power is only dependent on stored kinetic energy being converted to electrical energy. Grids with low inertia (i.e., little stored kinetic energy) will be less resilient to oppose changes in frequency compared to grids with higher inertia.

As the frequency falls, the deviation from nominal frequency increases. This causes the governors in the generating units to increase the power output, which is the first and primary control loop. This control loop typically responds after some seconds [23]. Furthermore, the secondary and tertiary control loop is activated if necessary, as mentioned in the introduction to this chapter.

Generators or motors controlled by power electronic converters, such as CFSM and DFIM, do not provide natural inertia response [30]. The power output (or input) from these units depend on the control of the converter, which makes the machine speed independent of the grid frequency. Grids with substantial penetration of converter controlled production can experience frequency instability [31]. However, modern power electronic converters have the advantage of a dynamic and rapid response, which can be used to emulate inertia, often referred to as synthetic inertia.

3.3 Synthetic Inertia

In recent years, synthetic inertia has received much attention due to increased integration of power electronic controlled generation in the grid. Such topologies are especially relevant for integration of modern wind turbines where DFIM and CFSM are becoming the new industry standards [32]. This has led to the development of a large number of different methods for implementing inertia emulation from converter controlled production.

The simplest method for implementing inertia response is to add a supplementary control loop to the existing control system. The additional control loop often changes the speed/-torque of the machine, releasing or absorbing energy. Also, a new method for inertia emulation is gaining attention know as virtual synchronous machine (VSM). The concept of VSM control is to emulate the dynamic and static operation of a synchronous machine. This is claimed to give many other advantages, such as virtual damping [33].

3.3.1 Supplementary Inertia Control

Even though there are a number of different control strategies for emulating inertia using an additional control loop, the principle is often the same. To emulate inertia, the speed/torque-control changes the speed of the machine in such a way that kinetic energy is released or absorbed depending on the power imbalance [34]. This is achieved by measuring the frequency and changing the speed reference according to frequency deviation or derivative. Similarly, the voltage on a DC link in a back-to-back converter can be changed to release and absorb energy in the capacitor.

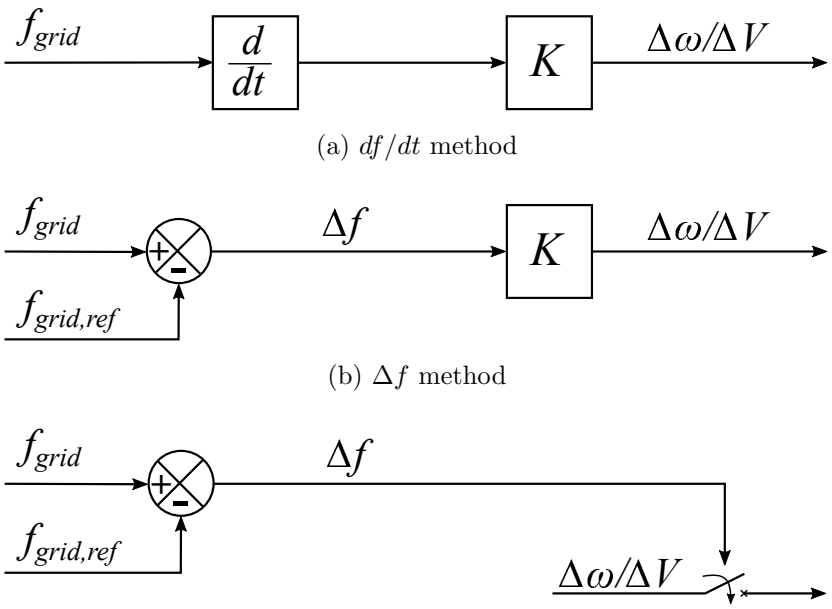

(a) df/dt method

(b) Δf method

(c) Trigger method

Figure 3.4: Different supplementary inertia control topologies

Inertia response based on frequency derivative (df/dt) is often referred to as natural inertia response [35]. The rate of change of frequency (ROCOF) is multiplied by a gain which is tuned based on available kinetic energy, as seen in Fig. 3.4a. This method gives a close to natural response, though it can cause power fluctuations and can be complicated to tune [31]. Another method is to respond based on the frequency deviation (Δf) as shown in Fig. 3.4b. This method offers a less complicated implementation; however, it can conflict with the primary frequency regulator [31]. Fig. 3.4c show one of the most straightforward implementations of inertia response. This method triggers a constant release of energy if the frequency deviation reaches a certain level.

3.3.2 Virtual Synchronous Machine

The principle of a VSM is to emulate the static and dynamic operation of a synchronous machine using a VSC. This can be achieved by taking advantage of the dynamic operation of modern inverters and the operation principle of synchronous machines. In 2007, Beck and Hesse were among the first to propose this idea, then labeling it VISMA [36]. Since then a number of approaches have been proposed with a wide range of complexity and terminology. A comparison and classification of different methods are proposed in [37] and [38].

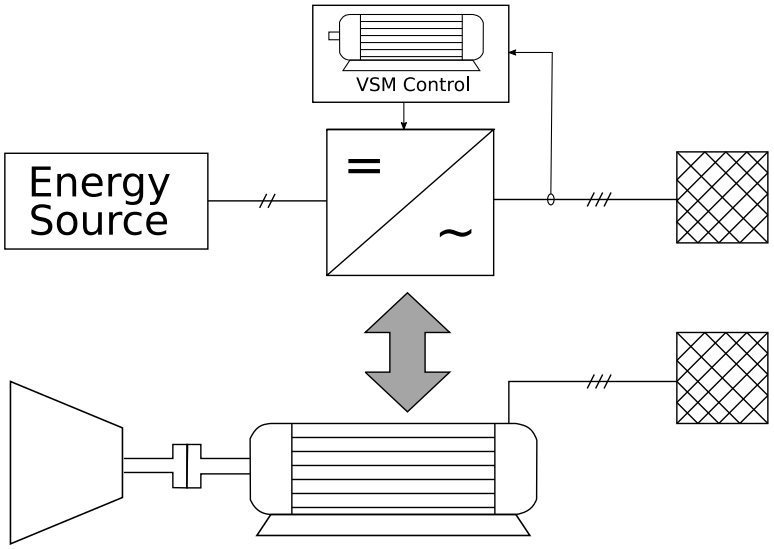

Figure 3.5: Basic concept of a virtual synchronous machine

The different VSM control methods can be classified into high-order models (as in [39][40][41]) and low-order models (as in [42][43][44]) [45]. High-order models are complex, representing the full dynamics of a synchronous machine, which can result in an unnecessary level of complexity [37]. Most of the research focuses on second-order models, which contains the mechanical part of a synchronous machine. The mechanical part reflects the rotor damping and inertia characteristics of a synchronous machine, which is described by the swing equation [46]. Some research also includes the electrical characteristic of synchronous machines by implementing the relationship between stator voltage and current [38]. In order to replicate a synchronous machine accurately, a full order model needs to be included in the system. This would result in a 7^{th} order model built of a 5^{th} order electrical model and 2^{th} order mechanical model [37].

Fig. 3.6 show the implementation of a typical VSM control scheme. As observed in the figure, the magnitude and phase of the converter output voltage are regulated to control reactive and active power respectively. The swing equation that calculates the phase angle based on the power error inherits the inertia response and damping.

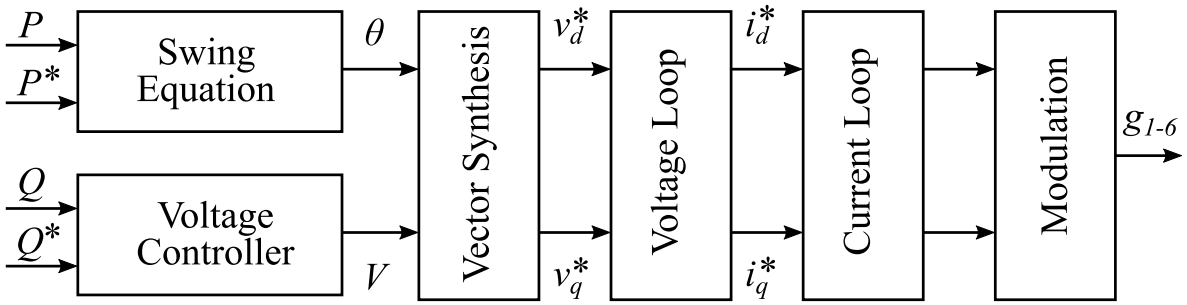

Figure 3.6: Typical VSM control with voltage and current control

Chapter 4

System Description

The system which will be investigated in this report consist of a converter-fed hydro-electric power plant connected to a grid through a transformer. The system is presented in Fig. 4.1 together with essential parameter values. As can be observed in the figure, the grid is represented by a large synchronous machine and two loads. The grid and hydro-electric power plant are separated through an ideal transformer. In this chapter, the construction and important characteristics of the system are described. The governor and AVR are presented in this chapter, while the control of the converter is the subject of the next two chapters. In Appendix C, the simulation models developed in MATLAB®/Simulink are presented, while all parameter values are given in Appendix B.

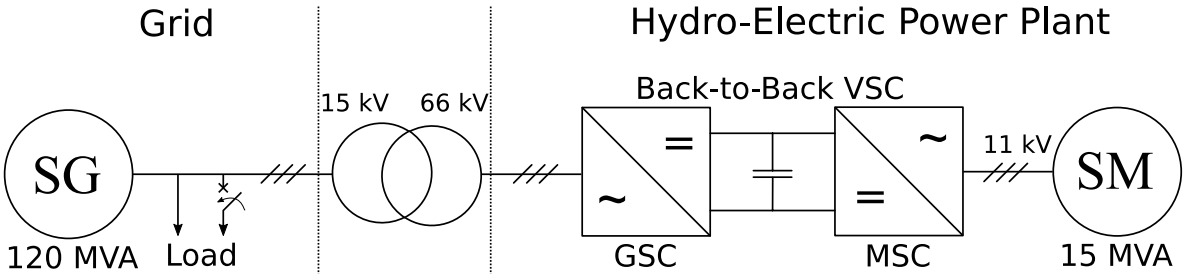

Figure 4.1: System overview

4.1 Hydro-Electric Power Plant

The hydro-electric power plant consists of a synchronous machine connected to a back-to-back VSC. A 15 MVA salient poled synchronous machine is chosen, with the parameter presented in Appendix B.1.1. The machine has the same control system as a traditional grid-connected synchronous machine as described in Chapter 3, i.e., a governor and AVR. A voltage level of 11 kV and 66 kV is chosen on the machine and grid side of the converter respectively [47].

4.1.1 Impedances

Between the GSC and transformer the impedance can be divided into line impedance ($Z_{g,L}$) and converter impedance ($Z_{g,C}$). The line impedance is the equivalent impedance in the line between the converter terminals and transformer, while the converter impedance is internal impedance in the converter. Between these impedances is the terminal voltage of the converter, v_T. On the machine-side, the line impedance is neglected. The resulting impedance is the converter impedance in series with the machine impedances, which will be elaborated in the next chapter.

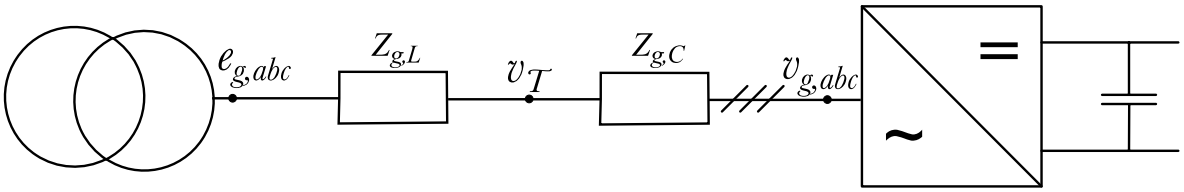

(a) Grid-side

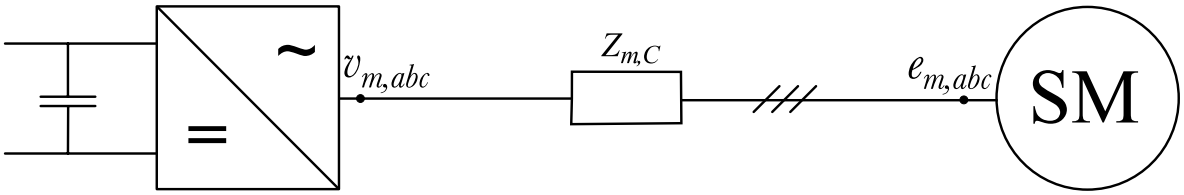

(b) Machine-side

Figure 4.2: Impedances and voltages

4.1.2 Governor and Turbine

The governor and turbine model is based on a simplified Francis turbine as shown in Fig. 4.3. The deviation from nominal speed/frequency is the input of the governor, which generate the desired gate opening based on the speed deviation. A simplified turbine is used to represent the turbine mechanics which generates the mechanical power/torque based on the gate opening from the governor. The parameter values for the governor and turbine model are presented in Appendix B.1.1.

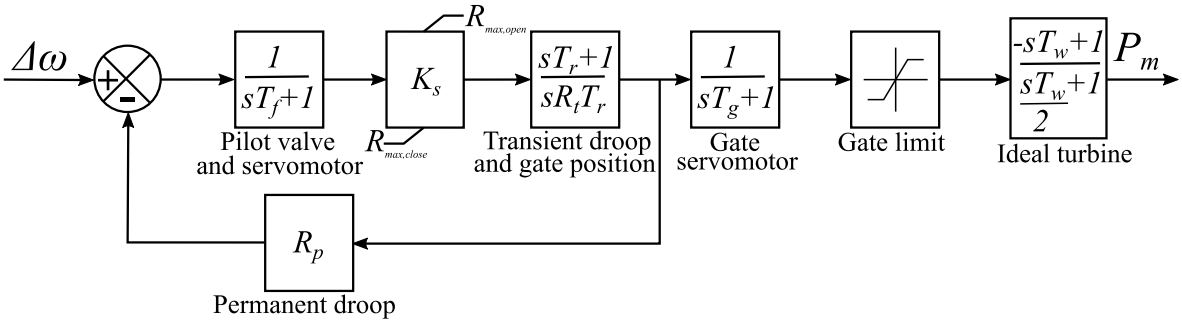

Figure 4.3: Governor and Turbine model based on a simplified Francis turbine

In the turbine transfer function, T_w represents the time required for the head to accelerate the water from standstill to a given velocity. This time constant varies with load and is typically in the range of 0.5 seconds to 4 seconds [27]. The transfer function inherits an important characteristic of the hydraulic turbine, which can be observed in Fig 4.4. As the gate position suddenly increase, the flow does not change instantly due to the water inertia. However, the pressure in the turbine reduces immediately, causing the power to decrease before increasing to the desired value.

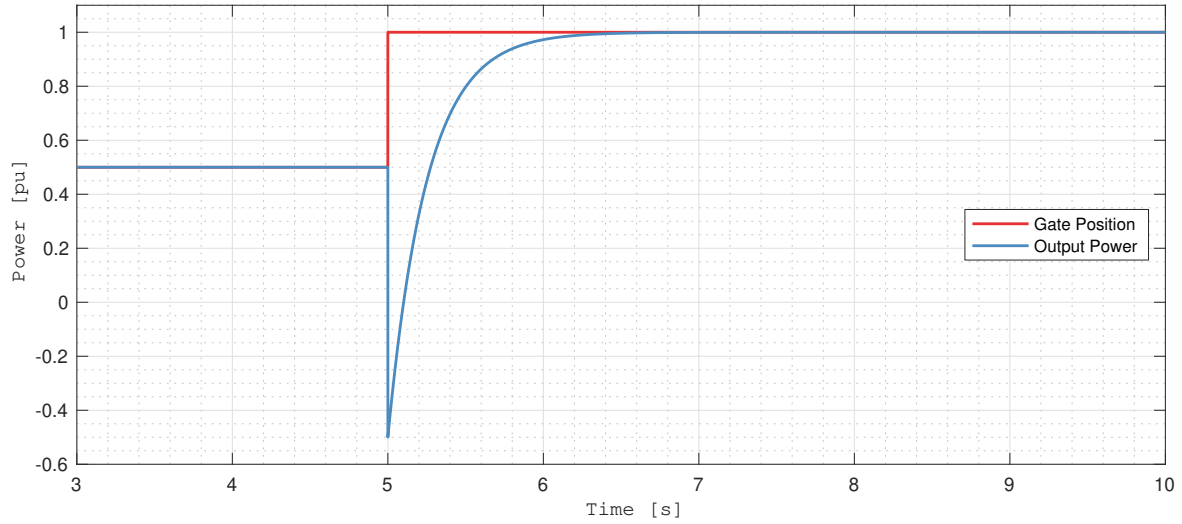

Figure 4.4: Power response form the turbine for a step in gate position

4.1.3 AVR

A simplified AVR is implemented in the excitation system which aims to keep the stator terminal voltage constant. The AVR is constructed of an outer loop controlling the terminal voltage and an inner field current loop as presented in Fig. 4.5. The terminal voltage (v_t) of the machine is measured and regulated using a PI-controller. From this controller, the reference

field current is generated, which is regulated to the desired value using a PI-controller. The parameter values for the PI-controllers are presented in Table B.5 in Appendix B.1.1.

As observed in the figure, the excitation system is not equipped with any power system stabilizer. However, since the active and reactive power can be controlled separately using the converter, it is claimed the there is no need for a power system stabilizer in adjustable speed units [48].

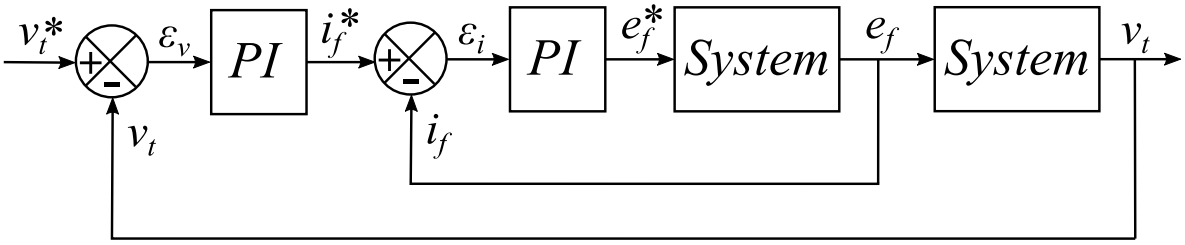

Figure 4.5: AVR control loop

4.1.4 Converter

The converter is rated correspondent to the machine, i.e., 15 MVA. In the simulation, it is favorable to use an average model of a VSC. An average model does not simulate the switching in the converter. However, it has the same average V-I terminal relationship on AC and DC side as a VSC [49].

A back-to-back VSC consist of two converters connected through an intermediate DC link. The converters are denoted grid-side converter (GSC) and machine-side converter (MSC), as seen in Fig. 4.1. The DC link voltage is chosen as twice the peak of the phase voltage, which is a restriction for the modulation. An overview of all parameter values for the converter is given in Appendix B.1.2.

4.2 Grid

The grid is simplified to a large synchronous generator connected to two loads. One large load acts as a constant base load while the other load is attached to the grid through a controllable switch. The generator is rated to 120 MVA, and is controlled like a typical grid-connected synchronous machine as shown in Fig. 3.1 with a governor and AVR. A standard MATLAB®/Simulink governor and turbine model are used where the governor and turbine are both represented as two separate time constants. The droop constant in the governor is set to 2%. The same AVR as described in Section 4.1.3 is used for the grid machine.

A voltage rating of 15 kV is chosen as it is a typical voltage level for large grid-connected

synchronous machines in the Nordic power system. Similarly, inertia constant of 3.5 seconds is typical for these types of machines [47].

There are two loads connected to the grid, one constant base load (Load 1) and one connected to the grid through a switch (Load 2). Both loads are wye-connected, and set to draw constant active power of 60 MW and 5 MW for Load 1 and Load 2 respectively. Load 2 will be connected/disconnected during steady-state operation to establish a power imbalance. The line is assumed to be ideal, i.e., there is no impedance in the line. For a full overview of all parameter values, see Appendix B.2.

Chapter 5

Classical Torque Control

Three main control responsibilities need to be accounted for in the system; machine speed, DC link voltage and power flow. In this chapter, classical torque control for the converter will be derived which allocates responsibilities in the following manner:

- Governor: Active power control
- Machine-side converter: Speed control
- Grid-side converter: DC link voltage control

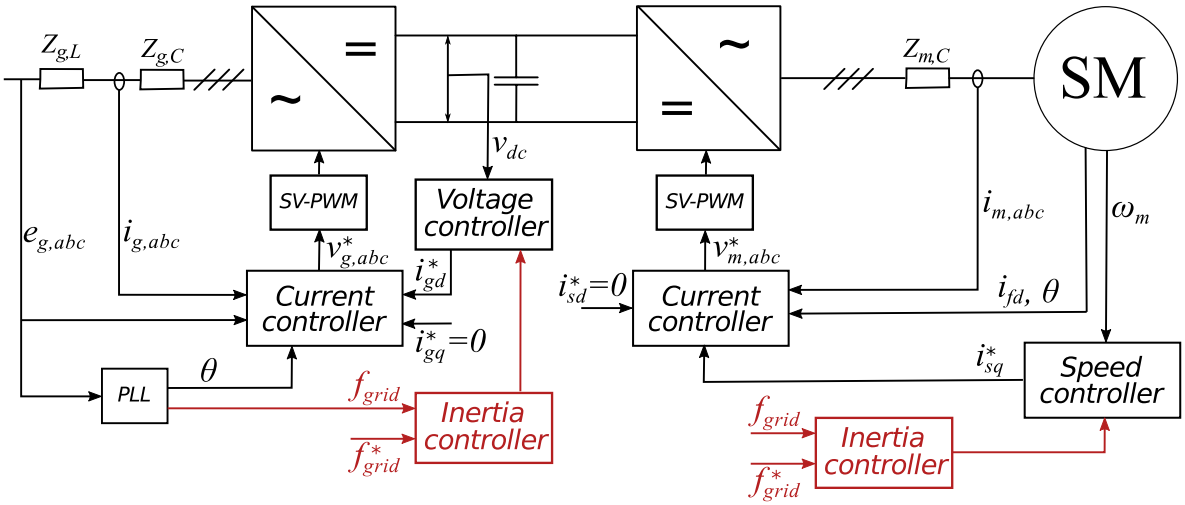

Figure 5.1: Overview of classical torque control with supplementary inertia control

In addition, supplementary control loops for inertia emulation will be added on both GSC and MSC, extracting stored energy in the capacitor and kinetic energy from rotation respectively. The inertia control loops will be in addition to the generic control loops and

will make the MSC and GSC responsible for short-term active power control. The complete control system for the converters is shown in Fig. 5.1, where the red part is the supplementary inertia control loops. As observed in the figure, both control systems consist of an inner current control an one outer control loop.

5.1 Synchronous Reference Frame (SRF)

To control time-varying currents and voltages it is favorable to represent them in a rotating dq-reference frame, often termed as a synchronous reference frame (SRF). This is achieved by synchronizing the reference frame with the control variables such that the variables can be represented as DC quantities. In addition, the d and q axis is perpendicular to each other which permits decoupling of the d and q axis. In other words, the d and q axis variables can be controlled independently of each other [50].

The transformation of a three-phase time-varying signal to a rotating dq-frame can be achieved by performing a Park transformation. To explain this it is common to use the Clark transformation. The Clark transformation represents a three-phase time-varying signal as a two-phase time-varying signal in a stationary reference frame, often termed as $\alpha\beta$-frame. Further, the Park transformation transforms this rotating two-phase signal to DC quantities by rotating the reference frame at synchronous speed. This is illustrated in Fig. 5.2 and mathematically described in Appendix A.1.

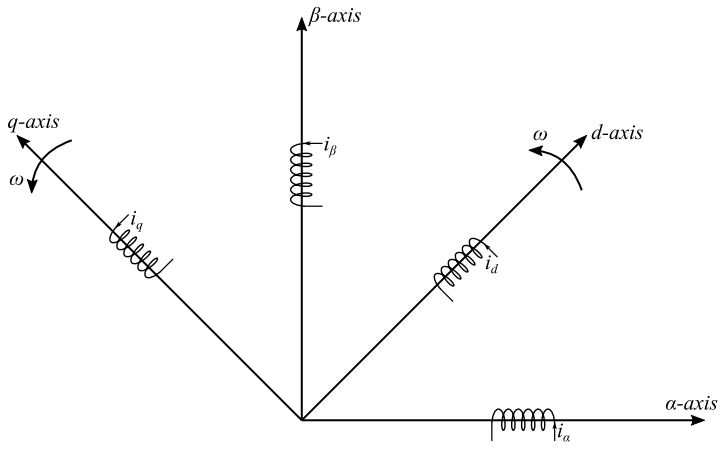

Figure 5.2: Stationary and rotating reference frames

Fig. 5.3 show the signal path from the transformation of measured signals, through the control system, and back to reference signals for the converter. After the control system, the signals are transferred back to a three-phase time-varying signal by performing an inverse transformation. In this work, the converters operate with a separate rotating axis. On the

GSC, the q-axis is aligned with a virtual grid flux vector while the d-axis is aligned with the grid voltage vector. For the MSC, the d-axis is aligned with the rotor flux and lags the q-axis by 90 electrical degrees.

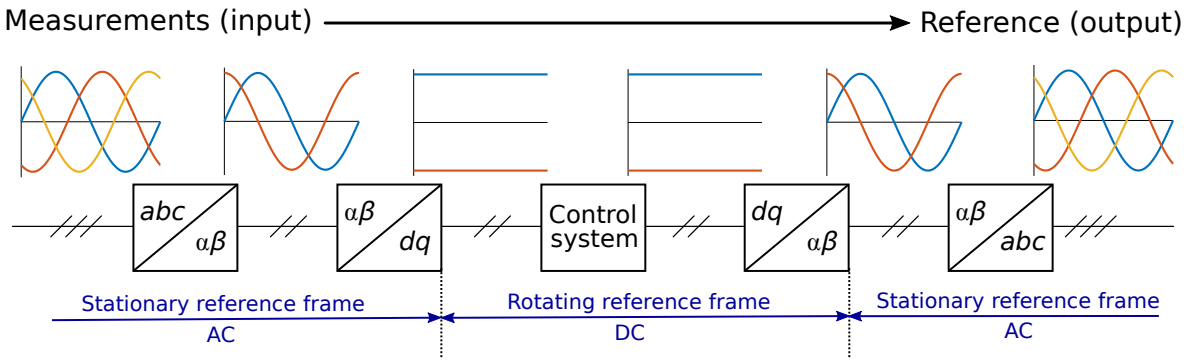

Figure 5.3: Signal reference frame through control system

5.2 Governor

The governor and turbine model is presented in Fig. 4.3, Chapter 4. In the classical torque control, the governor regulates the steady-state active power output from the plant by adjusting the flow of water into the turbine. To contribute to primary frequency regulation, the governor measures the grid frequency on the grid-side (from the PLL), and regulates power accordingly. This will result in similar primary frequency response from the governor as if the machine was directly grid-connected, with the lack of inertia support.

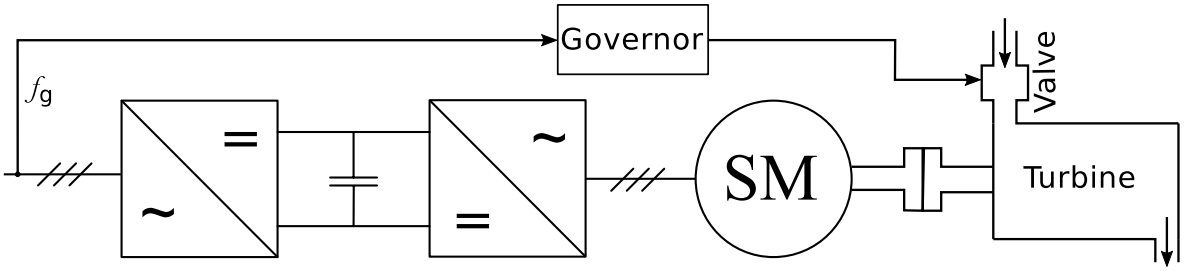

Figure 5.4: Governor control using classical torque control

5.3 Machine-Side Converter (MSC)

The MSC controls the electromagnetic torque and terminal voltage separately. The control consists of an inner current loop which controls the current and decouples the dq-axis to achieve independent control of the torque and voltage. The outer loops change the reference for i_{gq} and i_{gd} to control electromagnetic torque and terminal voltage respectively. In this report, only the control of electromagnetic torque is of interest, therefore the voltage control loop will not be derived. In addition, a supplementary inertia control loop emulates inertia by changing the speed reference. Fig. 5.5 show the final structure of the MSC control system which which is to be derived in this section. As seen in the figure, the control system consists of three main parts; the current controller, speed controller and inertia controller.

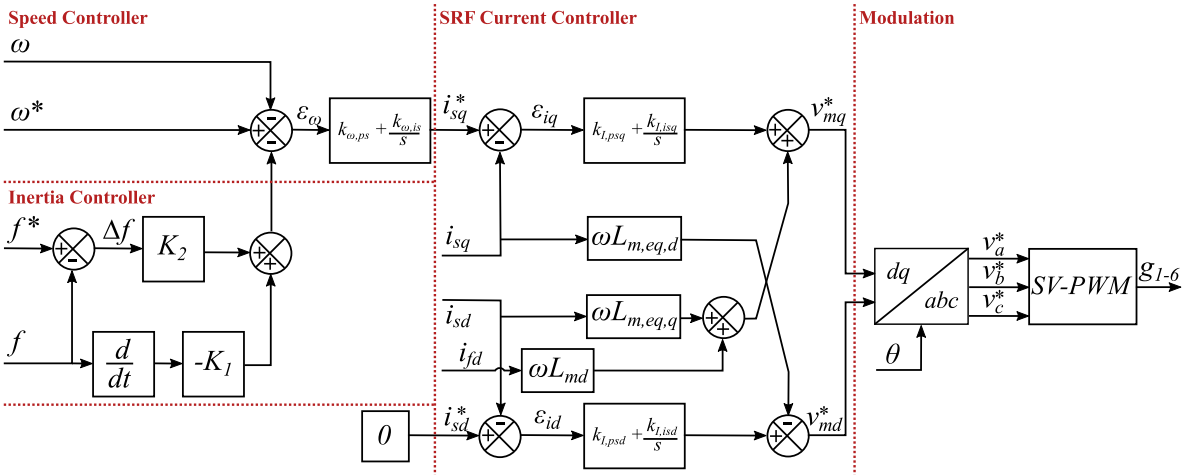

Figure 5.5: MSC final control system with modulation

5.3.1 Inner Loop: SRF Current Controller

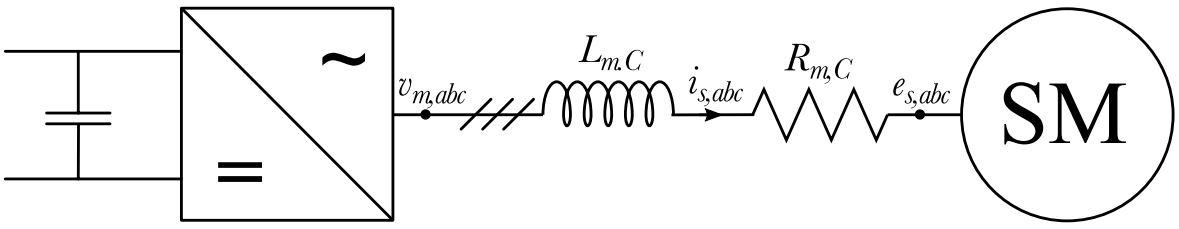

Figure 5.6: MSC-side system

The inner current loop aims to control the current on the AC-side and decouple the dq-axis to improve the dynamic performance of the system. The stator voltage equations for a salient poled synchronous machine with rotor field excitation can be expressed as [50]:

$$\begin{bmatrix} e_{sd} \\ e_{sq} \end{bmatrix} = R_s \begin{bmatrix} i_{sd} \\ i_{sq} \end{bmatrix} + \frac{d}{dt} \begin{bmatrix} \lambda_{sd} \\ \lambda_{sq} \end{bmatrix} + \underbrace{\omega \begin{bmatrix} 0 & -1 \\ 1 & 0 \end{bmatrix} \begin{bmatrix} \lambda_{sd} \\ \lambda_{sq} \end{bmatrix}}_{\textbf{Coupling}} \tag{5.3.1}$$

Where λ_{sd} and λ_{sd} are the d and q axis flux linkage respectively which can be expressed as:

$$\begin{aligned} \lambda_{sd} &= L_{sd} i_{sd} + L_{md} i_{rd} + L_{md} i_{fd} \\ \lambda_{sq} &= L_{sq} i_{sq} + L_{mq} i_{rq} \end{aligned} \tag{5.3.2}$$

In the equation above, L_{sd} and L_{sq} is the sum of the leakage inductance (L_{ls}) and magnetizing inductance ($L_{md/q}$) in the d and q windings respectively. Note that the magnetizing inductance is unequal ($L_{md} \neq L_{mq}$) due to the salient structure of the rotor. However, the leakage inductance is the same for both windings ($L_{ls} = L_{lsd} = L_{lsq}$) [50]. In order to simplify the stator voltage equations, the damper winding currents (i_{rd} and i_{rq}) in both axes can be neglected. This results in the following voltage equations:

$$\begin{bmatrix} e_{sd} \\ e_{sq} \end{bmatrix} = R_s \begin{bmatrix} i_{sd} \\ i_{sq} \end{bmatrix} + \frac{d}{dt} \begin{bmatrix} L_{sd} i_{sd} \\ L_{sq} i_{sq} \end{bmatrix} + L_{md} \frac{d}{dt} \begin{bmatrix} i_{fd} \\ 0 \end{bmatrix} + \underbrace{\omega \begin{bmatrix} 0 & -L_{sq} \\ L_{sd} & 0 \end{bmatrix} \begin{bmatrix} i_{sd} \\ i_{sq} \end{bmatrix} + \omega i_{fd} \begin{bmatrix} 0 \\ 1 \end{bmatrix}}_{\textbf{Coupling}} \tag{5.3.3}$$

As observed in Fig. 5.6, the converter resistance ($R_{m,C}$) is in series with the stator resistance (R_s). The equivalent resistance, $R_{m,eq}$, can be defined as the sum of these resistances. Similarly, the converter inductance ($L_{m,C}$) is in series with $L_{s,d/q}$. The equivalent inductances, $L_{m,eq,d/q}$, can be defined as the sum of these inductances. Using the stator voltage equation presented above and the equivalent impedances, the converter voltage, $v_{m,abc}$, can be represented in the dq-reference frame as:

$$\begin{aligned} \begin{bmatrix} v_{md} \\ v_{mq} \end{bmatrix} = R_{m.eq} \begin{bmatrix} i_{sd} \\ i_{sq} \end{bmatrix} + \frac{d}{dt} \begin{bmatrix} L_{m,eq,d} i_{sd} \\ L_{m,eq,q} i_{sq} \end{bmatrix} + L_{md} \frac{d}{dt} \begin{bmatrix} i_{fd} \\ 0 \end{bmatrix} \\ + \underbrace{\omega \begin{bmatrix} 0 & -L_{m,eq,d} \\ L_{m,eq,q} & 0 \end{bmatrix} \begin{bmatrix} i_{sd} \\ i_{sq} \end{bmatrix} + \omega i_{fd} \begin{bmatrix} 0 \\ 1 \end{bmatrix}}_{\textbf{Coupling}} \end{aligned} \tag{5.3.4}$$

From Eq. (5.3.4), it is evident that the d-q axis is coupled. To independently control these variables, the current controller needs to decouple the axis. In addition to decoupling the d and q axis, the current controller needs to regulate the current to the desired reference value.

In order to control the current, it is desirable to use a PI-controller and a feedback loop for the current. PI-controllers are widely used in industrial application due to a simple structure and low cost. PI-controllers eliminates forced oscillations and steady-state error [51]. Analyzing the equation above, the decoupling of the d-q axis variables and control of current can be achieved using:

$$\begin{aligned} v_{sd}^* &= \underbrace{(k_{I,psd} + \frac{k_{I,isd}}{s})}_{\textbf{PI}}(i_{sd}^* - i_{sd}) - \omega L_{m,eq,q} i_{sq} \\ v_{sq}^* &= \underbrace{(k_{I,psq} + \frac{k_{I,isq}}{s})}_{\textbf{PI}}(i_{sq}^* - i_{sq}) + \omega(L_{m,eq,d} i_{sd} + i_{fd} L_{md}) \end{aligned} \tag{5.3.5}$$

Where v_{sd}^* and v_{sq}^* are the converter voltage reference values in the d and q axis respectively. By inserting Eq. (5.3.5) in Eq. (5.3.4) it can be shown that the controller cancels out the coupling terms in both axes. The decoupling terms can be seen in the SRF current controller in Fig. 5.5. The current controller can be represented as a block diagram, as shown in Fig. 5.7. As seen in the figure, the current error is sent through a PI-controllers, which generates the reference voltage.

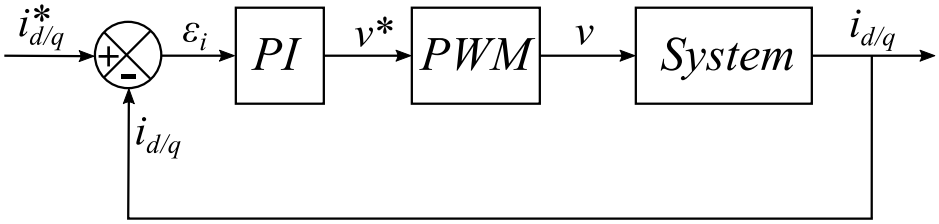

Figure 5.7: SRF inner current loop block diagram for both axes

5.3.2 Outer Loop: Speed Controller

The swing equation can be used to express the rotor motion of a synchronous machine as:

$$T_{em} - T_m = J\frac{d\omega}{dt} \tag{5.3.6}$$

During steady state operation the electromagnetic torque (T_{em}) and the mechanical torque (T_m) is equal. This leads to constant speed, as the acceleration term is zero. In order to change and control the speed of the machine, the electromagnetic torque can be controlled. Developed electromagnetic torque can be expressed as [50]:

$$T_{em} = \frac{p}{2}[L_{md}(i_{fd} + i_{rd})i_{sq} + \underbrace{(L_{sd} - L_{sq})i_{sd}i_{sq}}_{\textbf{Saliency}} - L_{mq} i_{rq} i_{sd}] \tag{5.3.7}$$

As with the current controller, the damper winding currents (i_{rd} and i_{rq}) can be neglected. Furthermore, the saliency can be neglected to simplify the expression. From this, the expression yields:

$$T_{em} = \frac{p}{2} L_{md} i_{fd} i_{sq} \tag{5.3.8}$$

From the equation above it can be observed that by controlling the current i_{sq} the torque/speed can be controlled. Similarly, it can be derived that the current i_{sd} can be controlled to control the voltage. The speed controller is shown as it is implemented in the control system in Fig. 5.5. As seen in the figure, the speed controller has two inputs; the speed reference and speed measurement feedback. The error between these inputs is sent through a PI-controller, which becomes the reference value for the q-axis current i^*_{sq}. This process can also be illustrated in a block diagram as shown in Fig. 5.8.

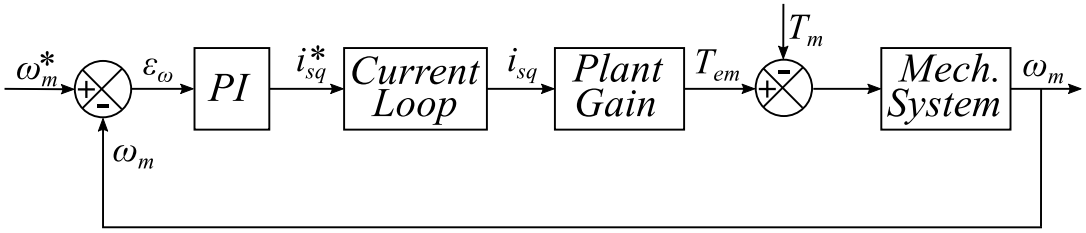

Figure 5.8: Outer speed loop block diagram for both axes

5.3.3 Supplementary Inertia Controller

Section 3.3 described a number of supplementary inertia control principles. In this section, both the df/dt-method and Δf-method will be derived. To describe the ROCOF method (or df/dt-method) the swing equation and energy equation of rotating masses can be used. The equations can be written as [52]:

$$\frac{P_{em} - P_m}{\omega_m} = J \frac{d\omega_m}{dt} \tag{5.3.9a}$$

$$E_{kin} = \frac{1}{2} J \omega_m^2 \tag{5.3.9b}$$

By linearizing Eq. (5.3.9a) around a steady state operation point and taking the derivative of both sides of Eq.(5.3.9b), Eq. (5.3.10a) and (5.3.10b) can be derived from Eq. (5.3.9a) and (5.3.9b) respectively. The full mathematical deduction of these two equations is presented in

Appendix A.5.

$$\Delta P_{em} = K' \frac{d\Delta f}{dt} \tag{5.3.10a}$$

$$\Delta P_{em} = -J\Delta\omega_m \tag{5.3.10b}$$

Eq. (5.3.10a) show the relation between a power imbalance in a grid and the frequency. From the equation, it is evident that a power imbalance in the grid will cause a change in frequency based on the derivative of the frequency multiplied by a constant. From Eq. (5.3.10b) it is evident that a reduction in the mechanical speed of a machine will cause a release of electrical power. Therefore, by controlling the speed deviation based on the ROCOF, inertia can be emulated similarly as the response would be for a grid-connected machine.

Another possible implementation is the frequency deviation method (or Δf-method). This method releases energy based on the deviation in frequency, similar to how droop control in a governor function. As with the ROCOF method, this method reduces the speed of the machine to release kinetic energy, according to Eq. (5.3.10b). This method can, however, conflict with the primary frequency controller in the governor.

Both methods described above can be combined in one controller. The derivative method will give a rapid and massive response as the frequency changes while the deviation part will prevent the machine from accelerating or decelerating back to nominal speed immediately after the initial frequency descent. The combined control system is shown in Fig. 5.9.

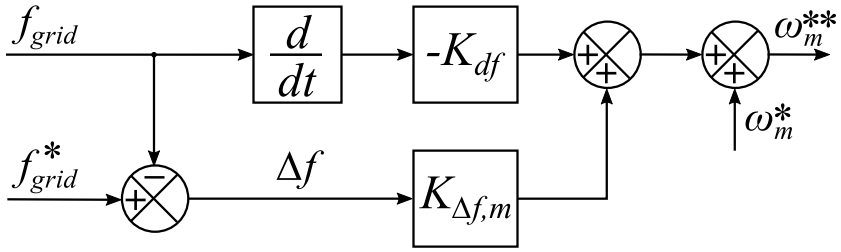

Figure 5.9: MSC inertia controller

5.4 Grid-Side Converter (GSC)

The GSC aims to control the DC link voltage by adjusting the flow of active power. The control consists of an inner current loop which controls the current and decouples the dq-axis similar to the MSC inner current loop. The current in the d and q axis controls the active and reactive power respectively. The outer voltage loop controls the active power reference such that the DC link voltage is kept constant. In this report, only active power control is of interest. Therefore a reactive power control loop will not be derived. Also, a supplementary inertia control loop emulates inertia by changing the DC link voltage reference. Fig. 5.10 show the final structure of the GSC control system which is to be derived in this section. As seen in the figure, the control system consists of three main parts; the current controller, DC link voltage controller and inertia controller.

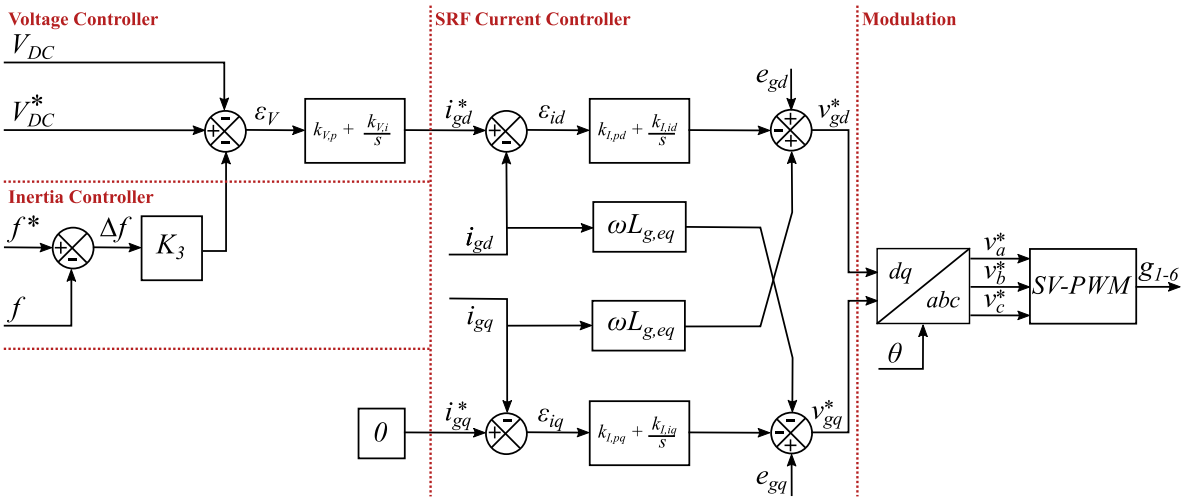

Figure 5.10: GSC final control system with modulation

5.4.1 Inner Loop: SRF Current Controller

The inner current loop aims to control the current on the AC-side and decouple the dq-axis to improve the dynamic performance of the system. Fig. 5.11 show the grid-side system with impedances, voltages and currents. In the figure, $e_{g,abc}$ is the three-phase grid voltage, $i_{g,abc}$ is the three-phase grid current and $v_{g,abc}$ is the three-phase converter voltage. Note that the current direction is chosen to be towards the converter. Between the grid voltage and converter voltage, there is an equivalent resistance and inductance ($R_{g,eq}$ and $L_{g,eq}$), which is the sum of the line and converter impedance presented in Fig. 4.2.

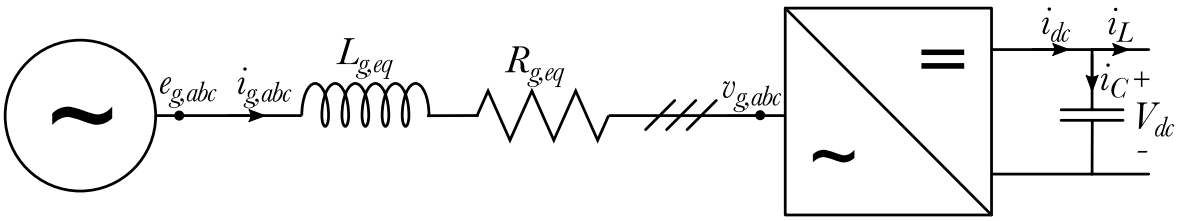

Figure 5.11: GSC-side system

Using KVL and KCL, the following equations can be derived:

$$e_{g,abc} = R_{g,eq} i_{g,abc} + L_{g,eq} \frac{di_{g,abc}}{dt} + v_{g,abc} \tag{5.4.1a}$$

$$C_{dc} \frac{dV_{dc}}{dt} = i_{dc} - i_L \tag{5.4.1b}$$

Using the Park transformation, Eq. (5.4.1ba) can be represented in the synchronous reference frame as:

$$\begin{bmatrix} e_{gd} \\ e_{gq} \end{bmatrix} = R_{g,eq} \begin{bmatrix} i_{gd} \\ i_{gq} \end{bmatrix} + L_{g,eq} \frac{d}{dt} \begin{bmatrix} i_{gd} \\ i_{gq} \end{bmatrix} + \underbrace{\omega L_{g,eq} \begin{bmatrix} 0 & -1 \\ 1 & 0 \end{bmatrix} \begin{bmatrix} i_{gd} \\ i_{gq} \end{bmatrix}}_{\textbf{Coupling}} + \begin{bmatrix} v_{gd} \\ v_{gd} \end{bmatrix} \tag{5.4.2}$$

From the equation above it is evident that the d-q axis is coupled. In order to control the current it is desirable to use a PI-controller and a feedback loop for the current. Analyzing the equation, the decoupling of the d-q axis variables and control of the current can be achieved using:

$$\begin{aligned} v_d^* &= -\underbrace{(k_{I,pd} + \frac{k_{I,id}}{s})}_{\textbf{PI}}(i_{gd}^* - i_{gd}) + \omega L_{g,eq} i_{gq} + e_{gd} \\ v_q^* &= -\underbrace{(k_{I,pq} + \frac{k_{I,iq}}{s})}_{\textbf{PI}}(i_{gq}^* - i_{gq}) - \omega L_{g,eq} i_{gd} + e_{gq} \end{aligned} \tag{5.4.3}$$

Where v_d^* and v_q^* are voltage reference values in the d and q axis respectively. By inserting Eq. (5.4.3) in Eq. (5.4.2) it can be shown that the controller cancels out the coupling terms in both axes. The decoupling terms can be seen in the SRF current controller in Fig. 5.10. The block diagram for the inner current control loop is equal to the MSC current loop shown Fig. 5.7.

5.4.2 Outer Loop: Voltage Controller

The outer voltage loop aims to control the DC link voltage to its reference value by controlling the flow of active power. If the governor increases power production, the GSC voltage control will forward this power, ensuring that the DC link voltage stays at the reference value. This also enables inertia response from the DC link as lowering and increasing the DC link voltage will inject and absorb active power. The equation for active and reactive power can be represented as (derived in Appendix A.3) [53]:

$$\begin{aligned} P &= \frac{3}{2} v_{gd} i_{gd} \\ Q &= -\frac{3}{2} v_{gd} i_{gq} \end{aligned} \tag{5.4.4}$$

From this, it is evident that i_{gd} and i_{gq} control active and reactive power respectively. The relation between i_{gd} and V_{dc} can be derived from Eq. (5.4.1b), and results in (derived in Appendix A.4):

$$C_{dc} \frac{d(\Delta V_{dc})}{dt} = \frac{3}{2} \frac{\bar{v}_d \Delta i_{gd}}{V_{dc}^*} \tag{5.4.5}$$

The equation above shows the relation between the d-axis current and DC link voltage. As shown in Eq. (5.4.4), a change in the d-axis current will change the active power. By controlling the DC link voltage based on the d-axis current reference, the active power flow is regulated such that the DC voltage is kept constant.

As observed in Fig 5.10, a PI-controller is used in the voltage controller. As with the speed controller, the voltage controller acts on the error from the feedback and reference value. This process can be represented in a block diagram as seen in Fig. 5.12.

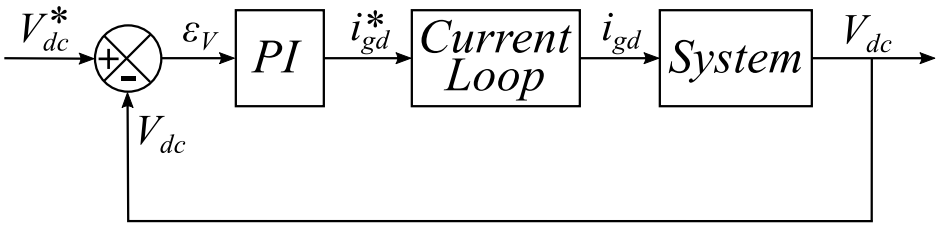

Figure 5.12: Outer voltage block diagram

5.4.3 Supplementary Inertia Controller

The capacitor in a back-to-back voltage source converter can store a considerable amount of energy. Similar to the kinetic energy inertia control system on the MSC, a supplementary control system can be added to the GSC to enable frequency support. Energy stored in a

capacitor is given by [54]:

$$E_{dc} = \frac{1}{2} C_{dc} V_{dc}^2 \tag{5.4.6}$$

Energy released for a given deviation in DC link voltage can be expressed as:

$$\Delta E_{dc} = \frac{1}{2} C_{dc} (V_{dc}^2 - (V_{dc} - \Delta V_{dc})^2) \tag{5.4.7}$$

Taking the derivative of Eq. (5.4.7), the equation can be written as Eq. (5.4.8). This is thoroughly described in Appendix A.6.

$$\Delta P_{em} = C_{dc} \Delta V_{dc} \tag{5.4.8}$$

By using the relation of power and voltage deviation above, an inertia controller based on frequency deviation or derivative can be implemented supplementary to the voltage controller. Fig. 5.13 show the supplementary controller using the Δf-method. There is, however, a limit to how much the voltage can be reduced given by the modulation, which needs to be accounted for in the implementation.

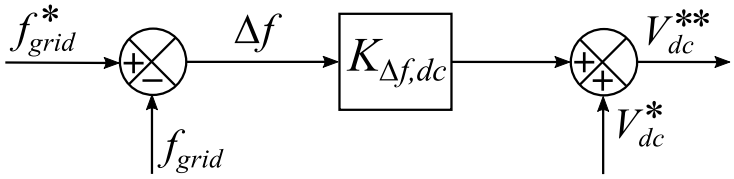

Figure 5.13: GSC inertia controller

5.5 Space vector modulation (SVM)

Space vector modulation is an algorithm for control of pulse width modulation (PWM), often referred to as space vector pulse with modulation (SV-PWM). This method combines traditional PWM with digital signal processors to achieve even better control of electric drives.

SV-PWM has been shown to generate less harmonic compared to sinusoidal PWM in both output voltage and current [55]. In addition, SV-PWM utilizes the DC voltage better, increasing the limit on the available output voltage by approximately 15% compared to sinusoidal PWM [50]. This is an important factor for the DC link inertia contribution which is dependent on reducing the DC link voltage for short-termed power response.

PWM can be implemented by comparing control voltages with a triangular waveform signal at switching frequency. The control system derived above generates sinusoidal signals

which need to be synthesized as space vectors. This can be done by synthesizes an average space vector. To implement this, the control voltages can be written as [50]:

$$\begin{bmatrix} v_{a,control} \\ v_{b,control} \\ v_{c,control} \end{bmatrix} = 2\frac{\hat{V}_{tri}}{V_{dc}} \begin{bmatrix} v_a^* - v_k \\ v_b^* - v_k \\ v_c^* - v_k \end{bmatrix} \tag{5.5.1}$$

Where

$$v_k = \frac{max(v_a^*, v_b^*, v_c^*) + min(v_a^*, v_b^*, v_c^*)}{2} \tag{5.5.2}$$

Using Eq. (5.5.1) and (5.5.2), SV-PWM can be implemented as presented in Fig. 5.14.

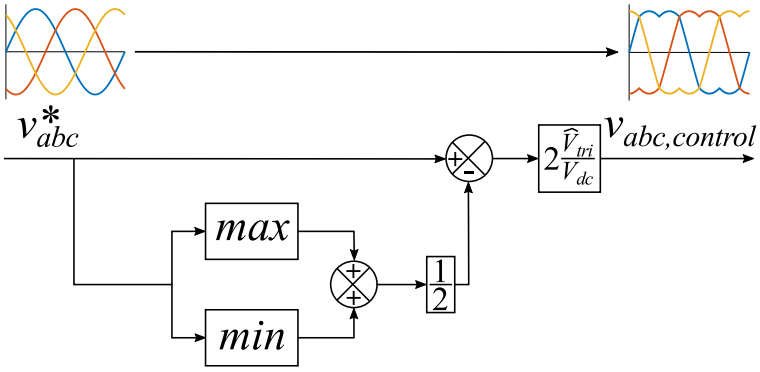

Figure 5.14: SV-PWM implementation

5.6 Tuning of Controllers

A number of methods exist for tuning PI-controllers which results in different performance of the controllers. The choice of method depends on the specification of the control system, such as measurement sensitivity, set-point following and robustness [56]. The current controllers and the speed and voltage controllers will be tuned according to modulus optimum and symmetrical optimum respectively.

5.6.1 Current Controllers: Modulus Optimum

From the current loop block diagram shown in Fig. 5.7, the open loop transfer functions can be expressed as:

$$
\begin{aligned}
G_{I,OL,GSC}(s) &= (k_{I,pd/q} + \frac{k_{I,id/q}}{s}) \frac{1}{1+T_{sw}s} \frac{1}{R_{g,eq} + L_{g,eq}s} \\
G_{I,OL,MSC}(s) &= \underbrace{(k_{I,psd/q} + \frac{k_{I,isd/q}}{s})}_{\textbf{PI}} \underbrace{\frac{1}{1+T_{sw}s}}_{\textbf{PWM}} \underbrace{\frac{1}{R_{m,eq} + L_{m,eq,d/q}s}}_{\textbf{System}}
\end{aligned} \tag{5.6.1}
$$

Where:

$$T_{sw} = \frac{1}{2f_{sw}} \tag{5.6.2}$$

Modulus optimum can be applied to this control system to achieve a satisfying response. This is a popular method due to simple implementation and rapid response. The method keeps the magnitude of the closed-loop function at unity for a wide frequency span as possible [57]. To use the method, a standard open loop transfer function can be considered:

$$g_{OL}(s) = (k_p + \frac{k_i}{s}) K_s \frac{1}{1+T_{sum}s} \frac{1}{1+T_1 s} \tag{5.6.3}$$

To tune according to modulus optimum, the PI-controller time constant is chosen to cancel the largest time constant, and the gain is set higher than unity. Based on the transfer function above, this can be achieved using the following relation:

$$k_i = \frac{1}{2K_s T_{sum}} \tag{5.6.4}$$

$$k_p = \frac{T_1}{2K_s T_{sum}} \tag{5.6.5}$$

Following this procedure, the resulting PI-controller parameter values are given in Table B.7 in Appendix B.1.2.

5.6.2 Voltage and Speed Controllers: Symmetrical Optimum

For the outer control loops, the current controller can be simplified to a time delay (T_{eq}). From the voltage and speed loop block diagrams, the open loop transfer function can be expressed as:

$$
\begin{aligned}
G_{V,OL,GSC}(s) &= (k_{V,p} + \frac{k_{V,i}}{s})\frac{1}{1+T_{eq}s}\frac{3\bar{v}_d}{2V_{dc}^*}\frac{1}{C_{dc}s} \\
G_{\omega,OL,MSC}(s) &= \underbrace{(k_{\omega,ps} + \frac{k_{\omega,is}}{s})}_{\textbf{PI}}\underbrace{\frac{1}{1+T_{eq}s}}_{\textbf{Cur.loop}}\underbrace{k_T}_{\textbf{P.gain}}\underbrace{\frac{1}{T_m s}}_{\textbf{System}}
\end{aligned}
\tag{5.6.6}
$$

Where:

$$T_{eq} = \frac{1}{f_{sw}} \tag{5.6.7}$$

Since the transfer function contains an integrator, modulus optimum cannot be used to tune the controllers. Instead, symmetrical optimum can be used to achieve satisfying performance. Symmetrical optimum produce maximum phase margin for the closed loop system, enabling high delay tolerance [58]. The method offers high disturbance rejection compared to other methods and easy implementation. To tune the regulator according to symmetrical optimum, the following general open loop transfer function with an integrator can be considered:

$$g_{OL}(s) = (k_p + \frac{k_i}{s})K_s\frac{1}{1+T_{eq}s}\frac{1}{T_1 s} \tag{5.6.8}$$

Using this function, the controller can be tuned according to the symmetrical optimum criterion by choosing the gains as:

$$k_i = \frac{T_1}{a^3 T_{eq}^2} \tag{5.6.9}$$

$$k_p = \frac{T_1}{aT_{eq}} \tag{5.6.10}$$

Where "a" is a design parameter which is usually chosen such that the bandwidth of the controller is at least one decade below the current controller bandwidth. Following this procedure, the resulting PI-controller parameter values are given in Table B.8 in Appendix B.1.2.

Chapter 6

Virtual Synchronous Machine Control

To implement VSM control on a converter-fed synchronous machine, the function of the MSC, GSC and governor is changed compared to classical torque control. The MSC and GSC control the DC link voltage and active power respectively, while the governor controls the machine speed. In this chapter, VSM control will be derived which allocates the control responsibilities in the following manner:

- Governor: Speed control
- Machine-side converter: DC link voltage control
- Grid-side converter: Active power control

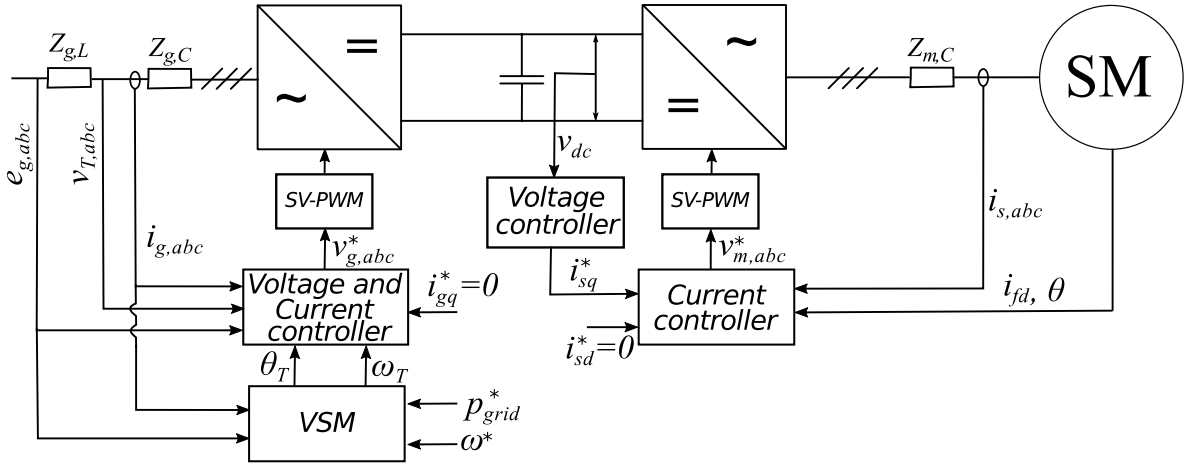

Figure 6.1: Overview of the converter control system using VSM control

In the classical torque control, the converter can only regulate the short-term response of power using stored energy while the governor controls the power output under normal operating conditions. For VSM control the GSC controls the power output while the MSC and governor control the DC link voltage and machine speed respectively. In principle, any energy source could be connected to the MSC, as the VSM control in the GSC do not take into account the type of power source. However, the power source will limit the amount of power the VSM can deliver. An overview of the control system is presented in Fig. 6.1 for both GSC and MSC. As can be observed in the figure, both converters have an inner current control similar to that of classical torque control.

In addition to the inner current control, the GSC is equipped with a voltage controller as can be observed in Fig. 6.1. Control of inverters can be classified into grid-feeding converters and grid-forming converters [45]. A grid-feeding converter can be simplified to a current source connected with a high impedance in parallel. Similarly, a grid-forming converter is equivalent to a voltage source with low impedance in series. The main difference between the two methods is the ability for stand-alone operation. The grid-feeding converter cannot regulate the voltage; therefore it is not able to operate individually. By implementing a grid-forming control method and VSM control, a converter can, in theory, operate without any synchronous generators in the grid and maintain a robust grid due to the presence of virtual inertia. As illustrated in Fig. 6.2, the main difference between these two methods is the presence of a voltage controller.

(a) Grid-feeding converter control

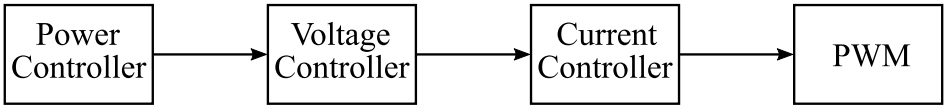

(b) Grid-forming converter control

Figure 6.2: Comparison of grid-feeding and grid-forming converter control

A number of methods to implement VSM exist today, with a wide range of design. Some methods focus on making the VSM self-synchronizing, such as in [31][59][60][61]. By doing this, the VSM can synchronize with the grid without any additional synchronization method such as a PLL. Such a method is implemented in this thesis, as presented in Fig. 6.1.

6.1 Governor

The governor in the hydro-electric power plant aims to control the speed of the generator. The structure of the governor is the same as for the classical torque control presented in Fig. 4.3. However, the governor now measures the mechanical speed of the machine which it regulates to a constant reference speed. This is similar to how a typical gird-connected synchronous machine is controlled, regulating the speed to synchronous speed.

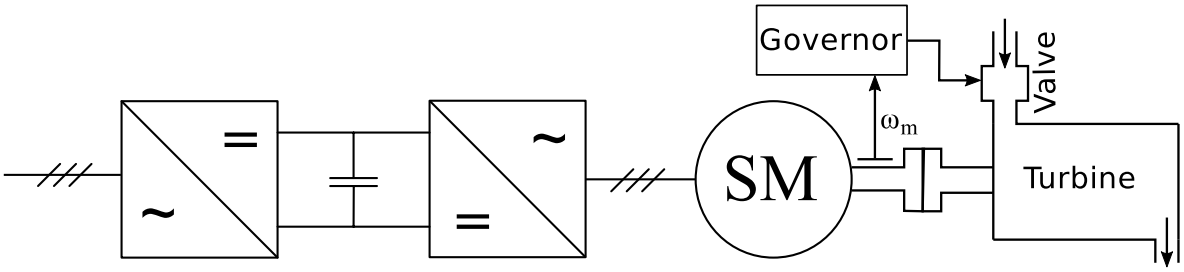

Figure 6.3: Governor control using VSM control

6.2 Machine-Side Converter (MSC)

As shown in Fig. 6.1, the MSC consist of an inner current loop and one outer voltage loop. The inner current loop is identical as for the classical torque control in Section 5.3, and aims to control the current and decouple the d and q axis variables. The outer loop aims to regulate the DC link voltage by controlling the active power/torque reference i_{sq}^*. In the previous chapter, the DC link voltage controller was derived for the GSC. The derivation is similar with the same tuning of the PI-controller. The current and DC link voltage controllers on the MSC are not derived in this section since it is similar to the classical torque control. An overview of the complete control system for the MSC is presented in Fig. 6.4.

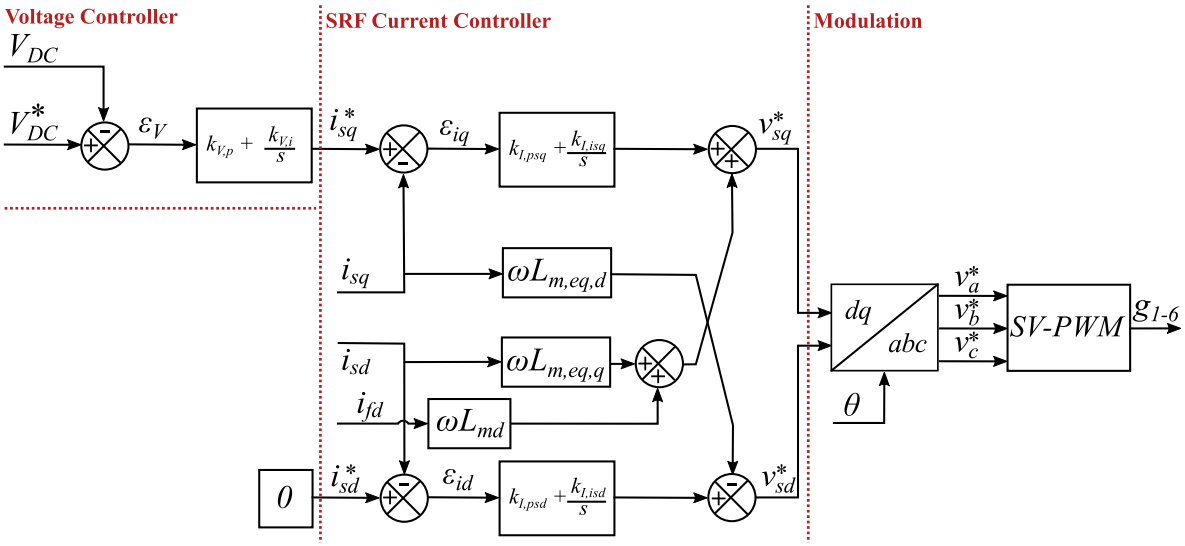

Figure 6.4: MSC final control system with modulation

6.3 Grid-Side Converter (MSC)

As shown in Fig. 6.5, the GSC consist of an inner SRF current loop, an SRF voltage loop and a power controller. The power controller aims to mimic the behavior of a grid-connected synchronous generator. This can be achieved by implementing the dynamic equations of a synchronous machine in the control system. The power controller also synchronizes the converter to the grid by calculating the angle based on the power balance.

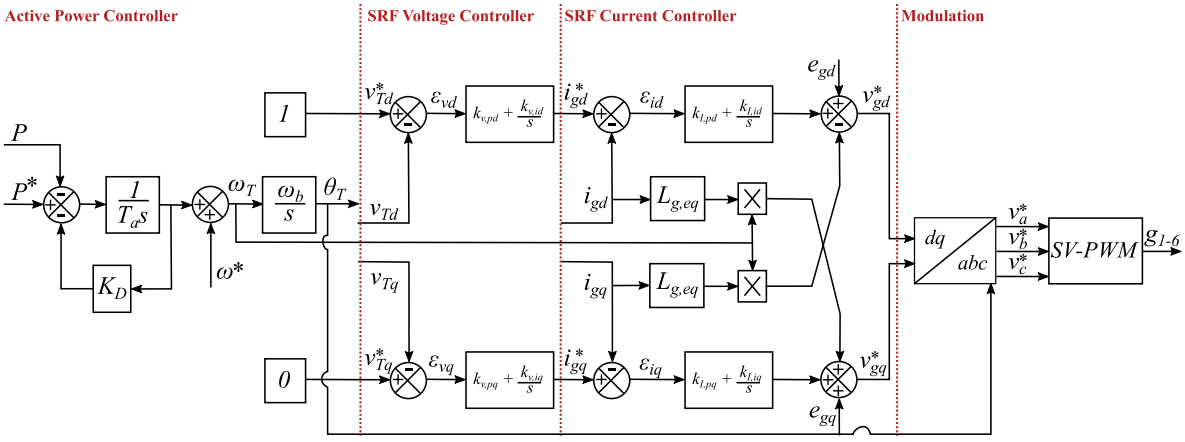

Figure 6.5: GSC final control system with modulation

6.3.1 SRF Current and Voltage Controller

As shown in Fig. 6.5, the control system consists of an inner current controller similar to the classical torque control and one outer voltage controller. As with the MSC, the inner current loop is identical as for the classical torque control in Chapter 5.3. The voltage controller aims to control the voltage on the converter terminals, v_T. Often a decoupling of an LCL-filter is performed in the voltage controller to improve transient stability, as explained in [33]. However, in this study, an average model of a VSC is used such that a filter is not required. The current reference is, therefore, calculated from the voltage error using a PI-controller as follows:

$$\begin{aligned} i_{sd}^* &= (k_{v,pd} + \frac{k_{v,id}}{s})(v_{Td}^* - v_{Td}) \\ i_{sq}^* &= (k_{v,pq} + \frac{k_{v,iq}}{s})(v_{Tq}^* - v_{Tq}) \end{aligned} \tag{6.3.1}$$

6.3.2 Power Controller and Synchronizer

The power controller aims to control the power output by changing the rotor angular position, θ. To achieve, the dynamic equations of a synchronous machine is implemented such that the power controller mimics the behavior of a synchronous machine. The VSM control synchronizes to the grid using the phase angle calculated from the swing equation. The swing equation can be written as [27]:

$$\frac{2H}{\omega_b}\frac{d^2\delta}{dt^2} + \frac{K_D}{\omega_b}\frac{d\delta}{dt} = P_m - P_{em} \tag{6.3.2}$$

With the following identities:

$$\begin{aligned} \omega_b \Delta\omega &= \frac{d\delta}{dt} \\ T_a &= 2H \end{aligned} \tag{6.3.3}$$

Substituting the above identities in the swing equation yields:

$$T_a s\Delta\omega + K_D\Delta\omega = P^* - P \tag{6.3.4}$$

Where T_a is the mechanical time constant and K_D represent the damping coefficient. The angle can be calculated as:

$$\theta_T = \frac{\omega_b}{s}\omega_T \tag{6.3.5}$$

Power Controller

In Fig. 6.6, the GSC represented as a VSM is shown connected to the grid. As observed in the figure, the impedance between the grid and the VSM is the line impedance $Z_{g,L}$. The converter impedance ($Z_{g,C}$) is between the terminal voltage (v_T) and the internal voltage of the converter ($V_{g,abc}$). This impedance is similar to the stator impedance of a synchronous machine.

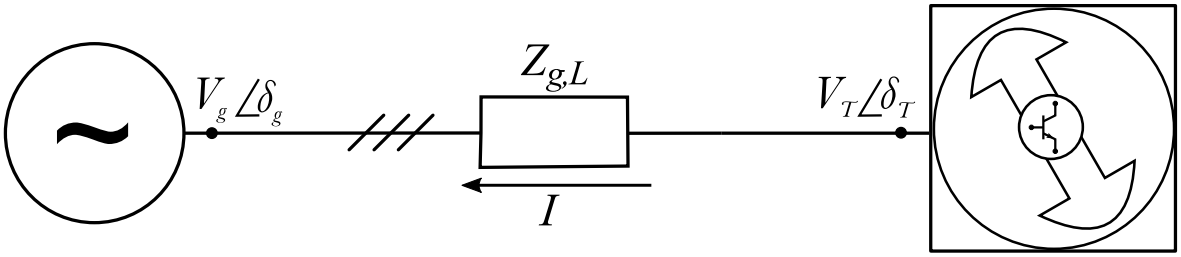

Figure 6.6: Simple schematic of power delivered from the VSM

In the figure above, the current flowing from the VSM to the grid can be expressed as:

$$I = \frac{V_T \angle \delta_T - V_g \angle \delta_g}{Z_L \angle \phi_L} \tag{6.3.6}$$

The power at the VSM terminal can be expressed as:

$$\begin{aligned} P_T =& \mathrm{Re}\left\{ V_T \angle \delta_T \left(\frac{V_T \angle -\delta_T - V_g \angle -\delta_g}{Z_L \angle -\phi_L} \right) \right\} \\ =& \mathrm{Re}\left\{ \frac{V_T^2}{Z_L} \angle \phi_L - \frac{V_T V_g}{Z_L} \angle (\delta_T - \delta_g + \phi_L) \right\} \\ =& \frac{V_T^2}{Z_L} \cos(\phi_L) - \frac{V_T V_g}{Z_L} \cos(\delta_T - \delta_g + \phi_L) \end{aligned} \tag{6.3.7}$$

From the equation above it can be observed that to change the active power either the voltage or angle needs to be regulated. Since the voltage controller aims to keep the terminal voltage constant, V_T can be assumed constant. Therefore, the angle is changed to control the active power. The relation between the angle δ and θ is given by [62]:

$$\theta_T(t) = \omega t + \delta_T(t) \tag{6.3.8}$$

Where δ is the rotor angular position with respect to a synchronously rotating reference while θ is the rotor angular position with respect to a stationary axis.

Understanding $\mathbf{K_D}$ and $\mathbf{T_a}$

To investigate the effect of changing the mechanical time constant (T_a) and damping coefficient (K_D), Eq. (6.3.7) can be further investigated. A linear approximation of the equation yields:

$$\begin{aligned} P + \Delta P = \frac{V_T^2}{Z_L}\cos(\phi_L) - \frac{V_T V_g}{Z_L}\cos(\delta_{T0} - \delta_{g0} + \phi_L) \\ + \underbrace{\frac{V_T V_g}{Z_L}\sin(\delta_{T0} - \delta_{g0} + \phi_L)}_{\mathbf{k_1}}[\Delta\delta_T - \Delta\delta_g] \end{aligned} \tag{6.3.9}$$

Which can be rewritten as:

$$P + \Delta P = \underbrace{\frac{V_T^2}{Z_L}\cos(\phi_L) - \frac{V_T V_g}{Z_L}\cos(\delta_{T0} - \delta_{g0} + \phi_L) - k_1(\delta_{T0} - \delta_{g0})}_{\mathbf{P}} + \underbrace{k_1(\delta_T - \delta_g)}_{\mathbf{\Delta P}} \tag{6.3.10}$$

Furthermore, a small signal analysis of the swing equation (presented i Eq. (6.3.4)) can be performed to find:

$$\frac{T_a}{\omega_b}\frac{d^2\Delta\delta}{dt^2} + \frac{K_D}{\omega_b}\frac{d\Delta\delta}{dt} = \Delta P^* - \Delta P \tag{6.3.11}$$

Substituting the expression for ΔP from Eq. (6.3.10), Eq. (6.3.11) can be written as:

$$\frac{T_a}{\omega_b}\frac{d^2\Delta\delta}{dt^2} + \frac{K_D}{\omega_b}\frac{d\Delta\delta}{dt} = \Delta P^* - k_1(\Delta\delta_T - \Delta\delta_g) \tag{6.3.12}$$

$$\frac{d^2\Delta\delta}{dt^2} + \frac{K_D}{T_a}\frac{d\Delta\delta}{dt} + \frac{k_1\omega_b}{T_a}\Delta\delta_T = (\Delta P^* + k_1\Delta\delta_g)\frac{\omega_b}{T_a} \tag{6.3.13}$$

Which can be written in the Laplace-domain as:

$$(s^2 + \frac{K_D}{T_a}s + \frac{k_1\omega_b}{T_a})\Delta\delta_T = (\Delta P^* + k_1\Delta\delta_g)\frac{\omega_b}{T_a} \tag{6.3.14}$$

From this, the following transfer functions can be derived:

$$\begin{aligned} \frac{\Delta\delta_T}{\Delta P^*} &= \frac{\frac{\omega_b}{T_a}}{s^2 + \frac{K_D}{T_a}s + \frac{k_1\omega_b}{T_a}} \\ \frac{\Delta\delta_T}{\Delta\delta_g} &= \frac{\frac{k_1\omega_b}{T_a}}{s^2 + \frac{K_D}{T_a}s + \frac{k_1\omega_b}{T_a}} \end{aligned} \tag{6.3.15}$$

Analyzing the equations above, the poles of the system yields:

$$s_{1,2} = -\frac{K_D}{T_a} \pm \frac{1}{2}\sqrt{\frac{K_D^2}{T_a^2} - 4\frac{k_1\omega_b}{T_a}} \tag{6.3.16}$$

From this, the system is stable as long as k_1 is greater than zero. Using the equation above, the natural frequency (ω_n) and damping (ζ) can be expressed as:

$$\begin{aligned} \omega_n &= \sqrt{\frac{k_1\omega_b}{T_a}} \\ \zeta &= \frac{K_D}{2}\sqrt{\frac{1}{T_a k_1 \omega_b}} \end{aligned} \tag{6.3.17}$$

From the above equations, it is clear that increasing the damping coefficient increases the damping in the system. Similarly, increasing the mechanical time constant decreases the damping and natural frequency.

Power Droop

There are two methods often used to control the steady-state power output of the VSM. The first is by adding a droop speed control on the power reference P^*, as shown in Fig. 6.7. This method requires the measurement of the frequency in some way, such as measuring it using a PLL. Furthermore, the speed reference (ω^*) in the swing equation is set as the measured grid frequency, as shown in Fig. 6.7.

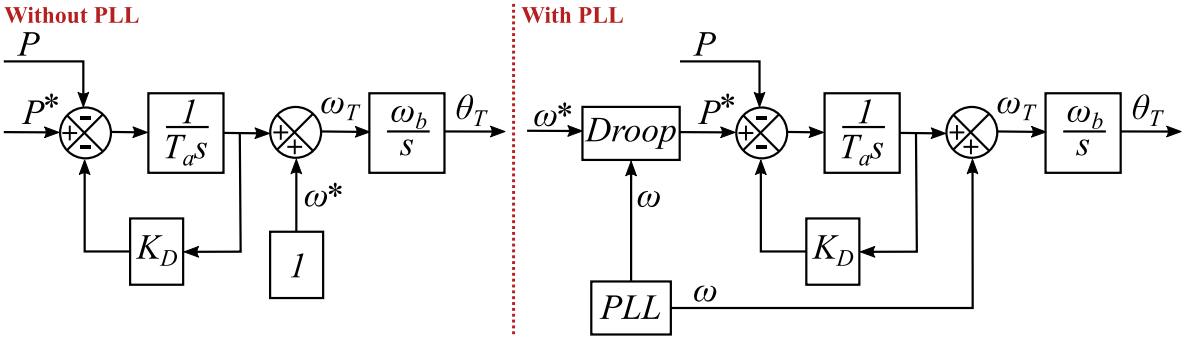

Figure 6.7: Power controller with and without a PLL

The other method is to use the damping coefficient (K_D) as a droop. This can be achieved by setting the speed reference (ω^*) in the swing equation to a constant of 1 pu. The advantage of this method is a more straightforward implementation and removal of the frequency measurement. However, the damping coefficient now works as a droop rather than as damping, which can make the system less stable. With this implementation, the power droop can be written as:

$$\Delta P = K_D \Delta\omega \tag{6.3.18}$$

Eq. (6.3.18) show that the damping coefficient in the swing equation is inversely linked to the droop gain in a droop controller.

6.4 Tuning of Controllers

Since the system is the same as with the classical torque control, the current controllers are tuned as described in Section 5.6. The tuning of the DC link voltage controller is the same as with the DC link voltage controller in torque control, which is also described in Section 5.6. Analyzing the SRF voltage loop, the transfer function can be simplified to the PI-controller and time constants representing the current controller and filter. This transfer function can be written as:

$$G_{v,OL,GSC}(s) = \underbrace{(k_{v,pd/q} + \frac{k_{v,id/q}}{s})}_{\textbf{PI}} \underbrace{\frac{1}{1+T_{eq}s}}_{\textbf{Cur.loop}} \underbrace{\frac{1}{T_{fi}s}}_{\textbf{Filter}} \tag{6.4.1}$$

The controllers can be tuned using modulus optimum, by canceling the current controller time constant. The result from the tuning is given in Table B.9 in Appendix B.1.2 using the method described for modulus optimum in Section 5.6

6.5 Comparison of Torque Control and VSM Control

The two control methods differ in how the control responsibilities are divided and the method inertia is emulated. As shown in Fig. 6.8a, the GSC, MSC and governor control the DC link voltage, machine speed and power respectively for the classical torque control. In addition, the GSC and MSC control the inertia support, which is short-termed active power. For the VSM control the GSC, MSC and governor control active power, DC link voltage and speed respectively. A comparison of the two methods is shown in Table 6.1. The response from the governor is typically slower than modern converters, which makes the decision of the control responsibility a question of prioritization. If speed control is the most important factor, then speed should be controlled by a converter. The argument is valid for power control and DC link voltage control. The classical torque control with supplementary inertia control uses the fast speed control to achieve short-termed power control. This way the control methods tries

to achieve the best of both worlds with both fast speed control and fast short-termed power control.

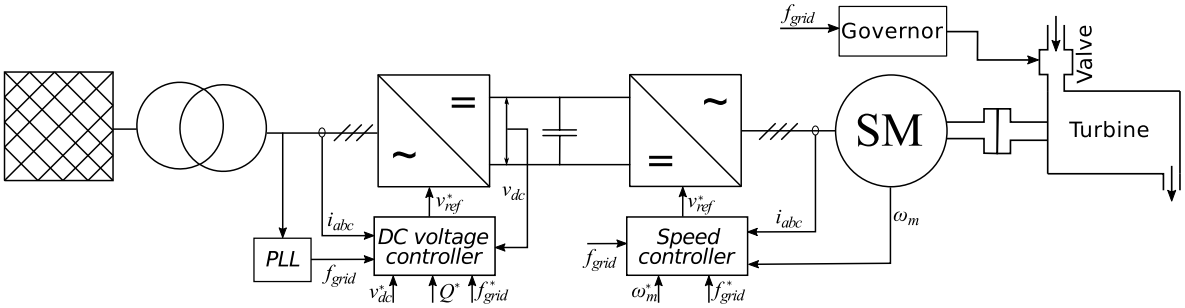

(a) Classical torque control with supplementary inertia controllers

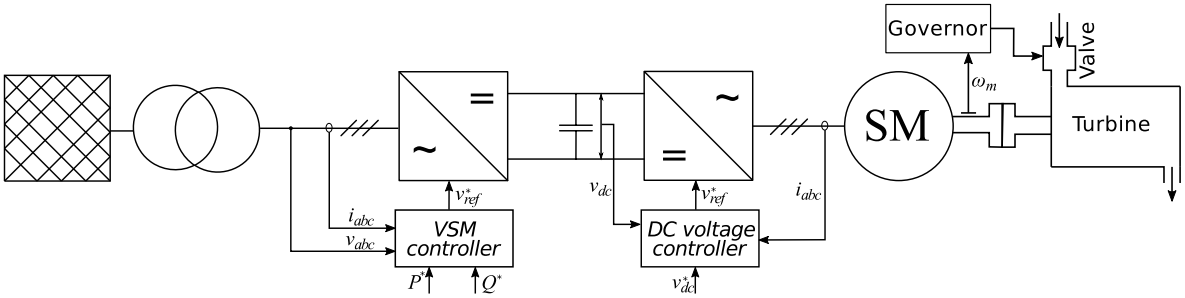

(b) Virtual synchronous machine control

Figure 6.8: Comparison of classical torque control and VSM control

Table 6.1: Comparison of control responsibilities for the two methods

Method	**GSC**	**MSC**	**Governor**
Classical torque control	DC link voltage	Machine speed	Active power
VSM control	Active power	DC link voltage	Machine speed

Other than the different allocation of control responsibilities, the most significant difference from a control implementation perspective is the possibility for self-synchronization using VSM control [31]. The VSM control also inherits other advantages such as natural damping and improved load sharing capability. However, the VSM control is a more complicated method to achieve inertia emulation compared to the other methods. In Case 1 in the following chapter, the performance of these two methods is compared during a load disturbance.

Chapter 7

Results and Discussion

The system simulated in this chapter is described in Chapter 4. Initially, the system operates at steady-state, and both the grid machine and hydro-electric power plant delivers active power to the load in the grid. The hydro-electric power plant deliverers 0.6 pu active power, while the grid machine delivers the remaining active power to the load. During steady-state operation Load 2 (described and quantified in Chapter 4) connects to the grid such that a load imbalance is established. This scenario will be the basis for the following two sections where the classical torque control (from Chapter 5) and VSM control (from Chapter 6) will be tested and analyzed separately. The goal of these two sections is to understand how the control method function and operate, and how the different parameters for inertia emulation in the controllers affect the performance.

In the third section of this chapter, three case studies are conducted. The goals of the three case studies are as follows:

- **Case 1**: *Comparison of classical torque control with supplementary inertia controllers and virtual synchronous machine control.* The goal of this case is to compare the inertia response for the two control strategies during the event described in the introduction to this chapter. Factors such as frequency nadir, oscillation in frequency and ROCOF are compared.

- **Case 2**: *Comparison of virtual synchronous machine and synchronous machine.* This case aims to understand how the VSM compares to a SM during the event described in the introduction to this chapter. The case investigates the influence of changing T_a and K_D, and compares this to a simulation of a SM and theory derived in the former chapter.

- **Case 3**: *Dynamic inertia for a VSM.* The goal of this case is to investigate advantages

with dynamic control of the inertia time constant using the VSM control method. Since the inertia time constant is set in the controller, it can be changed during operation depending on the state of the system to improve small-signal stability.

The results in this chapter are given in a per unit representation where the base values are based on the hydro-electric power plant, presented in Table B.3 in Appendix B.1.1.

7.1 Classical Torque Control with Inertia Controllers

In this section, the supplementary control scheme for the classical torque control will be tested and evaluated. The goal is to understand how both the kinetic inertia controller and capacitor inertia controller function. The different gain parameters (K_{df}, $K_{\Delta f,m}$ and $K_{\Delta f,dc}$) will be tuned for best performance.

7.1.1 Kinetic Inertia Control

Fig. 7.1 present the grid frequency for different values of K_{df} and $K_{\Delta f,m}$. As can be observed in the figure, increasing K_{df} results in an improved frequency nadir up to K_{df}=20. After this point the performance of the controller reduces. It is, therefore, reasonable to choose K_{df}=20 for this situation. Increasing $K_{\Delta f,m}$ improves the frequency nadir as shown in Fig 7.1b. However, $K_{\Delta f,m}$ also conflicts with the primary frequency control in the governor, which leads to more oscillation as the frequency recovers. $K_{\Delta f,m}$ is chosen to be 20 based on a trade-off between best inertia response and avoiding interference with the primary response.

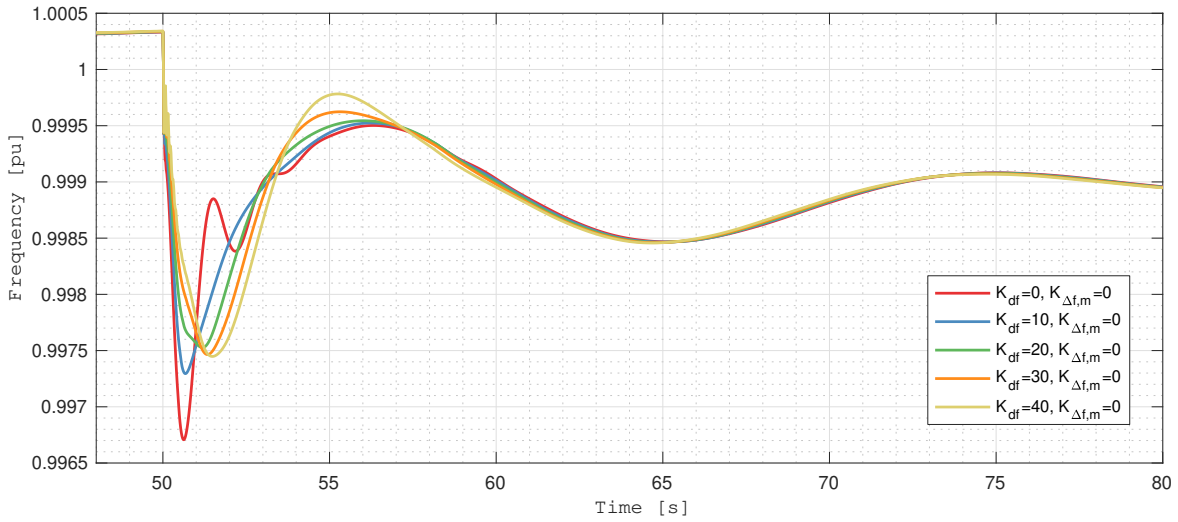

(a) Changing K_{df}

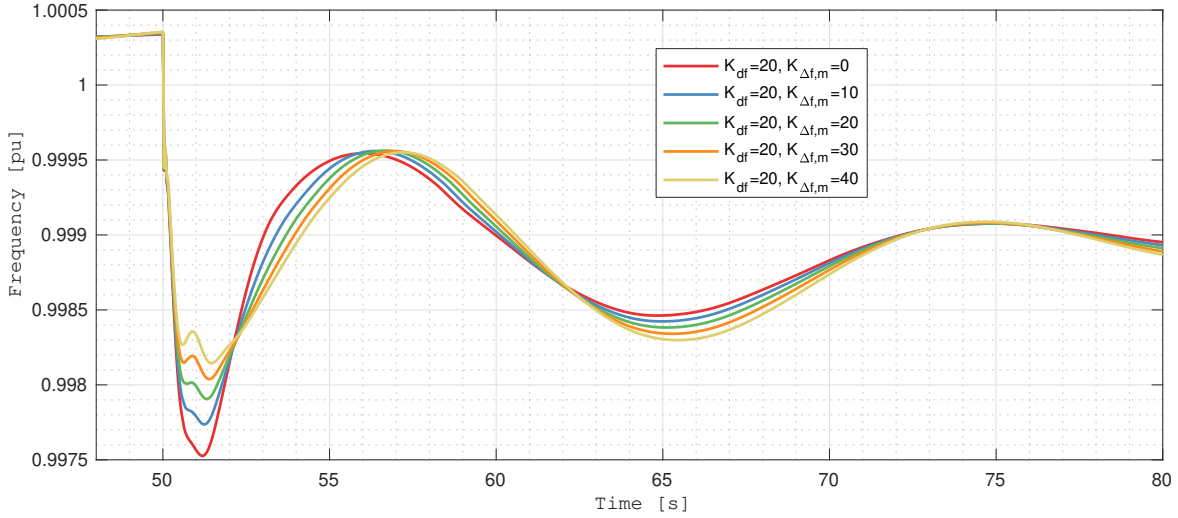

(b) Changing $K_{\Delta f,m}$

Figure 7.1: Grid frequency

In Fig. 7.2 and 7.3 it can be observed that as the machine decelerates it contributes to a short-term active power response. As seen in Fig. 7.2a, increasing K_{df} improves the inertia response, however, the consequence is reduced power output after the inertia response. This aftermath effect is the reason why the frequency response is worse for large values of K_{df}. Similarly, Fig. 7.2b shows the oscillation in power after inertia response due to the deviation inertia controller.

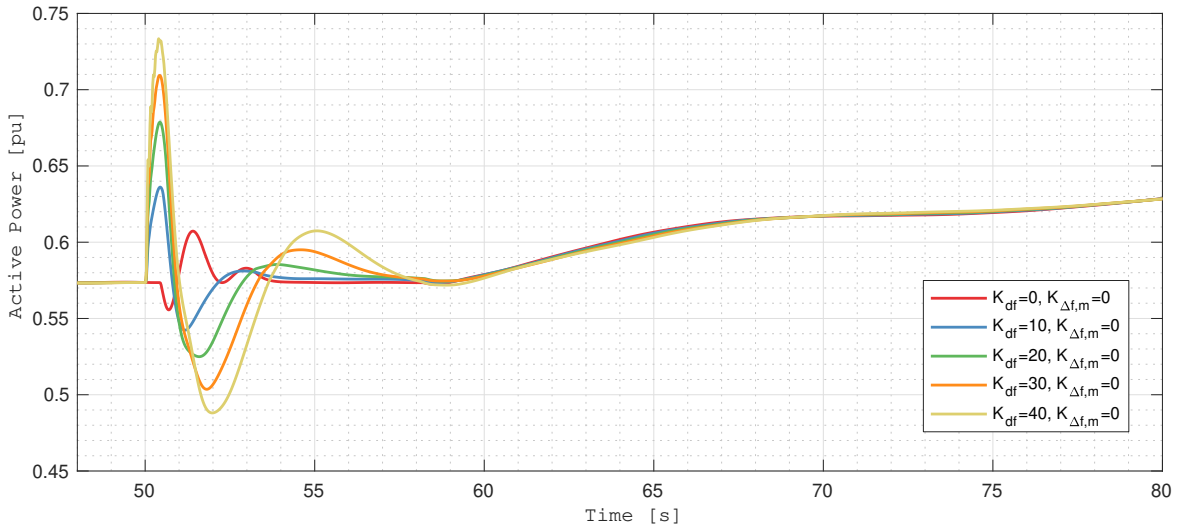

(a) Changing K_{df}

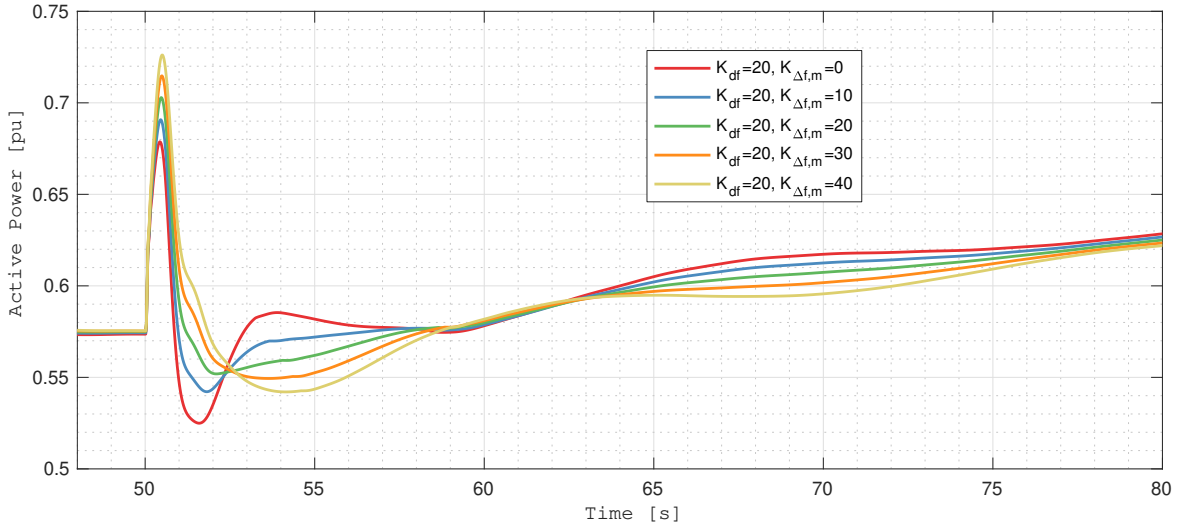

(b) Changing $K_{\Delta f,m}$

Figure 7.2: Active power delivered from the hydro-electric power plant

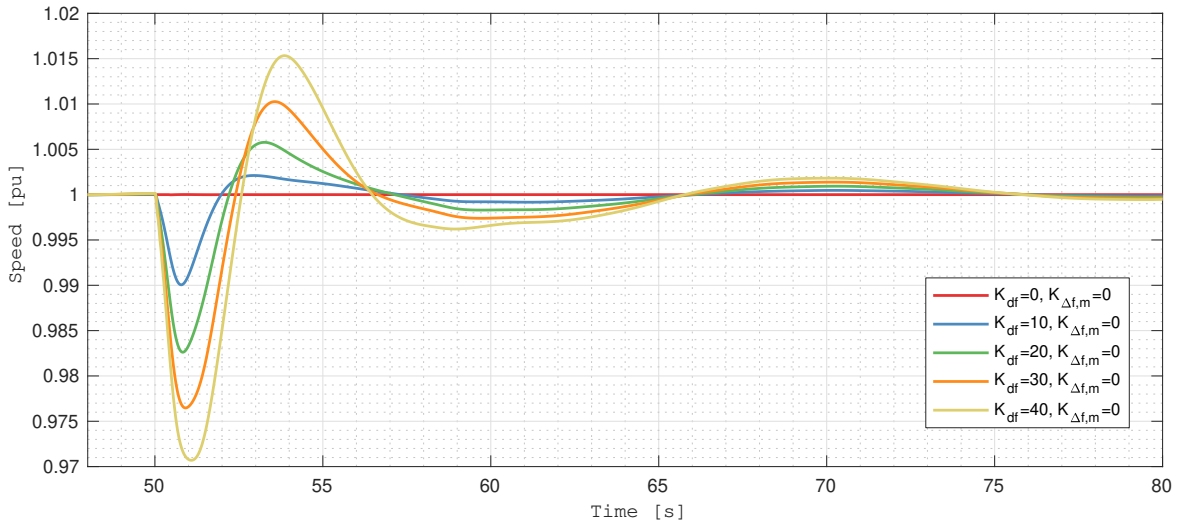

(a) Changing K_{df}

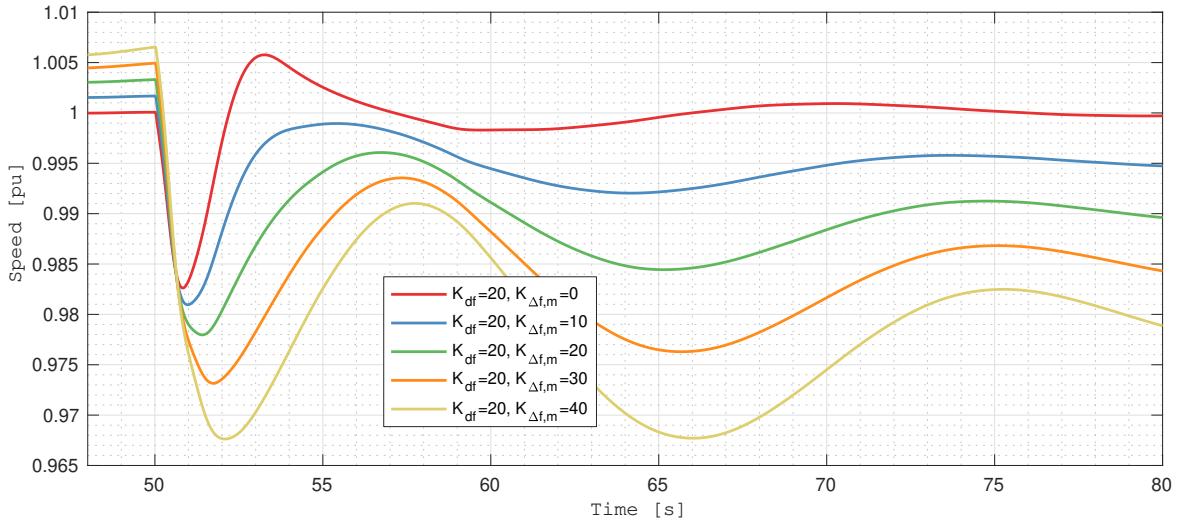

(b) Changing $K_{\Delta f,m}$

Figure 7.3: Hydro-electric synchronous machine speed (ω_m)

7.1.2 Capacitor Inertia Control

Enabling inertia support from the DC link capacitor as presented in Section 5.4.3 results in the frequency shown in Fig. 7.4. The frequency improves slightly, however, the inertia support from the capacitor is significantly less than the kinetic energy inertia support. The resulting active power presented in Fig. 7.5 show minor increase in active power delivered during the frequency event due to the capacitor inertia controller. Increasing the gain $K_{\Delta f,dc}$ would not increase the power output much as the DC link voltage saturates at the minimum allowable value which can be observed in Fig. 7.7.

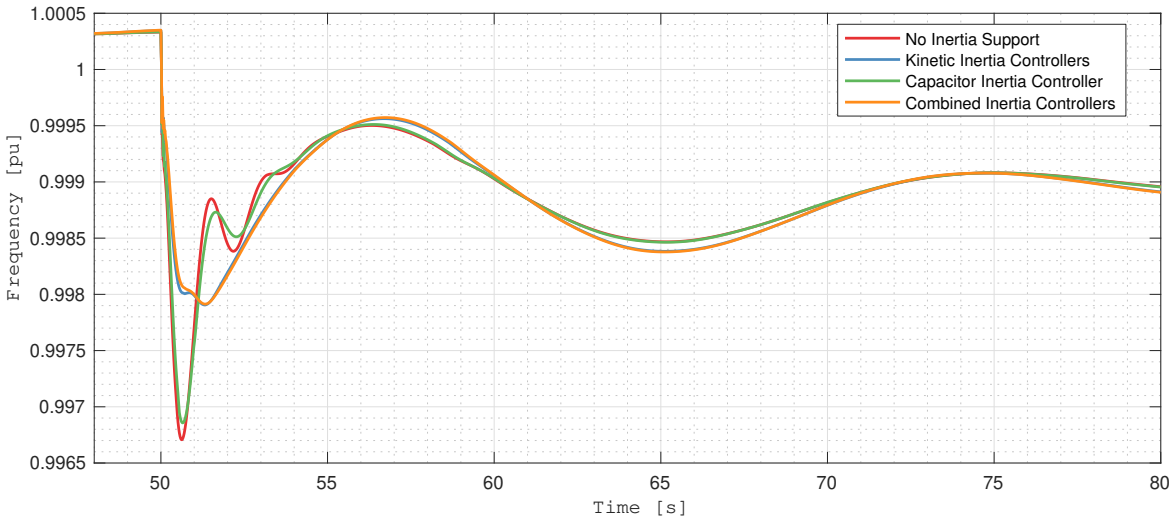

Figure 7.4: Grid frequency

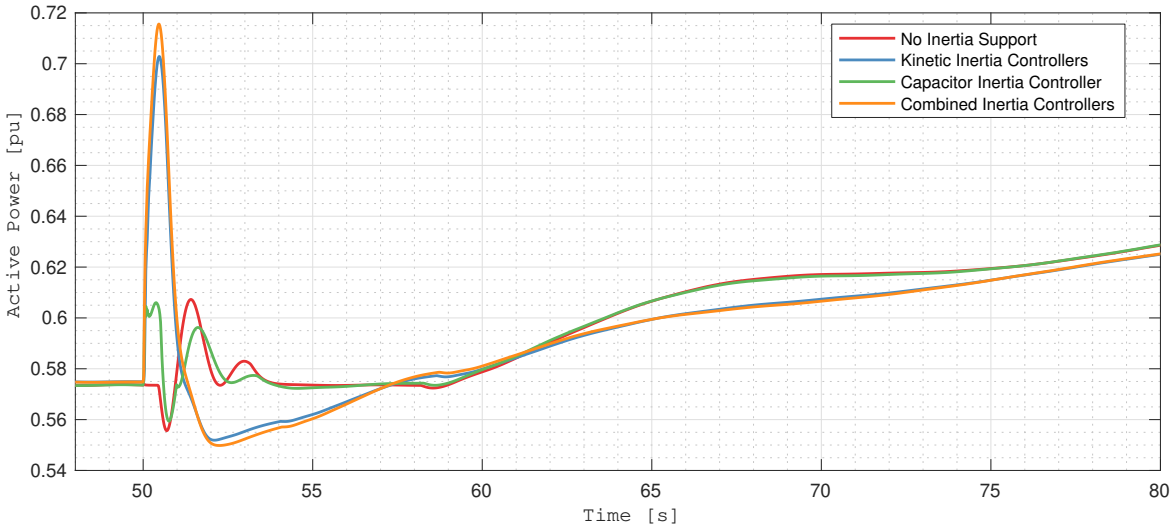

Figure 7.5: Active power delivered from the hydro-electric power plant

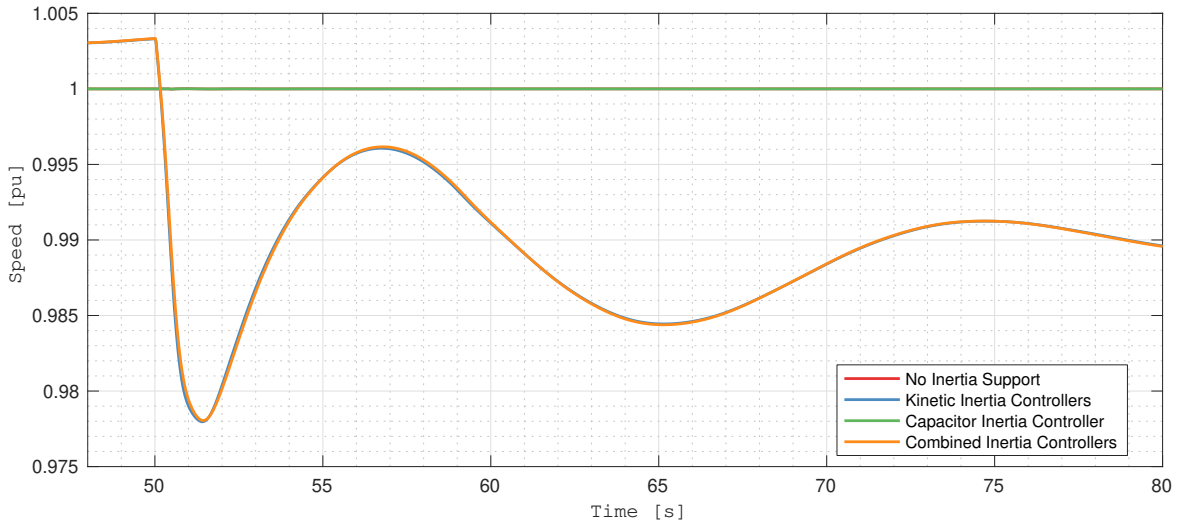

Figure 7.6: Hydro-electric synchronous machine speed (ω_m)

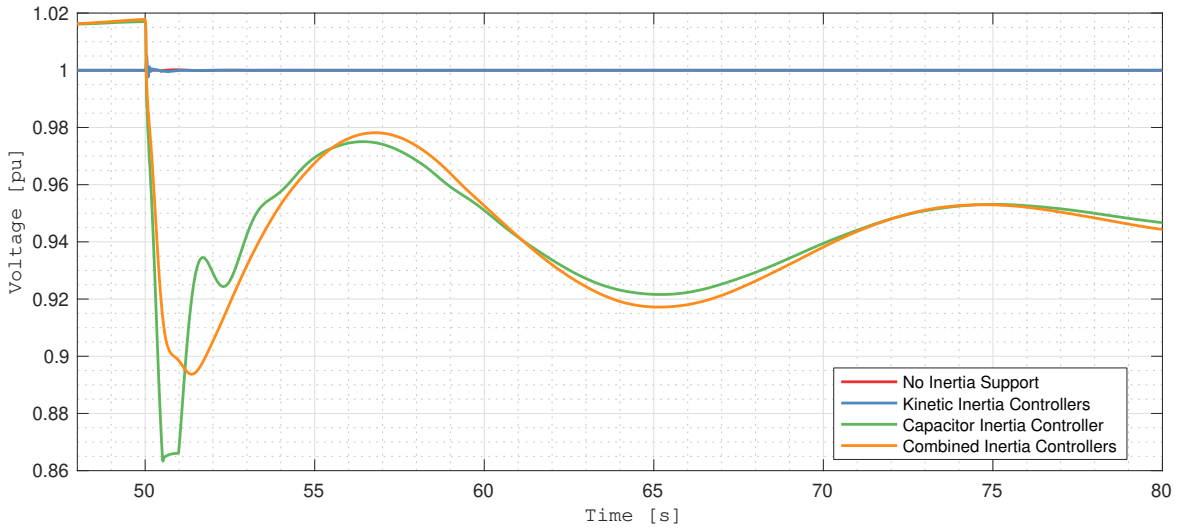

Figure 7.7: VSC DC link voltage (V_{dc})

7.2 Virtual Synchronous Machine Control

In this section, the VSM control method will be tested and evaluated during the case described in the introduction to this chapter. The VSM is set to deliver 0.6 pu active power, similar to the governor power set-point in the previous section. The goal is to investigate the performance of the VSM for different values of T_a and K_D.

7.2.1 Inertia Time Constant

Increasing the mechanical time constant T_a (equivalent to $2H$) improves the inertia contribution from the VSM, as observed in Fig. 7.8. Since the inertia time constant is set in the controller, the amount of synthetic inertia can be chosen freely. However, the contribution would, of course, be limited by the amount of available energy and rating of the converter, as will be discussed in the last section of this chapter. As observed in Fig. 7.9 and 7.8, changing the inertia time constant only affects the transient performance of the VSM. This is expected as the amount of inertia would not affect steady-state performance, as can be shown from Eq. (6.3.4).

The improved inertia response is also reflected in the active power, where the amplitude of the power increases for large values of T_a, as shown in Fig. 7.9. However, the consequence of large inertia is more oscillation after the power imbalance has occurred, i.e., the small-signal stability is worsened. In Case 3 in the following section, a solution for this will be suggested based on implementing dynamic inertia.

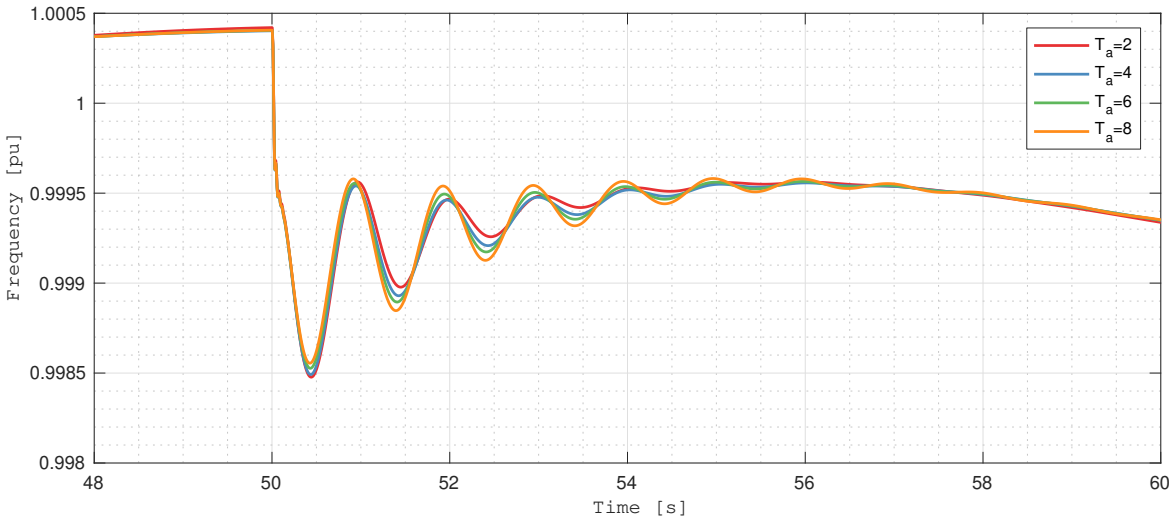

(a) Initial

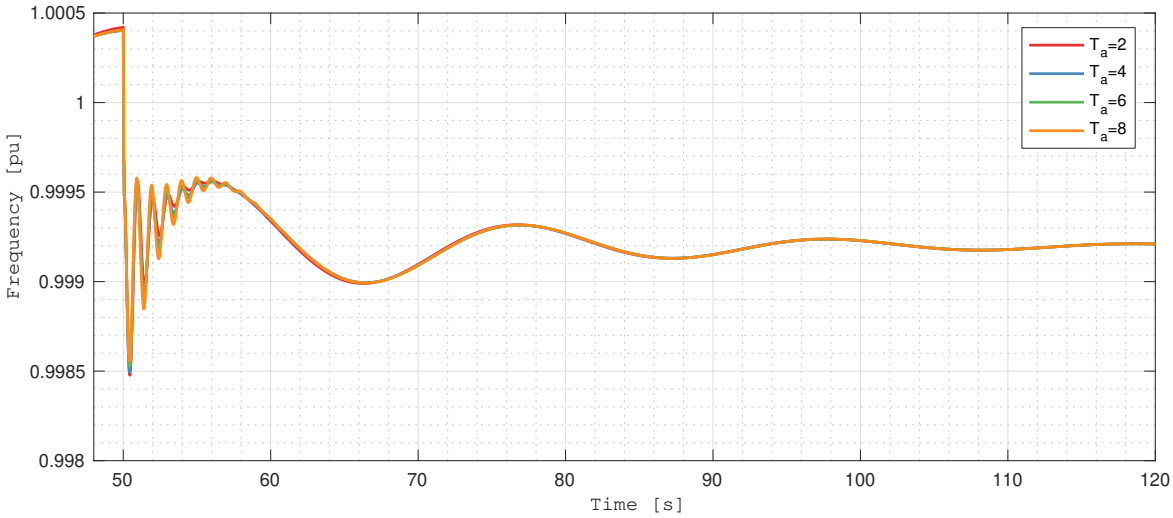

(b) Final

Figure 7.8: Grid frequency

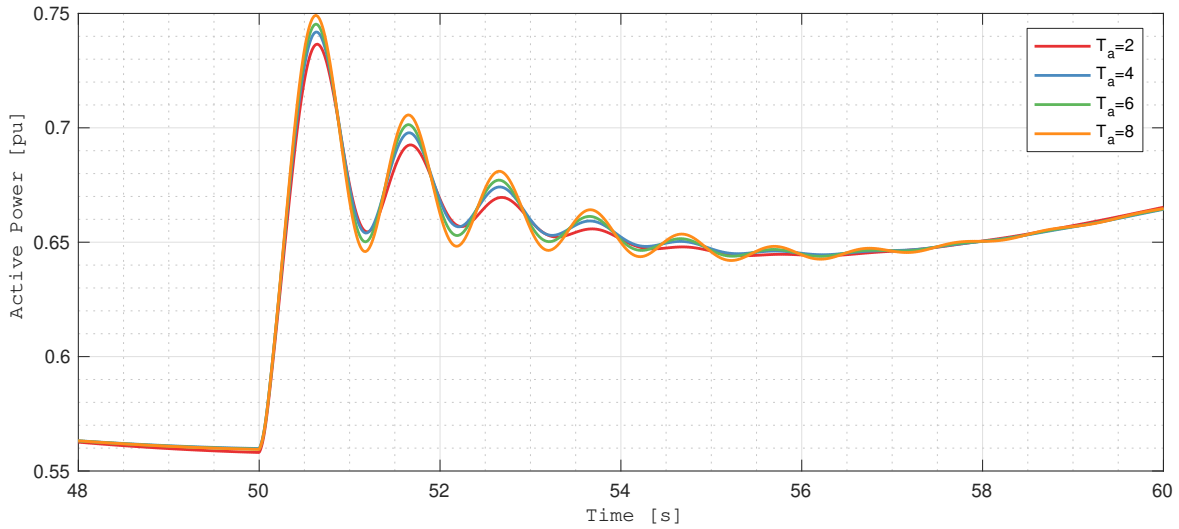

(a) Initial

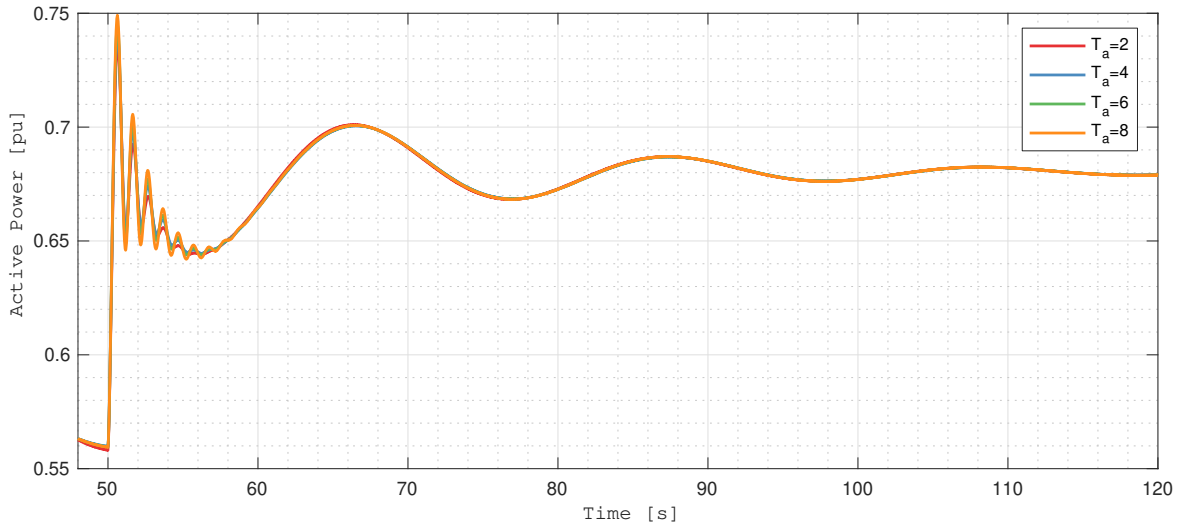

(b) Final

Figure 7.9: Active power delivered from the hydro-electric power plant

7.2.2 Damping Coefficient

Fig. 7.10 present the active power delivered from the VSM during the frequency event for different values of K_D. In the figure, it is clear that the VSM contribute to a significant amount of active power during the initial phase of the event. After the initial phase, the VSM stabilizes at a higher power output due to the droop mechanism in the VSM control. Comparing the result, increasing K_D causes the droop controller to be more aggressive, which is also clear from Eq. (6.3.18). For K_D=100, the frequency stabilizes at 0.994 pu, as observed in Fig. 7.11. Using Eq. (6.3.18), the increase in delivered active power for this deviation in

frequency can be calculated to be 0.08, i.e., from 0.6 to 0.68 pu. This can be observed in Fig. 7.10, which confirms that the damping coefficient represents the droop gain in steady-state operation.

It should be noted that the damping coefficient acts as a droop mechanism rather than as a damping in the system as discussed in the previous chapter. The effect of changing the damping coefficient in terms of system damping will be investigated in Case 2 in the next section.

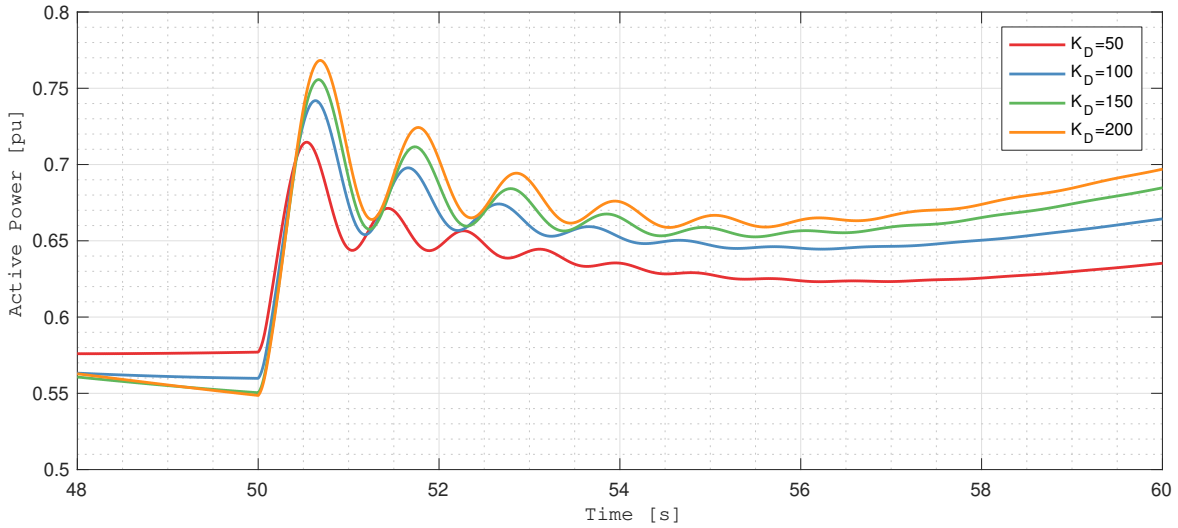

(a) Initial

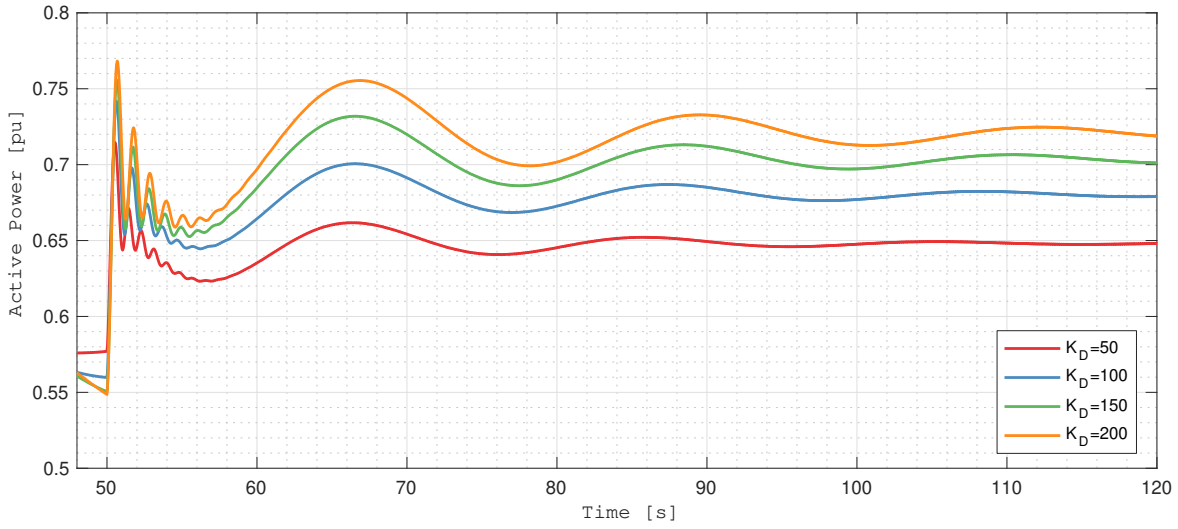

(b) Final

Figure 7.10: Active power delivered from the hydro-electric power plant

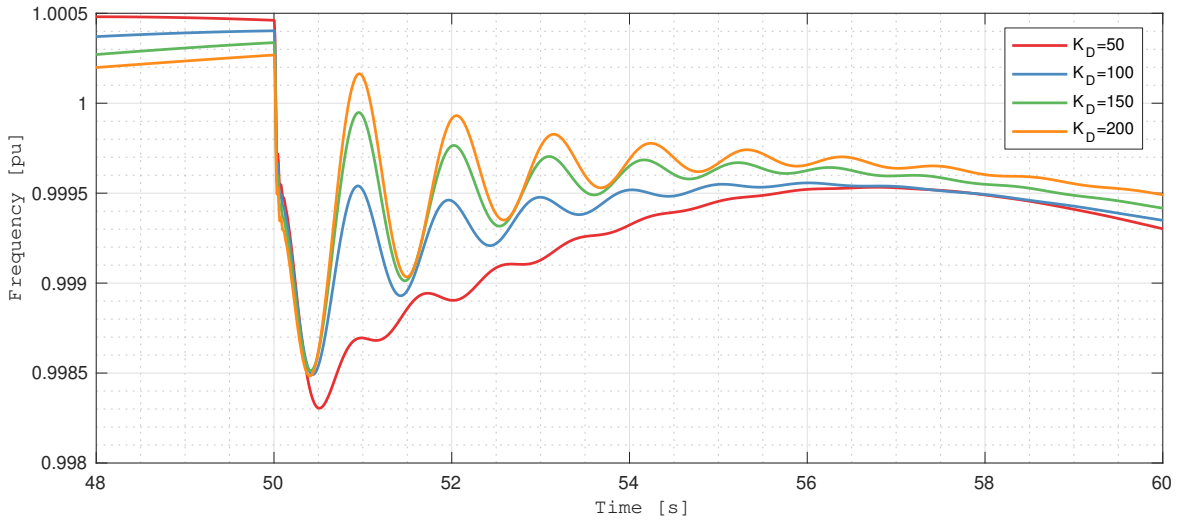

(a) Initial

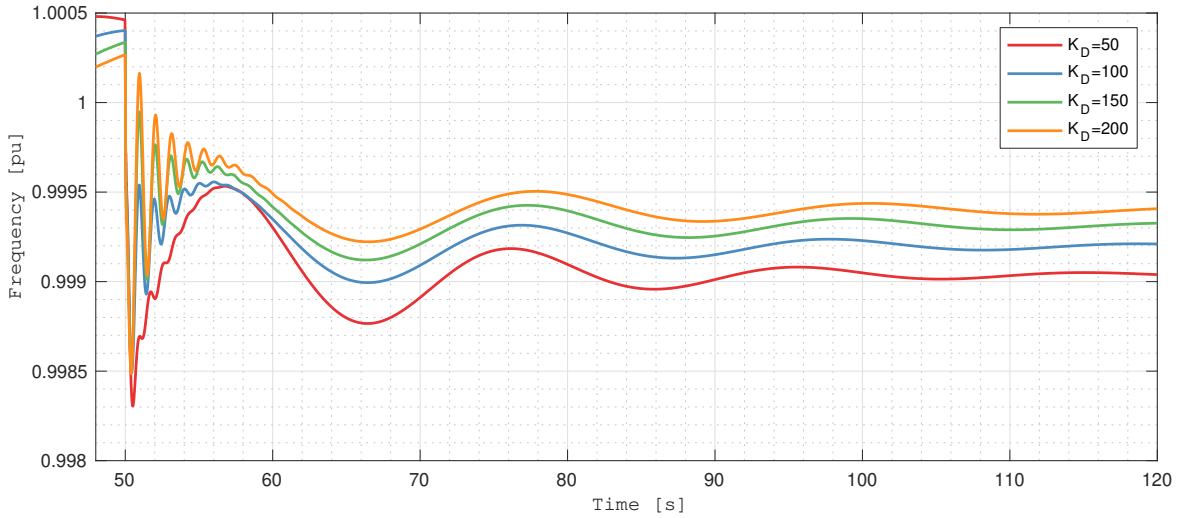

(b) Final

Figure 7.11: Grid frequency

Fig. 7.13 show the DC link voltage during the power imbalance event. It is clear that the DC link voltage controller on the MSC is fast enough to ensure that the DC link voltage is constant during transient events. Furthermore, it can be observed in Fig. 7.12 that the speed of the hydro-electric machine decelerates during the frequency event. This is expected as the governor in the plant respond slower than the VSM, and therefore it is not able to keep the speed constant as the VSM suddenly increase the power output.

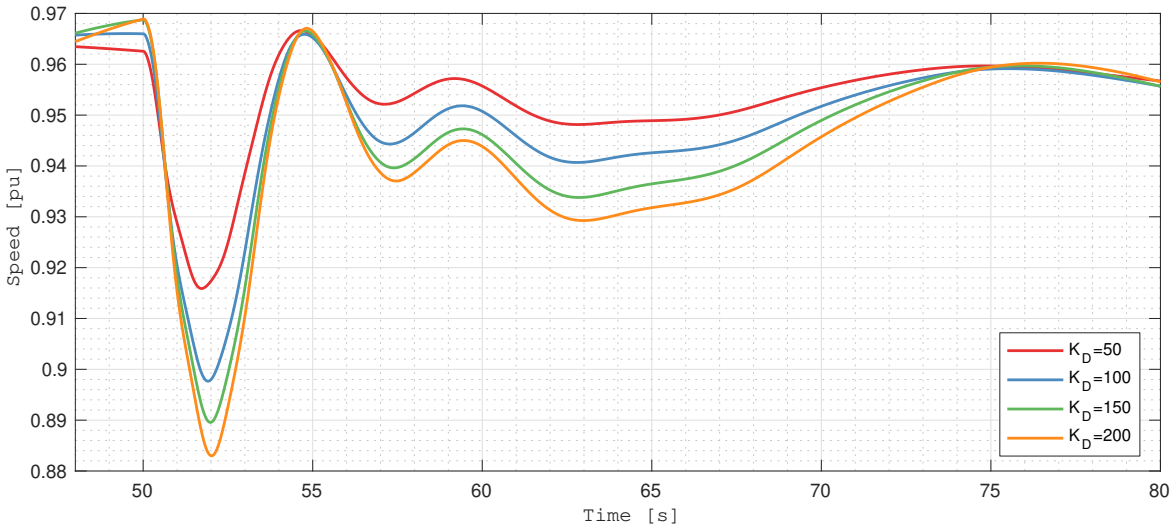

Figure 7.12: Hydro-electric synchronous machine speed (ω_m)

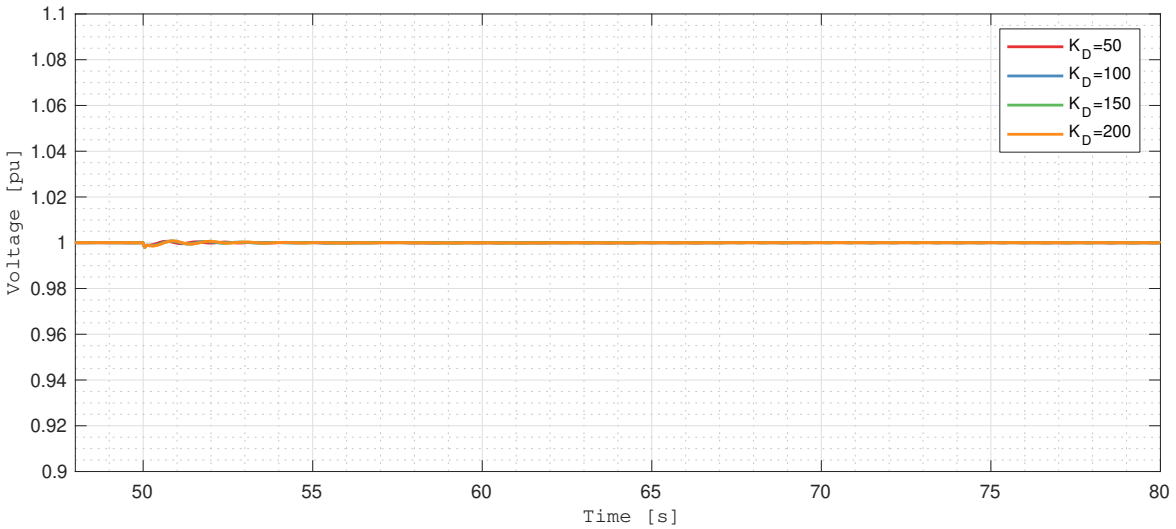

Figure 7.13: VSC DC link voltage (V_{dc})

7.3 Case Studies

7.3.1 Case 1: Comparison of VSM and Classical Torque Control

This case aims to compare the two control schemes under the same load disturbance as in the former sections. For the VSM control, K_D and T_a is chosen to be 100 and 4 respectively. The permanent droop gain in the governor for the classical torque control is chosen such that the system reaches the same steady-state level as the VSM. This is done such that the two control schemes can be compared on the same basis. The result labeled "No Inertia Support" is identical to the classical torque control without the inertia support.

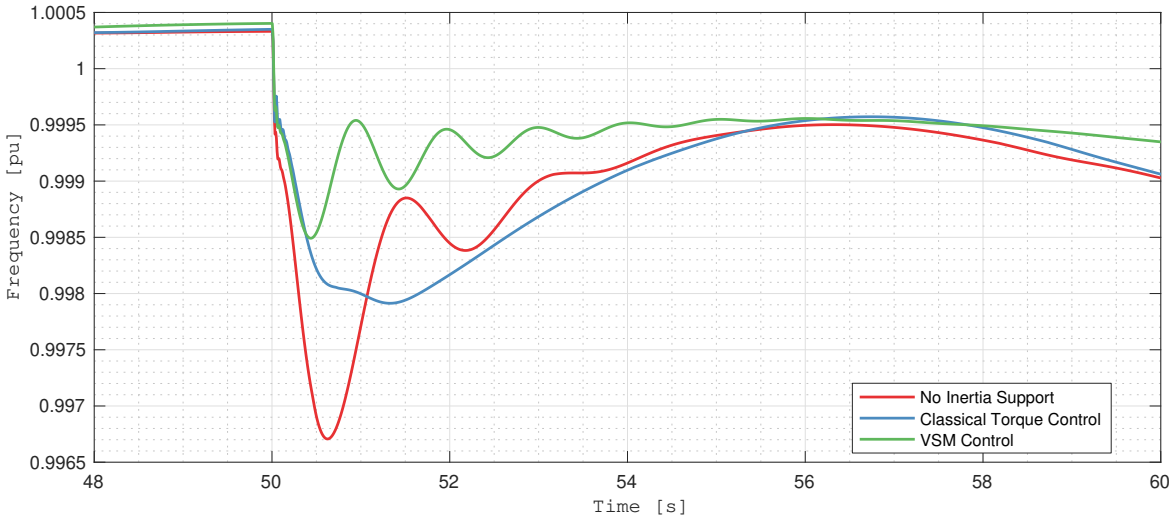

(a) Initial

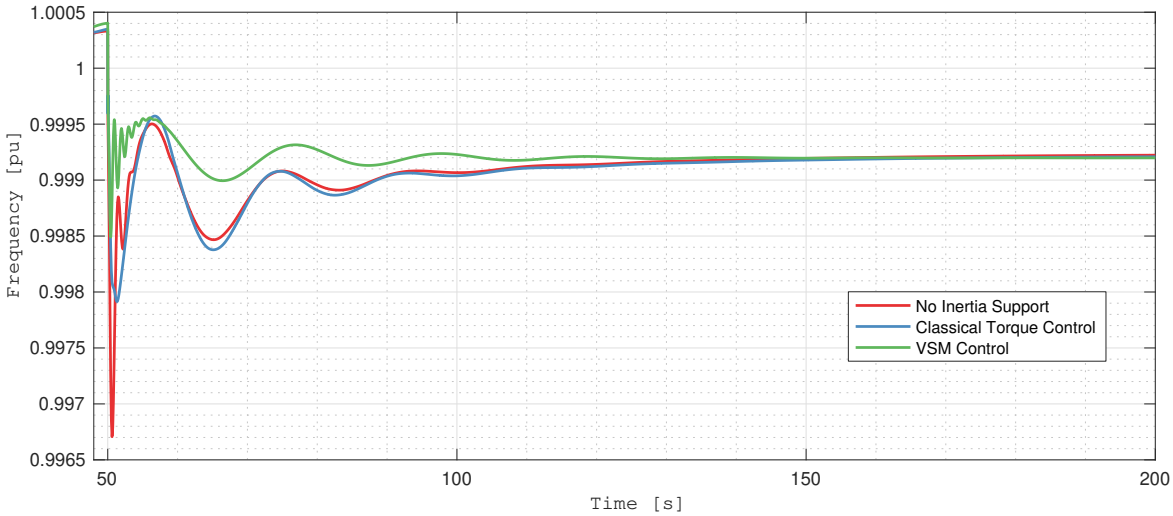

(b) Final

Figure 7.14: Grid frequency

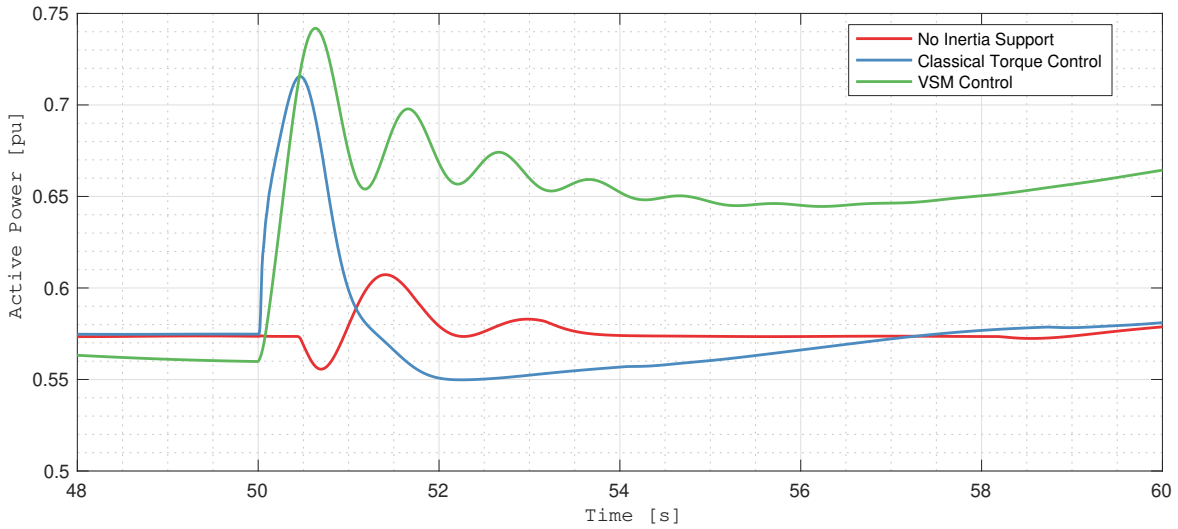

(a) Initial

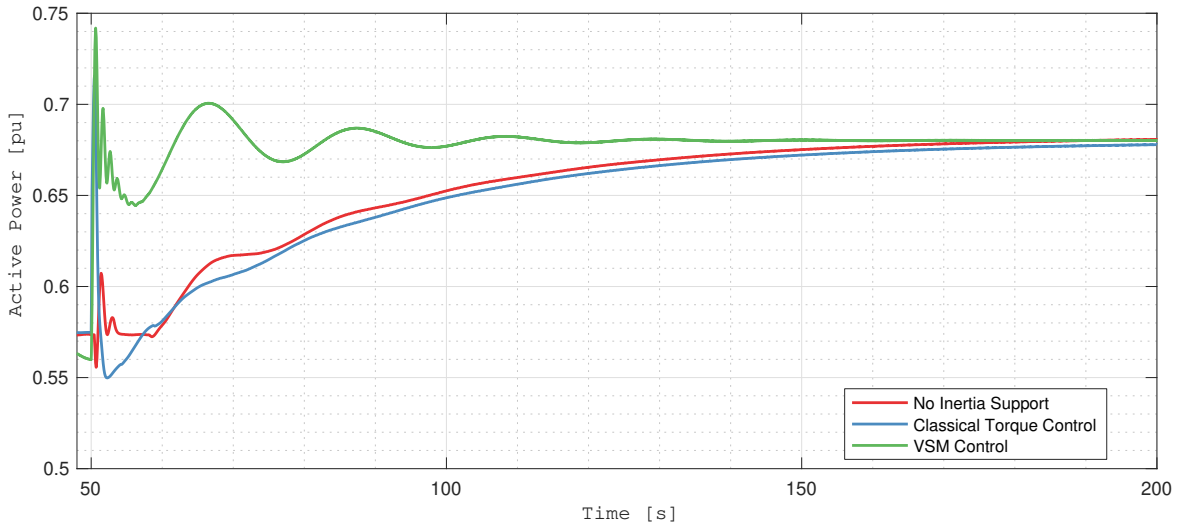

(b) Final

Figure 7.15: Active power delivered from the hydro-electric power plant

Fig. 7.14 shows the frequency behavior during this disturbance, both the initial and until it reaches steady-state. Compared to classical torque control, VSM control has an improved frequency nadir and reaches steady-state frequency faster. This can also be observed in Fig. 7.15, where the injected power is presented. As observed in the figure, the VSM respond fast and stabilizes at a higher power immediately after the disturbance. The inertia controller for the classical torque control respond similarly to the VSM, however, the primary frequency control is much slower. The reason for this is that the primary frequency control is regulated by the governor, which is a slow controller consisting of mechanical valves and gates. The result is a worse frequency nadir for the classical torque control compared to the VSM. However,

the frequency nadir is significantly improved compared to not having inertia controllers.

For the classical torque control with supplementary inertia control, the frequency nadir is improved from 0.9967 pu to 0.9979 pu compared to no inertia support. This corresponds to an improvement of 36.4% based on the steady-state frequency deviation[1]. Similarly, for the VSM control, the frequency nadir is improved from 0.9967 pu to 0.9985 pu compared to no inertia support. This corresponds to an improvement of 54.5% based on the steady-state frequency deviation.

Comparing the ROCOF, the initial value is equal for both inertia emulation methods and without inertia support. However, during the frequency descent, both inertia controllers improve the ROCOF, as can be observed in Fig. 7.15. The improvement on the initial ROCOF seems to be equal for both inertia emulation methods.

As can be observed in the figure, the VSM causes more oscillation during the initial phase of the event. This can could be improved by implementing the damping using a PLL, as discussed earlier. However, the oscillations are limited and are not causing any instabilities in the system. The classical torque control seems to reduce the initial oscillation compared to the case without inertia support. However, the amplitude of the oscillation towards steady-state operation is higher for the classical torque control compared to VSM control.

7.3.2 Case 2: Comparison of VSM and SM

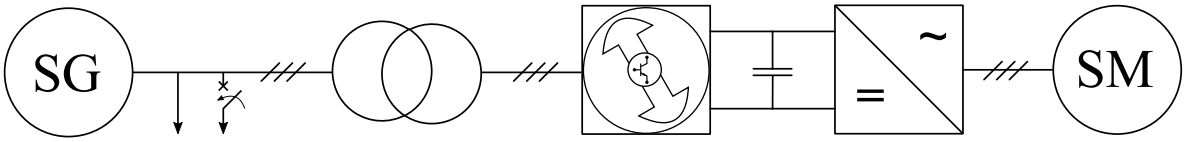

(a) System with VSM control simulated in MATLAB®/Simulink

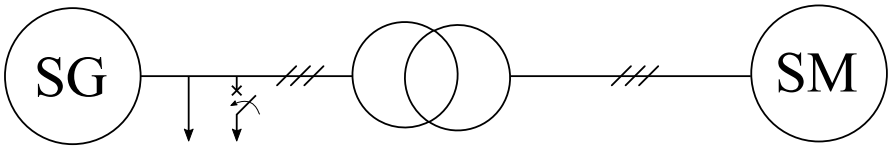

(b) System with a SM simulated in PowerFactory®

Figure 7.16: Topology of system simulated in MATLAB®/Simulink and PowerFactory®

The concept of VSM is to resemble the dynamics of a synchronous machine. This case aims to compare the dynamic operation of the VSM to an equivalent SM using the two systems shown in Fig. 7.16. The first figure illustrates the system with VSM control which has been used for the previous cases. In the second system, the converter-fed hydro-electric power plant is

[1]Calculated using $(\Delta f_{original} - \Delta f_{improved})/\Delta f_{original}$

replaced with a single synchronous machine which is equivalent to the VSM. This system is simulated using PowerFactory® as it is possible to set the damping coefficient K_D directly. The VSM control which is implemented in this thesis focus only on the mechanical system, and it is, therefore, the mechanical system which will be investigated in this case. To do this, the effect of changing the inertia time constant and damping factor can be studied.

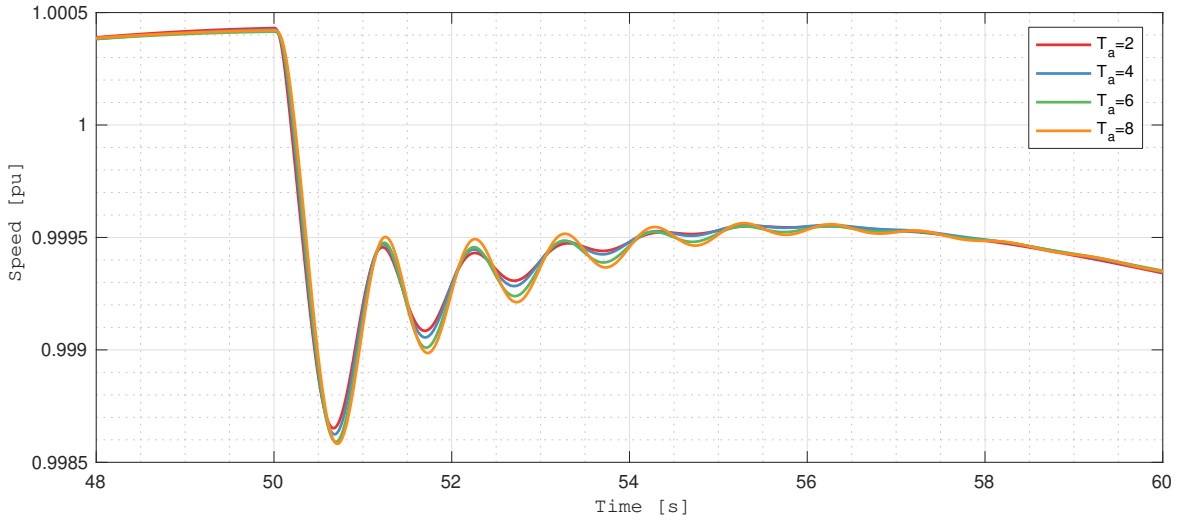

(a) VSM speed (ω_T) from MATLAB/Simulink®

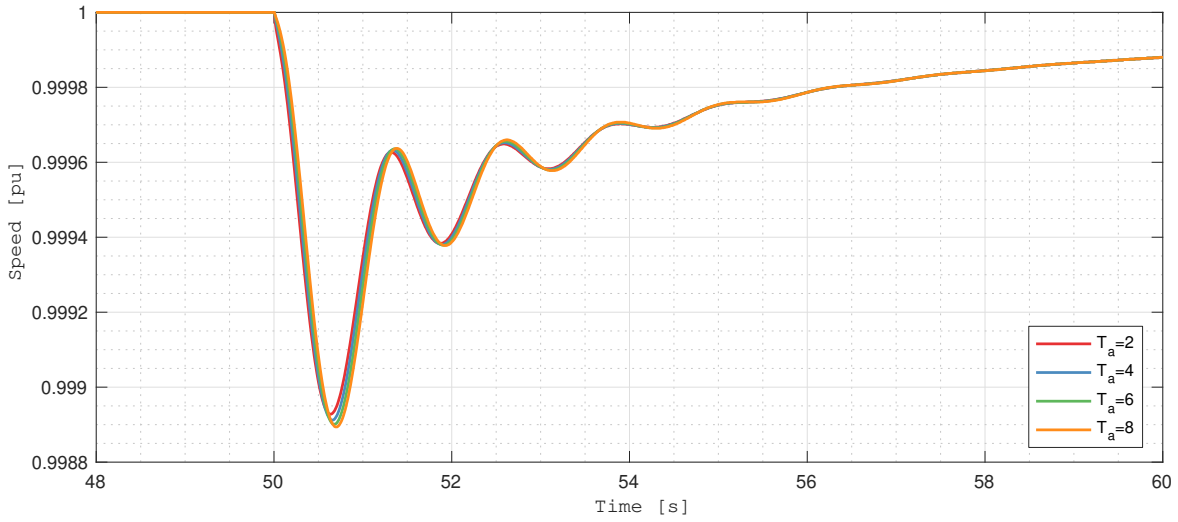

(b) SM speed from PowerFactory®

Figure 7.17: VSM/SM speed for different values of T_a

From Eq. (6.3.17), it is expected that increasing the inertia constant will reduce the damping and frequency of oscillation. The reduced damping can be observed in Fig. 7.17a, however, the change in frequency is difficult to observe. Running the same simulations in PowerFactory® with a SM instead of a VSM show similar results, as shown in Fig. 7.17b.

This suggests that the inertia time constant in the VSM work as intended.

Increasing the damping coefficient K_D is expected to increase the damping factor (ζ) according to Eq. (6.3.17). This is clear in the simulation of a SM in Fig. 7.18c, where increasing the damping coefficient increases the damping. However, this is not necessarily the case for the VSM since the damping coefficient here functions as a power droop. As discussed in Section 6.3.2, to obtain damping in the same manner as a grid-connected machine the reference speed in the controller needs to be measured using a synchronization method such as a PLL. Using a PLL as shown Fig. 6.7, results in the VSM speed presented in Fig. 7.18b for various values of K_D. As observed in the figure, this method gives similar results as the SM from PowerFactory®. This shows that a VSM can contribute to damping in a similar fashion as a grid-connected SM.

Note that the steady-state response from PowerFactory® and MATLAB®/Simulink is not equal since it is not feasible to get the same governor setting in the two cases. The power in the VSM is based on a simple droop control while a hydro governor and turbine drives the SM.

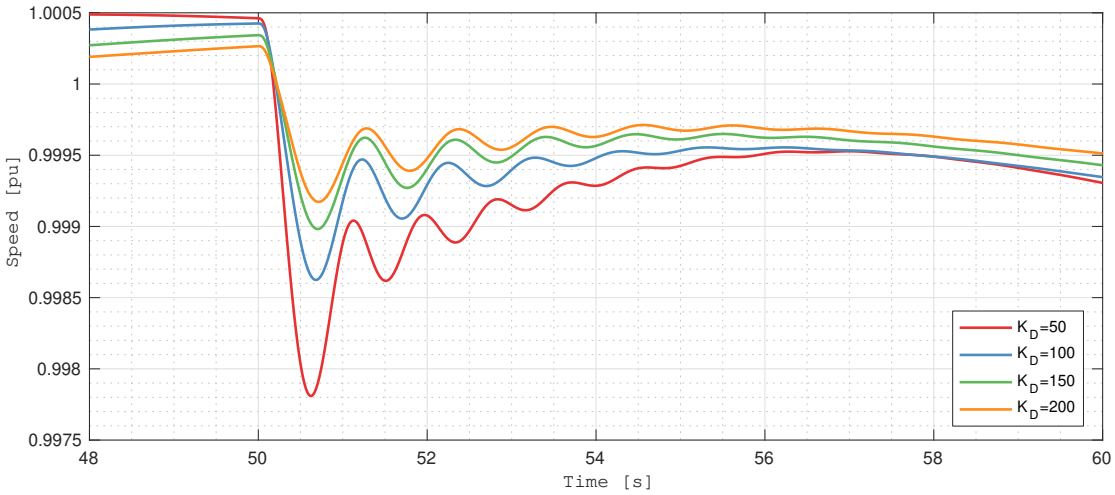

(a) VSM speed (ω_T) from MATLAB/Simulink® (without PLL)

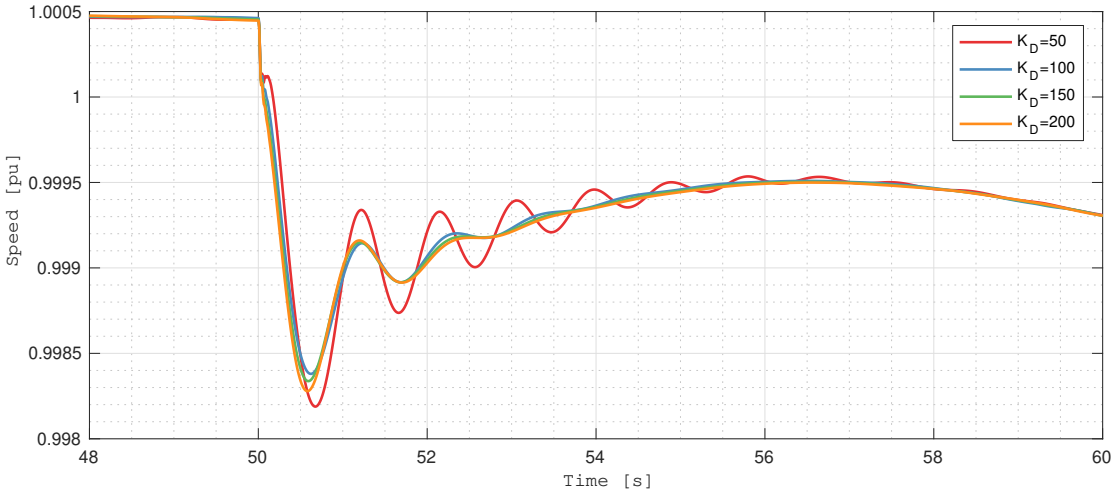

(b) VSM speed (ω_T) from MATLAB/Simulink® (with PLL)

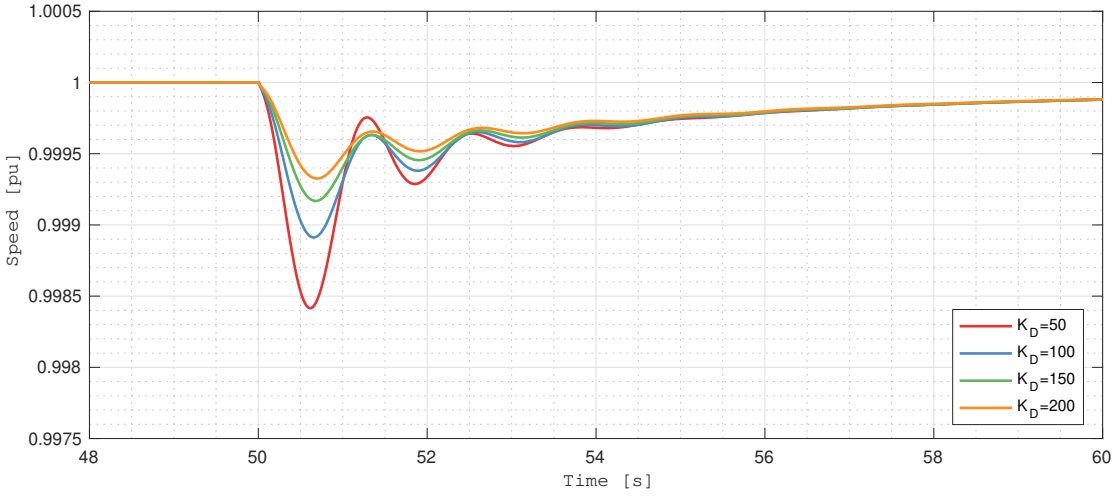

(c) SM speed from PowerFactory®

Figure 7.18: VSM/SM speed for different values of K_D

Fig. 7.19 shows swinging between the grid synchronous machine and the virtual synchronous machine. This is typical for a system with multiple synchronous machines, often termed local mode oscillations [27]. In Fig. 7.20, the same swinging can be observed between the machines from simulation in PowerFactory®. This indicates that the VSM acts similar to a grid-connected SM.

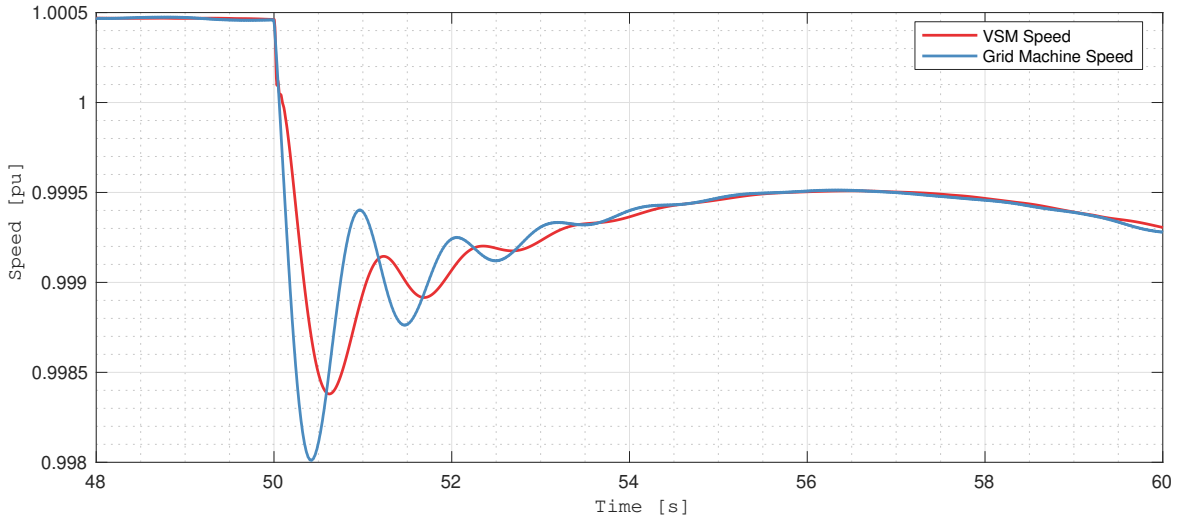

Figure 7.19: VSM and grid machine speed from MATLAB®/Simulink

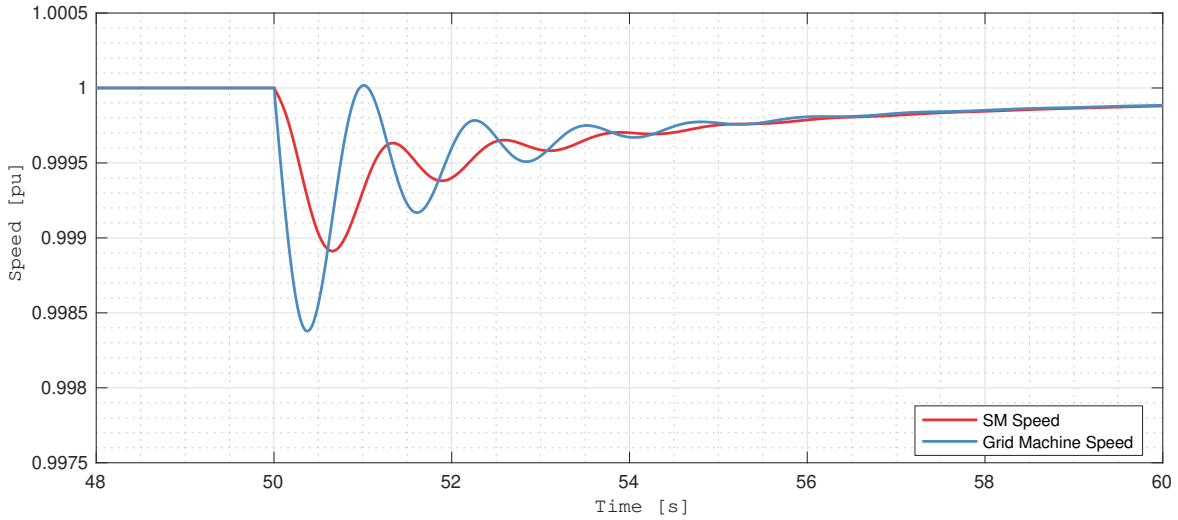

Figure 7.20: SM and grid machine speed from PowerFactory®

As discussed in Section 3.3.2, other VSM models includes a more detailed model of a SM with a mechanical and electrical part. For detailed models of a VSM, many of the advantages listed in Section 3.1 can be accurately emulated. However, some restrictions will apply such

as the amount of short circuit current a VSM can supply due to converter current limits.

7.3.3 Case 3: Dynamic Inertia from a VSM

Since the inertia time constant in a VSM is set in the controller, it can be changed during operation. By doing that, the amount of synthetic inertia in the system can be adjusted depending on the system status. This can, for instance, be beneficial to improve the small-signal stability. During normal grid operation, it is desirable to have a large inertia time constant to ensure a robust grid resilient to changes. However, after a load imbalance the large inertia worsen the small-signal stability, i.e. it leads to more oscillation, as observed in Section 7.2.1. This can also be observed in Eq. (6.3.17), where increased inertia leads to less damping in the system.

In this case, the mechanical time constant (T_a) is reduced after the load imbalance. This is achieved by setting a step on the inertia time constant as the frequency reaches the initial nadir in the frequency event. In an actual implementation, this should be implemented as an autonomous controller.

The frequency event is the same as described in the introduction to this chapter, i.e., a load is connected at 50 seconds. The mechanical time constant (T_a) is set to 10 seconds (which corresponds to an inertia time constant (H) of 5 seconds). Fig. 7.21 show the frequency for various steps from T_a=10 to 5 and 0.5. From the figure, it can be observed that reducing the inertia after the load imbalance can reduce the oscillation in grid frequency while maintaining the same frequency nadir. Similar to the frequency, from the delivered power shown in Fig. 7.22 it can be observed that the oscillation reduces when the inertia time constant is stepped to a lower value.

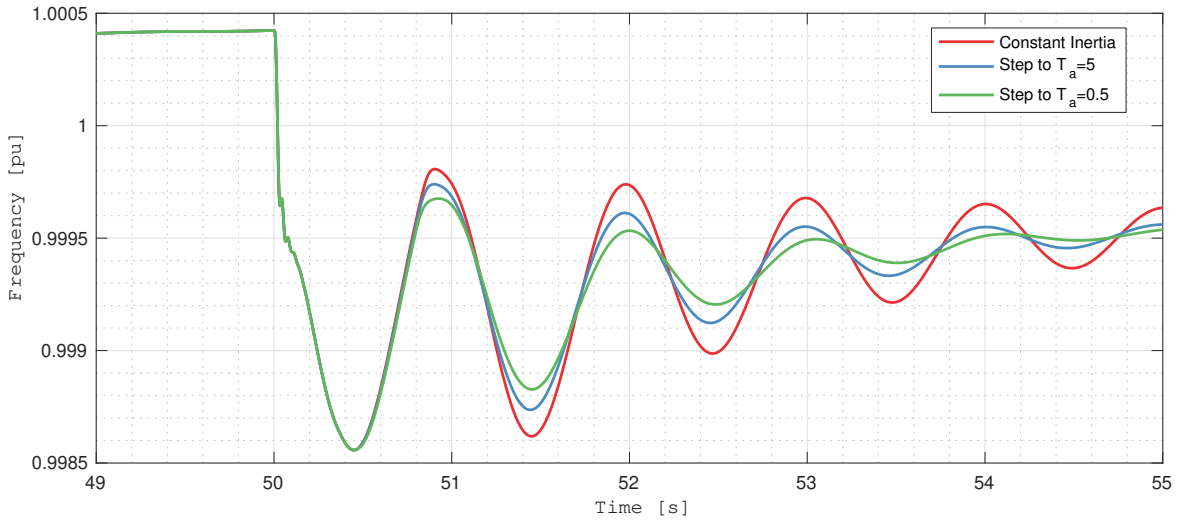

Figure 7.21: Grid Frequency

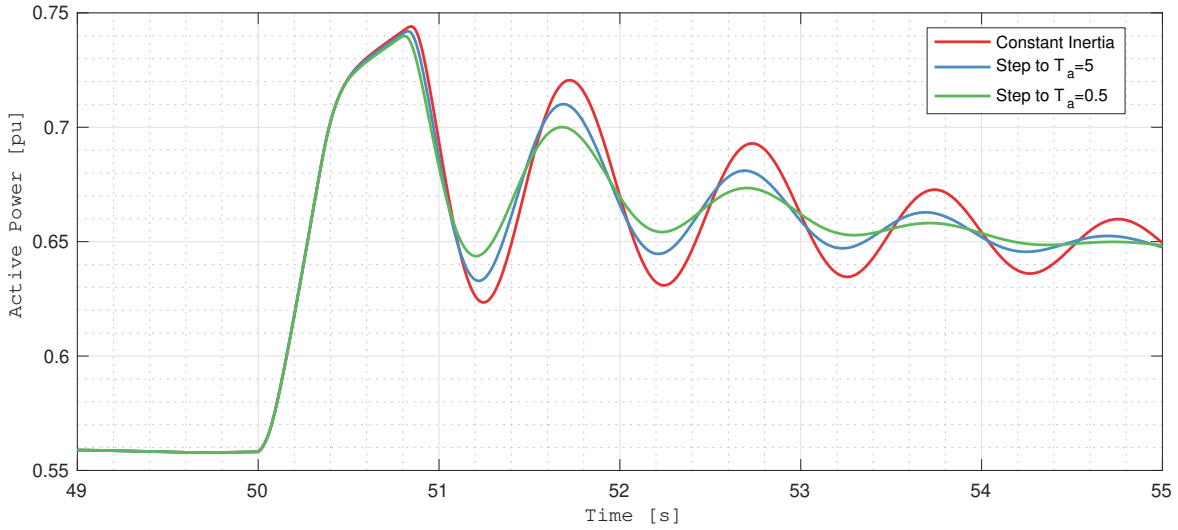

Figure 7.22: Active power delivered from the hydro-electric power plant

As shown in this case, implementing dynamic inertia support gives damping in the system, which is especially vital in weak AC grids. As seen in the results above, the inertia time constant can be changed during operation to improve the small-signal stability. In principle, the total amount of synthetic inertia can be controlled accurately such that the best system performance is achieved for any given situation. To benefit from this, the inertia time constant can be set to a large value during steady-state operation to maintain a robust grid resilient to changes. While in load events, the time constant can be reduced such that the small-signal stability is improved.

7.4 Evaluation of Results

The case studies conducted on the simulation models show that the implemented inertia controllers perform as intended. Both models accomplish to emulate inertia by controlling short-termed power delivered to the grid. By adjusting the various gains, the amount of inertia support can be varied to achieve different performance.

The two methods differ significantly in structure and control method. The supplementary inertia controllers worked satisfactory, presenting a way to enable inertia from a generic control structure. However, the VSM control method proved to be even better due to fast active power response. Another favorable feature of the VSM is setting the inertia time constant directly enables the possibility of controlling the amount of synthetic inertia during operation. This can also be performed by adjusting the gains in the supplementary inertia controllers. However, the implementation would be more difficult as the inertia time constant cannot be set directly as with the VSM. The classical torque control with supplementary inertia controllers does, however, make for an overall less complicated implementation compared to the VSM.

A significant difference between the two methods was the speed of the power controller. Since the governor controlled the primary controller in the classical model, the power controller acted significantly slower compared to the VSM method. However, the drawback for the VSM method is slower control of the machine speed. This might be problematic for various purposes where fast and accurate speed control is essential, such as MMPT to find the best speed for a given head. In the end, the allocation of control responsibility is a question of prioritization, where the governor controls the variable with the lowest prioritization. The slow response of the governor during the initial phase of the load event might be improved by adjusting the transient droop. However, a large transient droop with a long resetting time is often required for stable operation due to the mechanics in a hydropower plant [27]. The effect of changing the transient droop was therefore not investigated in this report.

As shown in this chapter, the amount of inertia support can be regulated by adjusting the various parameters. By doing this, it is possible to regulate the amount of synthetic inertia in the system by merely tuning the controllers differently. The synthetic inertia support from a converter-fed machine of a given size can, therefore, exceed the natural inertia support from a grid-connected machine of the same size. However, the cost of this is that the converter-fed machine uses more power during the initial phase of the load imbalance. This power needs to be restored after the imbalance, which can worsen the response after the frequency nadir. Synthetic inertia also has physical weaknesses since it is not a natural process. Instead, its implemented in a control system. This makes it more fragile to failure since the converter

with the control system consists of a complex architecture with many components.

As seen in the last case, the amount of synthetic inertia in the system can be regulated during operation. This enables the VSM to adjust the amount of inertia to obtain the best system performance for a given situation. In the last case, it is shown that changing the inertia during a load event improved the small-signal stability. This was taken advantage of by setting the inertia large during steady-state to improve frequency stability while reducing the inertia during the transient to strengthen small-signal stability. Doing this, damping in the system could be achieved by merely implementing dynamic inertia.

Except for Case 2, the simulation of the VSM was based on a model without a PLL. As discussed earlier, the damping coefficient acts as a droop when the PLL is removed. Since inertia support was the primary investigation of this report, this does not affect the results significantly. However, removing the damping can make the system less stable, especially in weak grids where the frequency deviates considerably from the nominal frequency. In larger more robust grids, such as the Nordic power system, it might be sufficient to use the method without a PLL. The advantage would be a more straightforward implementation due to the removal of the PLL. Besides, in the last case, it was shown that damping could be achieved by merely implementing dynamic inertia. This way, the damping could still be obtained even though the damping is not implemented as a damping coefficient.

7.5 Inertial Support Constraints

The most obvious constraint for the inertia support is the amount of available energy. In the simulations, it was assumed that the machine operated at nominal speed when the load imbalance occurred. However, the adjustable speed unit might operate at a lower speed, which leads to less available kinetic energy. Also, the machine might have a limit to the amount of speed decrease which is possible. This limit will determine the amount of inertia support available and can vary dependent on the restriction of the plant.

Fast deceleration of the machine can also lead to increased mechanical stress on both the machine and the turbine. This can reduce the lifetime of the machine and increase service cost. This is undesired, and additional restriction on the speed decrease might be necessary to take increased mechanical stress into account.

Regarding the electrical equipment, there are also some constraints related to their ratings. A short-term increase in power causes a fast increase in current and voltages, which can be problematic. Fast rise/fall of current and voltage can damage semiconductor devices and other electrical components such as the capacitor. For the plant to deliver more short-termed power than the rating of the power plant, the converter needs to be overrated (rated more than the

machine). This is not a feasible solution as converters at these power levels are expensive. Another solution is to modify the inertia controllers such that the power output never exceeds the rated power. However, this will limit the amount of inertia support available, depending on how much power the plant is delivering at the time of the power imbalance. If the plant runs at full capacity, it would not be capable of supporting the grid with synthetic inertia.

Chapter 8

Conclusion

8.1 Summary and Concluding Remarks

This work contributes to research on inertia support from converter-fed synchronous machines in hydro-electric power plants. Simulation models of a converter-fed hydropower plant connected to a grid have been established. Two separate models have been developed. The first model investigates inertia support using supplementary controllers added on a classical torque control scheme. The other model investigates a method often termed virtual synchronous machine control, where the converter mimics the operation of a synchronous machine. The overall goal has been to derive and test these control methods during a load imbalance in a weak AC grid.

The implemented inertia emulation for the classical torque control works as intended. By changing the gains in the inertia controller, it was observed that the amount of inertia support was changed. It was also observed that increasing the gains beyond a certain level caused problems, such as conflict with the primary controller and too large speed deviations. Using the method in a load imbalance situation, the frequency nadir improved from 0.9967 pu to 0.9979 pu compared to no inertia support. This corresponds to an improvement of 36.4% based on the steady-state frequency deviation. The method also improved initial ROCOF and reduced oscillation in frequency.

The implemented VSM control method also works as intended. It was observed how the different parameters in the control system changed the performance of the system. By varying these parameters, it was observed that the amount of synthetic inertia and damping in the system could be changed. In the load imbalance case, the frequency nadir improved from 0.9967 pu to 0.9985 pu compared to no inertia support. This corresponds to an improvement of 54.5% based on the steady-state frequency deviation. Also, the VSM control method made

it possible to control the inertia time constant during operation, which in this thesis was labeled dynamic inertia. Doing this, better performance was achieved as the inertia was set high during steady-state to improve frequency stability and reduced after the load event to achieve improved small-signal stability.

Comparing the two methods, it was found that the VSM method was superior in the context of inertia support due to fast power control. In the classical torque model, the converter only controlled the short-term power response. The steady state power was controlled by the governor, which is significantly slower. The result was a more seamless response with the VSM.

8.2 Recommendations for Future Work

8.2.1 Laboratory Work

In the initial phase of working on this thesis, the possibility for a laboratory setup was investigated. A number of challenges arose, mostly related to lack of equipment. Fig. 8.1 present two different suggested laboratory setups which could be used to test the methods derived in this thesis. The first is a full-scale system where both control methods can be investigated. The synchronous machine in the plant can be driven by a motor which should mimic the behavior of a hydro turbine. The other method is a simplified version where the hydro-electric power plant is replaced by a converter connected to a DC source. In this case, only the VSM method would be possible to investigate since the dynamics in the hydropower plant is neglected.

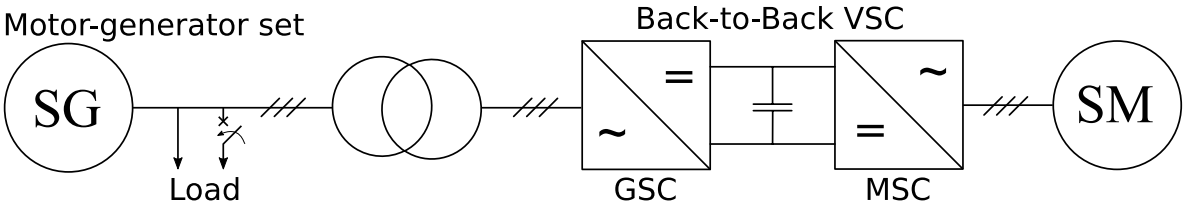

(a) Full-scale system

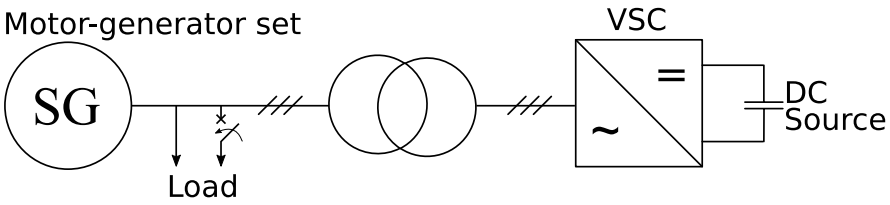

(b) Simplified setup for analysis of VSM

Figure 8.1: Suggested laboratory setups

The grid can be represented by a synchronous machine driven by a mechanical power source such as in the simulation. In Fig. 8.1, it is suggested to use a synchronous machine driven by a DC motor. Such a setup is present at the National Smart Grid Laboratory at NTNU, and the control system needed to get it operating is under development [47].

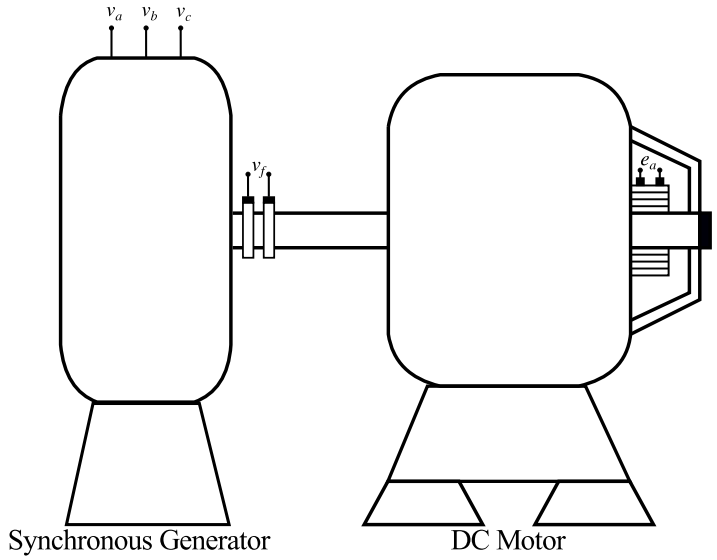

Figure 8.2: Motor-generator set suggested for grid representation

The results from laboratory experiments can be compared with the results from the thesis, verifying the methods and concepts derived. The challenge is, however, to establish a realistic small-scale system which is comparable to the large-scale system used in this report.

8.2.2 Simulation Model

This report was limited to investigate the importance of synthetic inertia on frequency stability, with some investigation on small-signal stability. However, more in-depth research on other stability issues should be performed. The last case investigates solutions related to improving small-signal stability using dynamic inertia in a VSM. This is a research area with little existing studies. However, the results obtained in this thesis indicate a potential, which would be interesting to investigate further.

As discussed previously, the VSM model used in this thesis contains only the mechanical parts of a synchronous machine. This model can be further developed to include a higher-order model with an electrical part. With a focus on inertia support, it would be interesting to compare different order models of a VSM. Another development which can be done to further investigate the VSM model with a PLL. In this way, the damping of the system can be more thoroughly analyzed.

A further development on the classical torque control would be to change the control responsibilities such that the GSC controls the active power. This would make for an interesting comparison to the VSM control as the power controller has the same potential since both methods control active power using the GSC. The suggested power control is shown in Fig. 8.3. The power reference should be determined similarly as the VSM power droop to get the same steady-state response. Supplementary inertia controllers can be added to this setup to enable inertia emulation.

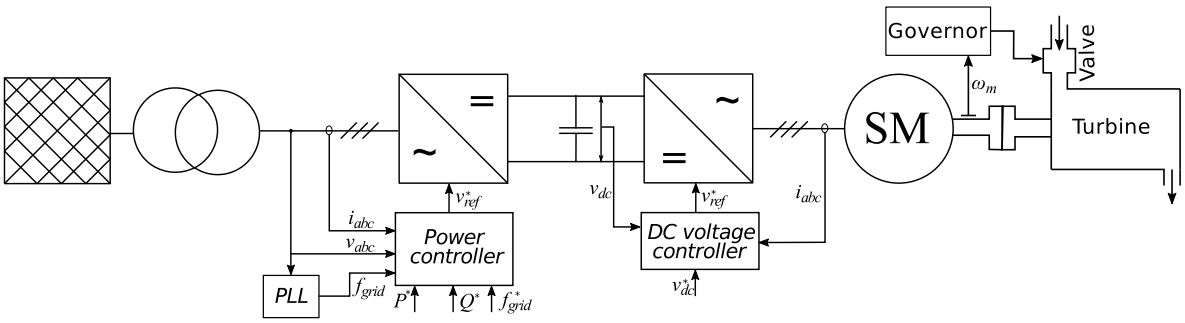

Figure 8.3: Suggested control setup

Table 8.1: Comparison of control responsibilities for suggested methods

Method	**GSC**	**MSC**	**Governor**
Classical torque control	DC link voltage	Machine speed	Active power
VSM control	DC link voltage	Machine speed	Active power

Bibliography

[1] Vera Silva, Miguel Lopez-Botet-Zulueta, and Ye Wang. Impact of high penetration of variable renewable generation on frequency dynamics in the continental Europe interconnected system. *IET Renewable Power Generation*, 2016.

[2] CIRED. Smart Grids on the Distribution Level – Hype or Vision? CIRED's point of view Final Report Members of the Working Group. 2013.

[3] Bradford P Roberts and Chet Sandberg. The Role of Energy Storage in Development of Smart Grids. *Proc. IEEE*, 2011.

[4] Tracy Lane Bill Girling, Hans-Willhelm Schiffer, Nnamdi Ibeanu Corina Radu, and Et. Al. *World Energy Resources: Hydropower*. World Energy Council, 2016.

[5] JA Suul, Kjetil Uhlen, and Tore Undeland. Variable speed pumped storage hydropower for integration of wind energy in isolated grids: case description and control strategies. *Nordic Workshop on Power and Industrial Electronics*, 2008.

[6] Jürgen Bublitz. Position Paper on Energy Efficiency - the Role of Power Electronics. Technical Report March, 2007.

[7] Salvatore D'Arco, Jon Are Suul, and Olav B. Fosso. A Virtual Synchronous Machine implementation for distributed control of power converters in SmartGrids. *Electric Power Systems Research*, 2015.

[8] Michael Manwaring, Debbie Mursch, and Kelly Tilford. Challenges and Opportunities For New Pumped Storage Development. Technical Report 5, National Hydropower Association, 2013.

[9] Mostafa Valavi and Arne Nysveen. Variable-Speed Operation of Hydropower Plants : Past , Present , and Future. *2016 XXII International Conference on Electrical Machines (ICEM)*, 2016.

[10] J Janning and A Schwery. Next generation variable speed pump-storage power stations. *13th European Conference on Power Electronics and Applications*, 2009.

[11] Peter K. Steimer, Osman Senturk, Steve Aubert, and Stefan Linder. Converter-fed synchronous machine for pumped hydro storage plants. *IEEE Energy Conversion Congress and Exposition (ECCE)*, 2014.

[12] Thomas Hildinger and Ludger Ködding. Modern Design for Variable Speed Motor-Generators. In *Enhanching existing hydropowerplant facilities*, Grenoble, 2014. Voith.

[13] C. Bueno and J. A. Carta. Wind powered pumped hydro storage systems, a means of increasing the penetration of renewable energy in the Canary Islands. *Renewable and Sustainable Energy Reviews*, 2006.

[14] Takao Kuwabara, Akira Shibuya, Hideo Furuta, Eizou Kita, and Keiichi Mitsuhashi. Design and dynamic response characteristics of 400 MW adjustable speed pumped storage unit for Ohkawachi Power Station. *IEEE Transactions on Energy Conversion*, 11(2), 1996.

[15] Chao Yang, Xiaobo Yang, and Yao Chen. Integration of variable speed hydropower generation and VSC HVDC. *17th European Conference on Power Electronics and Applications, EPE-ECCE Europe*, 2015.

[16] H. Schlunegger. Pumping efficiency: A 100 MW converter for the Grimsel 2 pumped storage plan, 2014.

[17] H. Schlunegger and A. Thöni. 100 MW full-size converter in the Grimsel 2 pumped-storage plant, 2013.

[18] Kalyan Kumar. Power System Stability and Control. Technical report, Indian Institute of Technology Madras, Chennai.

[19] Prabha Kundur, John Paserba, Venkat Ajjarapu, Göran Andersson, Anjan Bose, Thierry Van Cutsem, Claudio Canizares, Nikos Hatziargyriou, David Hill, Vijay Vittal, Alex Stankovic, and Carson Taylor. Definition and Classification of Power System Stability. *IEEE Transactions on Power Systems*, 19, 2004.

[20] Erik Ørum, Minna Laasonen, and Et al. Future System Inertia. Technical report, European Network of Transmission System Operators for Electricity Contents (ENTSO-E), 2015.

[21] Beate Nesje. The need for Inertia in the Nordic Power System. Master's thesis, Norwegian University of Science and Technology, 2015.

[22] Statnett. Om Reservemarkeder, Accessed 20.03.2018. URL `http://www.statnett.no/Kraftsystemet/Markedsinformasjon/`.

[23] Jan Machowski, Janusz W. Bialek, and James R. Bumby. *Power System Dynamics: Stability and Control*. Wiley, 2 edition, 2008.

[24] Ned Mohan. *First Course on Power Systems*. MNPERE, 1 edition, 2006.

[25] Yong Chen, Ralf Hesse, Dirk Turschner, and Hans Peter Beck. Investigation of the virtual synchronous machine in the island mode. *IEEE PES Innovative Smart Grid Technologies Conference Europe*, 2012.

[26] A.E. Fitzgerald, C. Kingsley Jr., and S.D. Umans. *Electric Machinery*. McGraw-Hill, 5 edition, 1992.

[27] Prabha Kundur. *Power System Stability and Control*. McGraw-Hill Education, 1 edition, 1994.

[28] Ned Mohan. *Electric Machines and Drives: A First Course*. John Wiley & Sons, 2012.

[29] J.B. Ekanayake, N. Jenkins, and G. Strbac. Frequency Response from Wind Turbines. *Wind Engineering*, 32, 2008.

[30] N. Jenkins O. Anaya-Lara, F.M. Hughes and G. Strbac. Contribution of DFIG-based wind farms to power system short-term frequency regulation. *IEE Proceedings-Generation, Transmission and Distribution*, 153, 2006.

[31] Lei Shang, Jiabing Hu, Xiaoming Yuan, and Yongning Chi. Understanding inertial response of variable-speed wind turbines by defined internal potential vector. *Energies*, 10, 2017.

[32] Olimpo Anaya-Lara, David Campos-Gaona, Edgar Moreno-Goyita, and Grain Adam. *Offshore Wind Energy Generation: Control, Protection, and Integration to Electrical Systems*. John Wiley & Son, New Delhi, India, 1 edition, 2014.

[33] Salvatore D'Arco, Jon Are Suul, and Olav B. Fosso. Control system tuning and stability analysis of Virtual Synchronous Machines. *2013 IEEE Energy Conversion Congress and Exposition, ECCE 2013*, 2013.

[34] Yi Wang, Jianhui Meng, Xiangyu Zhang, and Lie Xu. Control of PMSG-Based Wind Turbines for System Inertial Response and Power Oscillation Damping. *IEEE Transactions on Sustainable Energy*, 6, 2015.

[35] Z. Wu, X. Wang, W. Gao, M. Kang, M. Hwang, Y. Kang, V. Gevorgian, and E. Muljadi. Frequency support of PMSG-WTG based on improved inertial control. *IEEE Power and Energy Society General Meeting*, 2016.

[36] Hans Peter Beck and Ralf Hesse. Virtual synchronous machine. *9th International Conference on Electrical Power Quality and Utilisation, EPQU*, 2007.

[37] Salvatore D'Arco and Jon Are Suul. Virtual synchronous machines - Classification of implementations and analysis of equivalence to droop controllers for microgrids. *IEEE Grenoble Conference PowerTech*, 2013.

[38] Hasan Alrajhi Alsiraji and Ramadan El-Shatshat. Comprehensive assessment of virtual synchronous machine based voltage source converter controllers. *IET Generation, Transmission & Distribution*, 11, 2017.

[39] Yong Chen, Ralf Hesse, Dirk Turschner, and Hans-Peter Beck. Dynamic Properties of the Virtual Synchronous Machine (VISMA). *Renewable Energies and Power Quality Journal*, 1(9), 2011.

[40] Ralf Hesse, Dirk Turschner, and Hans-peter Beck. Micro grid stabilization using the Virtual Synchronous Machine (VISMA). *Proceedings of the International Conference on Renewable Energies and Power Quality (ICREPQ'09)*, 2009.

[41] Shuthakini Pulendran and Joseph Euzebe Tate. Hysteresis control of voltage source converters for synchronous machine emulation. *15th International Power Electronics and Motion Control Conference (EPE/PEMC)*, 2012.

[42] M. P.N. Van Wesenbeeck, S. W.H. De Haan, P. Varela, and K. Visscher. Grid tied converter with virtual kinetic storage. *IEEE Bucharest PowerTech: Innovative Ideas Toward the Electrical Grid of the Future*, 2009.

[43] Frequency-droops Converter-based Microgrids, Salvatore D Arco, and Jon Are Suul. Equivalence of Virtual Synchronous Machines and. 5, 2014.

[44] G. Delille, B. François, and G. Malarange. Dynamic frequency control support by energy storage to reduce the impact of wind and solar generation on isolated power system's inertia. *IEEE Transactions on Sustainable Energy*, 3, 2012.

[45] Bo Zhang, Xiangwu Yan, Dongxue Li, Xueyuan Zhang, Jinzuo Han, and Xiangning Xiao. Stable Operation and Small-Signal Analysis of Multiple Parallel DG Inverters Based on a Virtual Synchronous Generator Scheme. *Energies*, 11, 2018.

[46] Yong Chen, Ralf Hesse, Dirk Turschner, and Hans-peter Beck. Comparison of methods for implementing virtual synchronous machine on inverters. *In International Conference on Renewable Energies and Power Quality*, 1, 2012.

[47] Trond Toftevaag. Personal communication, 2018.

[48] Steve Auber. Power on tap from variable speed pumped water storage scheme. *Energize*, (July), 2012.

[49] Magnar Hernes, Kjell Ljøkelsøy, Tormod Kleppa, and Olve Mo. Average model of PWM converter. Trondheim, 2003. SINTEF Energy Research.

[50] Ned Mohan. *Advanced Electric Drives: Analysis, Control, and Modeling Using MATLAB / Simulink*. John Wiley & Sons, Hoboken, New Jersey, 2014.

[51] K Smriti Rao and Ravi Mishra. Comparative study of P, PI and PID controller for speed control of VSI-fed induction motor. *International Journal of Engineering Development and Research*, 2, 2014.

[52] M. Pavella and P. G. Murthy. *Transient Stability of Power Systems: Theory and Practice*. John Wiley & Sons, Chichester, 1 edition, 1994.

[53] C. Bajracharya, M. Marta, S. Are, and T. Undeland. Understanding of tuning techniques of converter controllers for VSC-HVDC. *Proceedings of the Nordic Workshop on Power and Industrial Electronics*, 2008.

[54] Ned Mohan, Tore M. Undeland, and William P. Robbins. *Power Electronics Converters, Applications, and Design*. Wiley, 3 edition, 2003.

[55] E Hendawi, F Khater, and A Shaltout. Analysis, Simulation and Implementation of Space Vector Pulse Width Modulation Inverter. *Aee '10: Proceedings of the 9th Wseas International Conference on Applications of Electrical Engineering*, 2010.

[56] R. Vilanova, V. M. Alfaro, O. Arrieta, and C. Pedret. Analysis of the claimed robustness for PI/PID robust tuning rules. *18th Mediterranean Conference on Control and Automation, MED'10 - Conference Proceedings*, (July), 2010.

[57] J. A. Suul, M. Molinas, L. Norum, and T. Undeland. Tuning of Control Loops for Grid Connected Voltage Source Converters. *2nd IEEE International Conference on Power and Energy*, (PECon 08), 2008.

[58] Han Wee Low. Control of Grid Connected Active Converter. Master's thesis, Norwegian University of Science and Technology, Trondheim, 2013.

[59] Mahdi Ashabani and Yasser Abdel-Rady. Integrating VSCs to Weak Grids by Nonlinear Power Damping Controller Capability. 2014.

[60] Uros Markovic, Petros Aristidou, and Gabriela Hug. Virtual Induction Machine Strategy for Converters in Power Systems with Low Rotational Inertia. *10th Bulk Power Systems Dynamics and Control Symposium*, 2017.

[61] Qing Chang Zhong, Phi-Long PL Nguyen, Zhenyu Ma, and Wanxing Sheng. Self-synchronised Synchronverters: Inverters without a Dedicated Synchronisation Unit. *IEEE Transactions on Power Electronics*, 29, 2014.

[62] Duncan Glover, Mulukutla Sarma, and Thomas Overbye. *Power System Analysis & Design*, volume 53. Cengage Learning, 5 edition, 2012.

[63] Jens G. Balchen, Trond Andresen, and Bjarne A. Foss. *Reguleringsteknikk*. Department of Engineering Cybernetics, NTNU, 5 edition, 2003.

[64] Chandra Bajracharya. Control of VSC-HVDC for wind power. Master's thesis, Norwegian University of Science and Technology, Trondheim, 2008.

Appendix A

Identities and Deduction

A.1 Park Transformation

The voltage invariant Park transformation when the rotating frame is aligned with the a-axis is given as [27]:

$$\begin{bmatrix} u_d \\ u_q \\ u_0 \end{bmatrix} = \frac{2}{3} \begin{bmatrix} \cos(\omega t) & \cos\left(\omega t - \frac{2\pi}{3}\right) & \cos\left(\omega t + \frac{2\pi}{3}\right) \\ -\sin(\omega t) & -\sin\left(\omega t - \frac{2\pi}{3}\right) & -\sin\left(\omega t + \frac{2\pi}{3}\right) \\ \frac{1}{2} & \frac{1}{2} & \frac{1}{2} \end{bmatrix} \begin{bmatrix} u_a \\ u_b \\ u_c \end{bmatrix} \tag{A.1}$$

Inverse transformation is given by [27]:

$$\begin{bmatrix} u_a \\ u_b \\ u_c \end{bmatrix} = \frac{2}{3} \begin{bmatrix} \cos(\omega t) & -\sin(\omega t) & 1 \\ \cos\left(\omega t - \frac{2\pi}{3}\right) & -\sin\left(\omega t - \frac{2\pi}{3}\right) & 1 \\ \cos\left(\omega t + \frac{2\pi}{3}\right) & -\sin\left(\omega t + \frac{2\pi}{3}\right) & 1 \end{bmatrix} \begin{bmatrix} u_d \\ u_q \\ u_0 \end{bmatrix} \tag{A.2}$$

The voltage invariant Park transformation when the rotating frame is 90 degrees behind a-axis is given as [27]:

$$\begin{bmatrix} u_d \\ u_q \\ u_0 \end{bmatrix} = \frac{2}{3} \begin{bmatrix} \sin(\omega t) & \sin\left(\omega t - \frac{2\pi}{3}\right) & \sin\left(\omega t + \frac{2\pi}{3}\right) \\ \cos(\omega t) & \cos\left(\omega t - \frac{2\pi}{3}\right) & \cos\left(\omega t + \frac{2\pi}{3}\right) \\ \frac{1}{2} & \frac{1}{2} & \frac{1}{2} \end{bmatrix} \begin{bmatrix} u_a \\ u_b \\ u_c \end{bmatrix} \tag{A.3}$$

Inverse transformation is given by [27]:

$$\begin{bmatrix} u_a \\ u_b \\ u_c \end{bmatrix} = \frac{2}{3} \begin{bmatrix} \sin(\omega t) & \cos(\omega t) & 1 \\ \sin\left(\omega t - \frac{2\pi}{3}\right) & \cos\left(\omega t - \frac{2\pi}{3}\right) & 1 \\ \sin\left(\omega t + \frac{2\pi}{3}\right) & \cos\left(\omega t + \frac{2\pi}{3}\right) & 1 \end{bmatrix} \begin{bmatrix} u_d \\ u_q \\ u_0 \end{bmatrix} \tag{A.4}$$

A.2 Taylor Series Expansion

Consider a general function f_i with the given evolution of state x_i:

$$\frac{dx_i}{dt} = f_i(x_1, ..., x_n, u_1, ..., u_m) \tag{A.1}$$

In order to linearize the non-linear equation above Taylor Series expansion can be applied. Linerizing this equation around the equilibrium point $\bar{x}_1, ..., \bar{x}_n, \bar{u}_1, ..., \bar{u}_m$ yields [63]:

$$\frac{d\Delta x_i}{dt} = \sum_{j=1}^{n} \left.\frac{\partial f_i}{\partial x_j}\right|_{x_j=\bar{x}_j} \Delta x_j + \sum_{j=1}^{m} \left.\frac{\partial f_i}{\partial u_j}\right|_{u_j=\bar{u}_j} \Delta u_j \tag{A.2}$$

A.3 Power in dq-Reference Frame

The apparent power for the voltage invariant dq-frame can be expressed as:

$$\begin{aligned} S &= \frac{3}{2} v_{dq} i_{dq}^* \\ &= \frac{3}{2}(v_d + jv_q)(i_d - ji_q) \\ &= \frac{3}{2}(\underbrace{(v_d i_d + v_q i_q)}_{\mathbf{P}} + j\underbrace{(v_q i_d - v_d i_q)}_{\mathbf{Q}}) \end{aligned} \tag{A.1}$$

$$\begin{aligned} P &= \frac{3}{2}(v_d i_d + v_q i_q) \\ Q &= \frac{3}{2}(v_q i_d - v_d i_q) \end{aligned} \tag{A.2}$$

Since the d-axis is placed along the voltage vector, the q-axis voltage is equal to zero ($v_q = 0$). Using this, the above equations yields:

$$\begin{aligned} P &= \frac{3}{2} v_d i_d \\ Q &= -\frac{3}{2} v_d i_q \end{aligned} \tag{A.3}$$

A.4 Relation Between $\mathbf{V_{dc}}$ and $\mathbf{i_d}$

Neglecting converter losses, the relation between active power one the AC and DC-side is:

$$\frac{3}{2} v_d i_d = V_{dc} i_{dc} \tag{A.1}$$

Substituting Eq. (A.1) in Eq. (5.4.1b) yields:

$$C_{dc}\frac{dV_{dc}}{dt} = \frac{3}{2}\frac{v_d i_d}{V_{dc}} - i_L \tag{A.2}$$

Since this equation is non-linear, it needs to be linearized around a steady state operating point. Applying Taylor Series expansion as described in Appendix A.2 the following can be found:

$$C_{dc}\frac{d(\Delta V_{dc})}{dt} = \frac{3}{2}\frac{\bar{v}_d \Delta i_d}{V^*_{dc}} + \frac{3}{2}\frac{\bar{i}_d \Delta v_d}{V^*_{dc}} - \frac{3}{2}\frac{\bar{v}_d \bar{i}_d}{V^{*2}_{dc}}\Delta V_{dc} - \Delta i_L \tag{A.3}$$

Neglecting the disturbance i_L and focusing on the input i_d the equation above can be simplified to [64]:

$$C_{dc}\frac{d(\Delta V_{dc})}{dt} = \frac{3}{2}\frac{\bar{v}_d \Delta i_d}{V^*_{dc}} \tag{A.4}$$

A.5 Kinetic Energy Inertia Power

The swing equation can be written as:

$$\frac{P_{em} - P_m}{\omega_m} = J\frac{d\omega_m}{dt} \tag{A.1}$$

Since this equation is non-linear it needs to be linearized around a steady state operating point. Applying Taylor Series expansion as described in Appendix A.2 the following can be found:

$$J\frac{d\Delta\omega_m}{dt} = \frac{1}{\omega^*_m}\Delta P_{em} - \frac{1}{\omega^*_m}\Delta P_m - \frac{\bar{P}_{em}}{\omega^{*2}_m}\Delta\omega_m + \frac{\bar{P}_m}{\omega^{*2}_m}\Delta\omega_m \tag{A.2}$$

Assuming that P_m is constant during a short period of time ($\Delta P_m = 0$) and looking at P_{em} the following can be found:

$$J\frac{d\Delta\omega_m}{dt} = \frac{1}{\bar{\omega}_m}\Delta P_{em} \tag{A.3}$$

Which can be written as:

$$\Delta P_{em} = K\frac{d\Delta\omega_m}{dt} = K'\frac{d\Delta f}{dt} \tag{A.4}$$

Energy stored in the rotation can generally be expressed as:

$$E_{kin} = \frac{1}{2}J\omega_m^2 \tag{A.5}$$

The energy released for a given reduction in speed can be expressed as:

$$\Delta E_{kin} = -\frac{1}{2} J(\omega_m^2 - (\omega_m - \Delta\omega_m)^2) \tag{A.6}$$

Further, the derivative of both sides of the equation expresses the power released for a given reduction in speed:

$$\frac{\Delta E_{kin}}{dt} = \Delta P_{em} = -\frac{1}{2} J \frac{d}{dt}(\omega_m^2 - (\omega_m - \Delta\omega_m)^2) \tag{A.7}$$

Solving the equation above results in:

$$\Delta P_{em} = -\frac{1}{2} J(2\omega_m - 2(\omega_m - \Delta\omega_m)) \tag{A.8}$$

Which can be written as:

$$\Delta P_{em} = -J\Delta\omega_m \tag{A.9}$$

A.6 Capacitor Energy Inertia Power

Energy stored in a capacitor can generally be expressed as:

$$E_{dc} = \frac{1}{2} C_{dc} V_{dc}^2 \tag{A.1}$$

The energy released for a given reduction in voltage can be expressed as:

$$\Delta E_{dc} = \frac{1}{2} C_{dc}(V_{dc}^2 - (V_{dc} - \Delta V_{dc})^2) \tag{A.2}$$

Further, the derivative of both sides of the equation express the power released for a given reduction in speed:

$$\frac{\Delta E_{dc}}{dt} = \Delta P_{em} = \frac{1}{2} C_{dc} \frac{d}{dt}(V_{dc}^2 - (V_{dc} - \Delta V_{dc})^2) \tag{A.3}$$

Solving the equation above results in:

$$\Delta P_{em} = \frac{1}{2} C_{dc}(2V_{dc} - 2(V_{dc} - \Delta V_{dc})) \tag{A.4}$$

Which can be written as:

$$\Delta P_{em} = C_{dc}\Delta V_{dc} \tag{A.5}$$

Appendix B

Parameter Values

B.1 Hydro-Electric Power Plant

B.1.1 Synchronous Machine

Table B.1: Synchronous machine ratings

Machine parameter	**Rated Values**
Power	15 MVA/MW
Stator voltage (star connected)	11 kV
Inertia constant	2 s
Frequency	50 Hz

Table B.2: Synchronous machine reactances and time constants

Explanation	**Value**
d-axis transient short-circuit time constant	0.5 s
d-axis subtransient short-circuit time constant	0.02 s
q-axis subtransient short-circuit time constant	0.02 s
d-axis synchronous reactance	0.8 pu
q-axis synchronous reactance	0.5 pu
d-axis transient reactance	0.25 pu
q-axis transient reactance	0.5 pu
d-axis subtransient reactance	0.15 pu
q-axis subtransient reactance	0.16 pu
Stator leakage reactance	0.06 pu

Table B.3: Machine base values

Explanation	**Symbol**	**Base value**
Power (rated)	$S_{s,base}$	15 MVA
Frequency (rated)	f_n	50 Hz
Voltage (peak value of rated line to neutral voltage)	$V_{s,base}$	8981.5 V
Current (peak value of rated line current)	$I_{s,base}$	1113.4 A
Impedance	$Z_{s,base}$	8.06 Ω
Speed (electrical)	$\omega_{el,base}$	100π rad/s
Speed (mechanical)	$\omega_{m,base}$	104.7 rad/s
Inductance	$L_{s,base}$	0.0257 H
Torque	$T_{em,base}$	143 kNm

Table B.4: Governor and turbine parameter values

Parameter	**Symbol**	**Value**
Pilot valve and servomotor time constant	T_f	0.05 s
Governor Time Constant	T_r	8 s
Temporary Droop	R_t	0.2
Permanent Droop	R_p	0.06
Servo Time Constant	T_g	0.2 s
Water Time Constant	T_w	0.5 s
Minimum Gate Limit	G_{min}	0
Maximum Gate Limit	G_{max}	1
Servo gain	K_s	5
Maximum Gate Opening Rate	$R_{max,open}$	0.16 pu/s
Maximum Gate Closing Rate	$R_{max,close}$	0.16 pu/s

Table B.5: AVR PI-controller parameter values

Explanation	**Value**
Voltage loop proportional constant	0.1
Voltage loop integral constant	1
Current loop proportional constant	0.0955
Current loop integral constant	6.36

B.1.2 Converter and Line

Table B.6: Converter parameter values

Converter parameter	**Rated Values**
Power	15 MVA/MW
DC-link voltage	107.8 kV
Capacitor	77.5 μF
Machine-side voltage	11 kV
Grid-side voltage	66 kV

Table B.7: Current controllers parameter values (Classical torque control and VSM control)

Parameter	**Value**
$k_{I,pd}$	0.24
$k_{I,id}$	1.5
$k_{I,pq}$	0.24
$k_{I,iq}$	1.5
$k_{I,psd}$	8.1
$k_{I,isd}$	29
$k_{I,psq}$	8.1
$k_{I,isq}$	34

Table B.8: Voltage and speed controllers parameters (Classical torque control)

Parameter	**Value**
$k_{V,p}$	42.6
$k_{V,i}$	3.2
$k_{\omega,ps}$	363.5
$k_{\omega,is}$	12084

Table B.9: SRF voltage controller and DC link voltage controller (VSM control)

Parameter	**Value**
$k_{s,pd}$	0.023
$k_{s,id}$	10
$k_{s,pq}$	0.023
$k_{s,iq}$	10
$k_{V,p}$	42.6
$k_{V,i}$	3.2

Table B.10: Line parameter values

Explanation	**Value**
Converter inductance	0.0124 pu
Converter resistance	0.0025 pu
Line inductance	0.0074 pu
Line resistance	0.0012 pu

B.2 Grid

Table B.11: Synchronous machine ratings

Machine parameter	**Rated Values**
Power	120 MVA/MW
Stator voltage (star connected)	15 kV
Inertia constant	3 s
Frequency	50 Hz

Table B.12: Synchronous machine reactances and time constants

Explanation	**Value**
d-axis transient short-circuit time constant	0.5 s
d-axis subtransient short-circuit time constant	0.02 s
q-axis subtransient short-circuit time constant	0.02 s
d-axis synchronous reactance	0.8 pu
q-axis synchronous reactance	0.5 pu
d-axis transient reactance	0.25 pu
q-axis transient reactance	0.5 pu
d-axis subtransient reactance	0.15 pu
q-axis subtransient reactance	0.16 pu
Stator leakage reactance	0.06 pu

Table B.13: Load 1

Explanation	**Rated Value**
Power	60 MW
Voltage	15 kV

Table B.14: Load 2

Explanation	**Rated Value**
Power	5 MW
Voltage	15 kV

Appendix C

Simulation Models

In this appendix, the simulation models implemented in MATLAB®/Simulink is presented. In all the models, discrete blocks and a discrete solver are used with a sampling time of 0.002 seconds. For the physical part of the simulation (electrical and mechanical system), the Simscape Power System library is used. The machine in the hydro-electric power plant is modeled using the built-in model *Synchronous Machine Salient Poled (standard)*. Similarly, the grid machine is modeled using *Synchronous Machine Model 2.1 (fundamental)*.

C.1 Hydro-Electric Power Plant

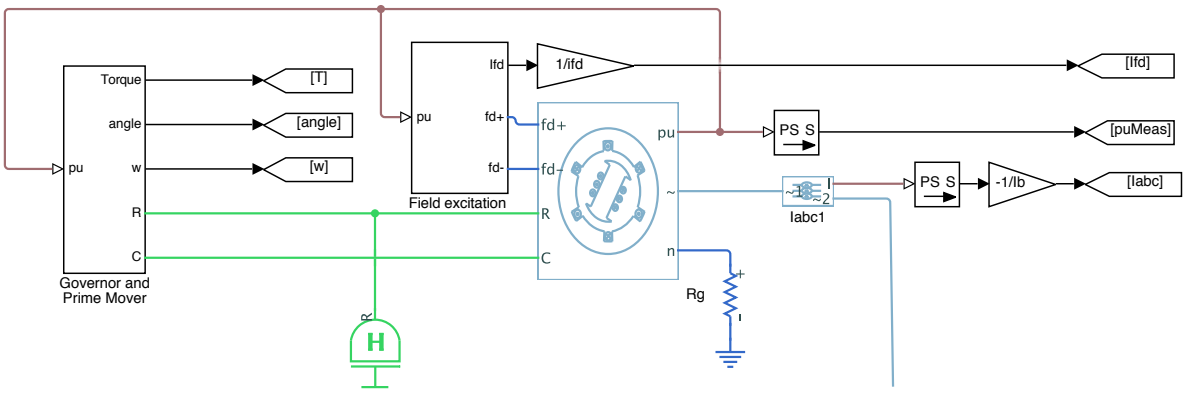

Figure C.1: Synchronous machine with measurements, excitation, governor and turbine

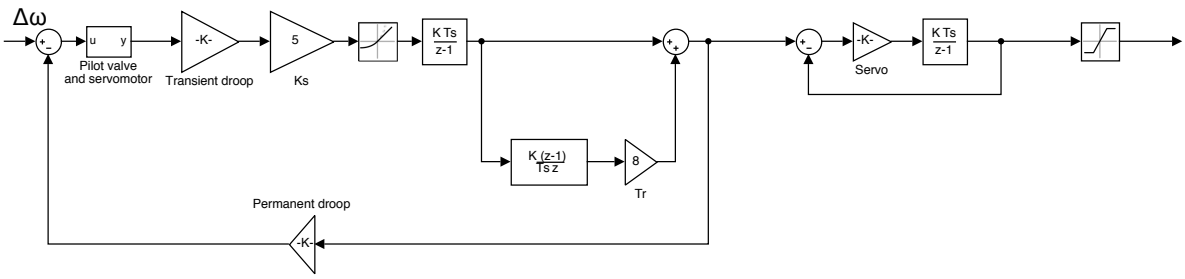

Figure C.2: Governor

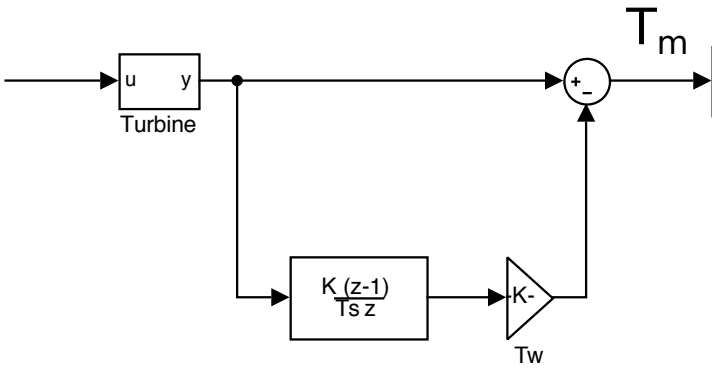

Figure C.3: Turbine

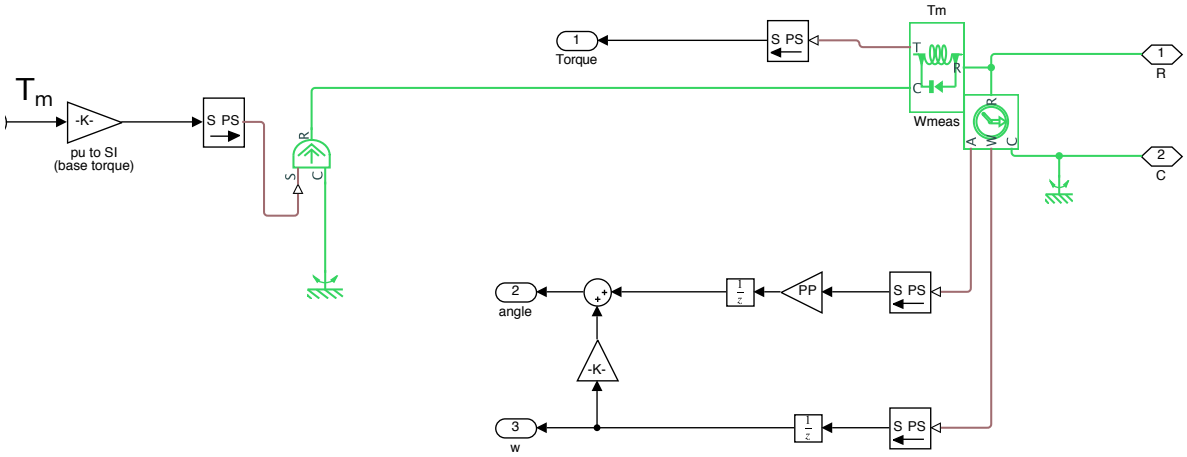

Figure C.4: Conversion to physical system after turbine

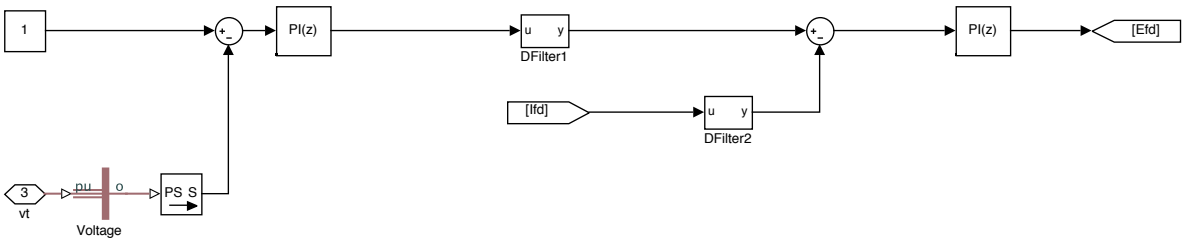

Figure C.5: AVR

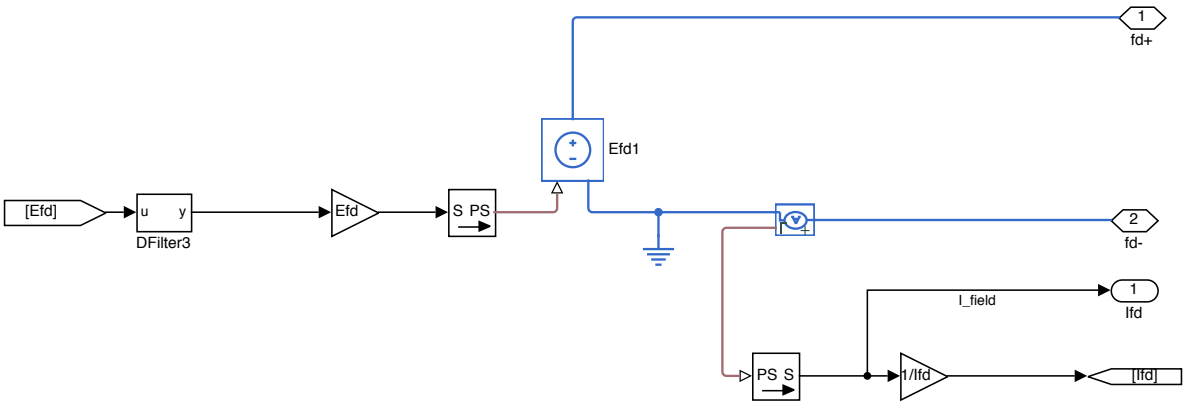

Figure C.6: Exciter

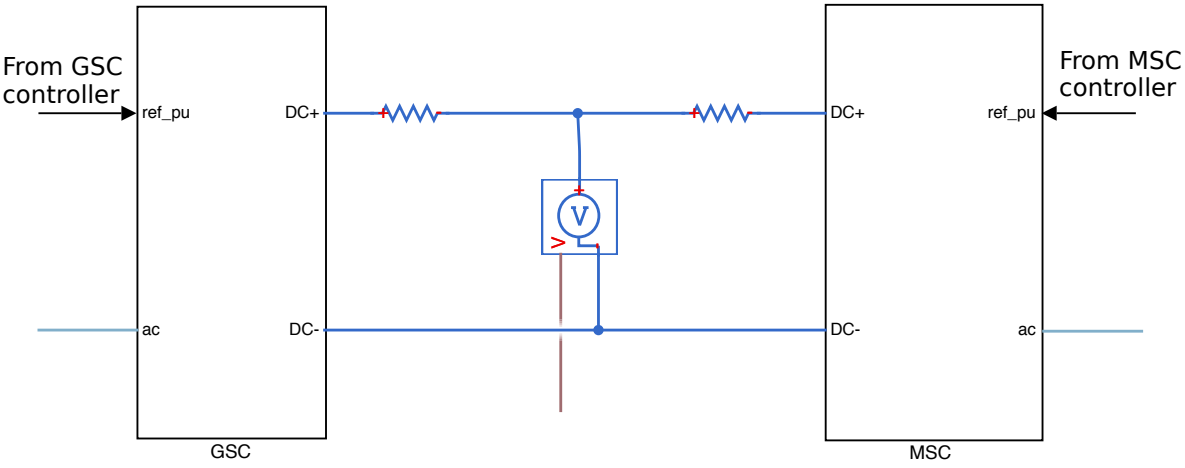

Figure C.7: Back-to-back converter

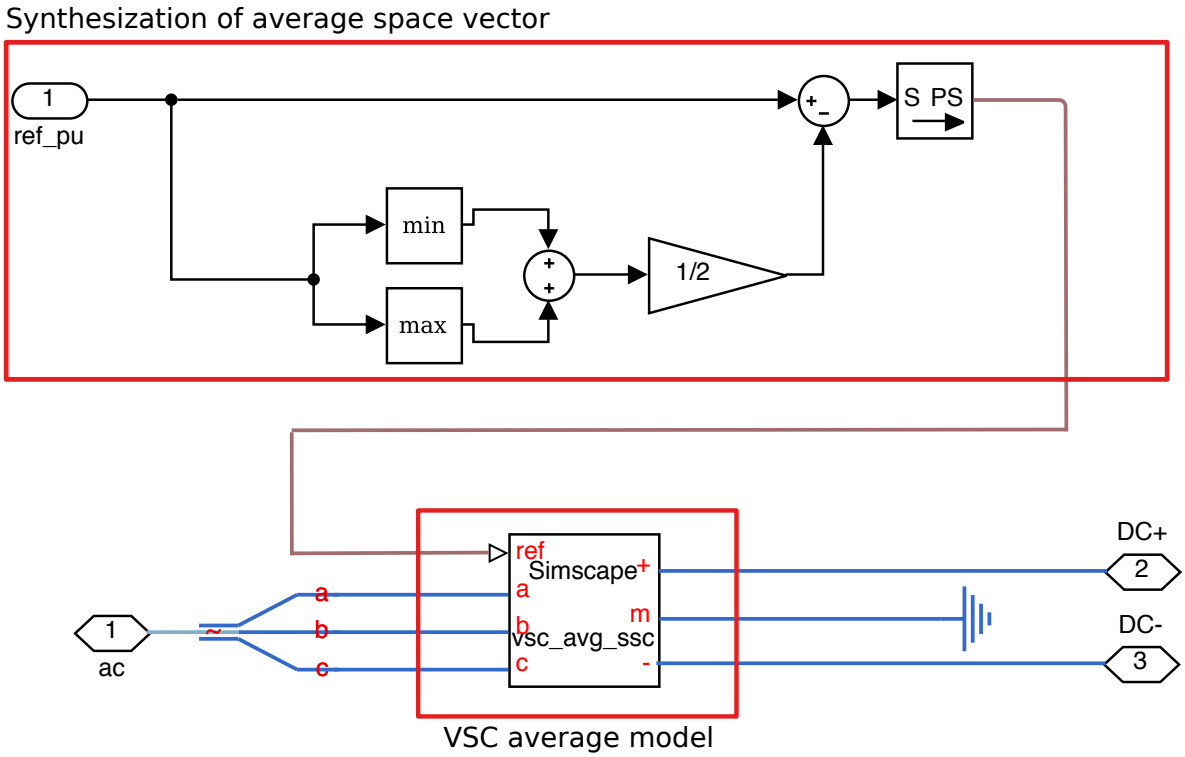

Figure C.8: VSC average model and modulation (same for GSC and MSC)

C.1.1 GSC: Classical Torque Control

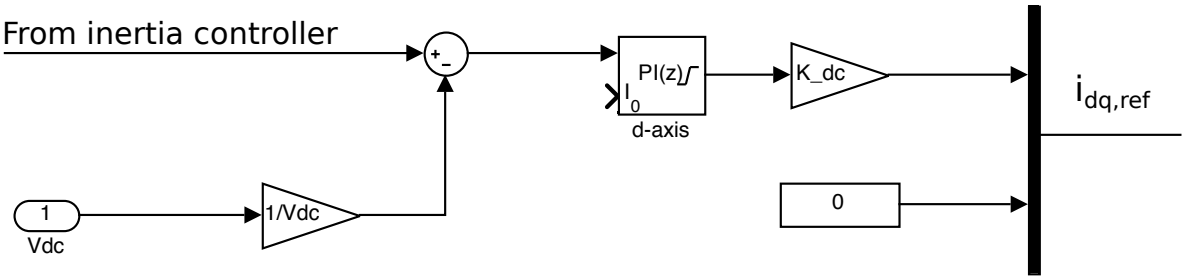

Figure C.9: Outer loop: Voltage control

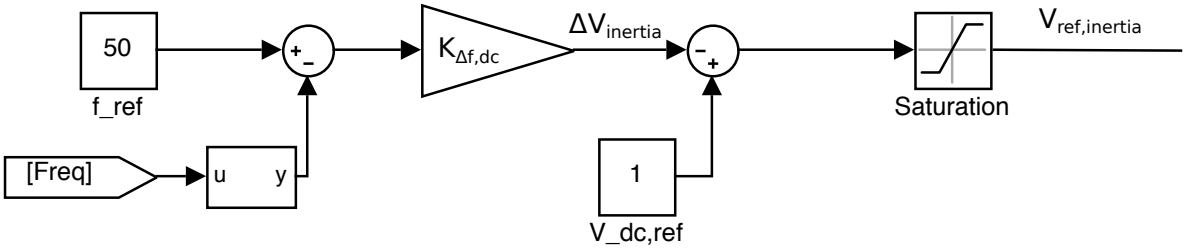

Figure C.10: Supplementary inertia control

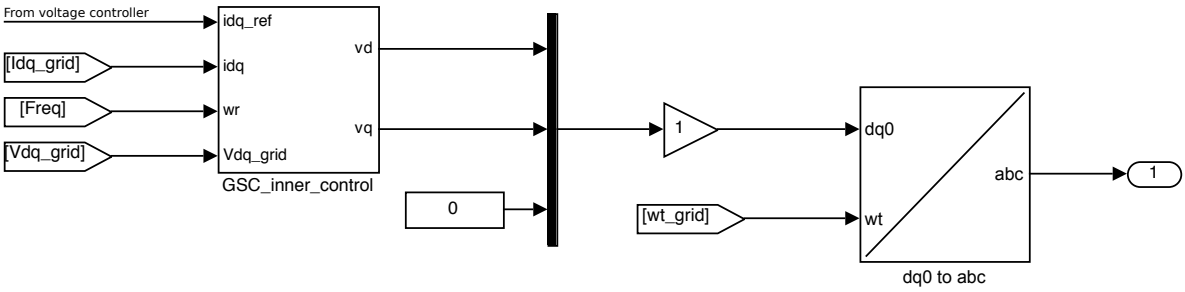

Figure C.11: Current control block with transformation

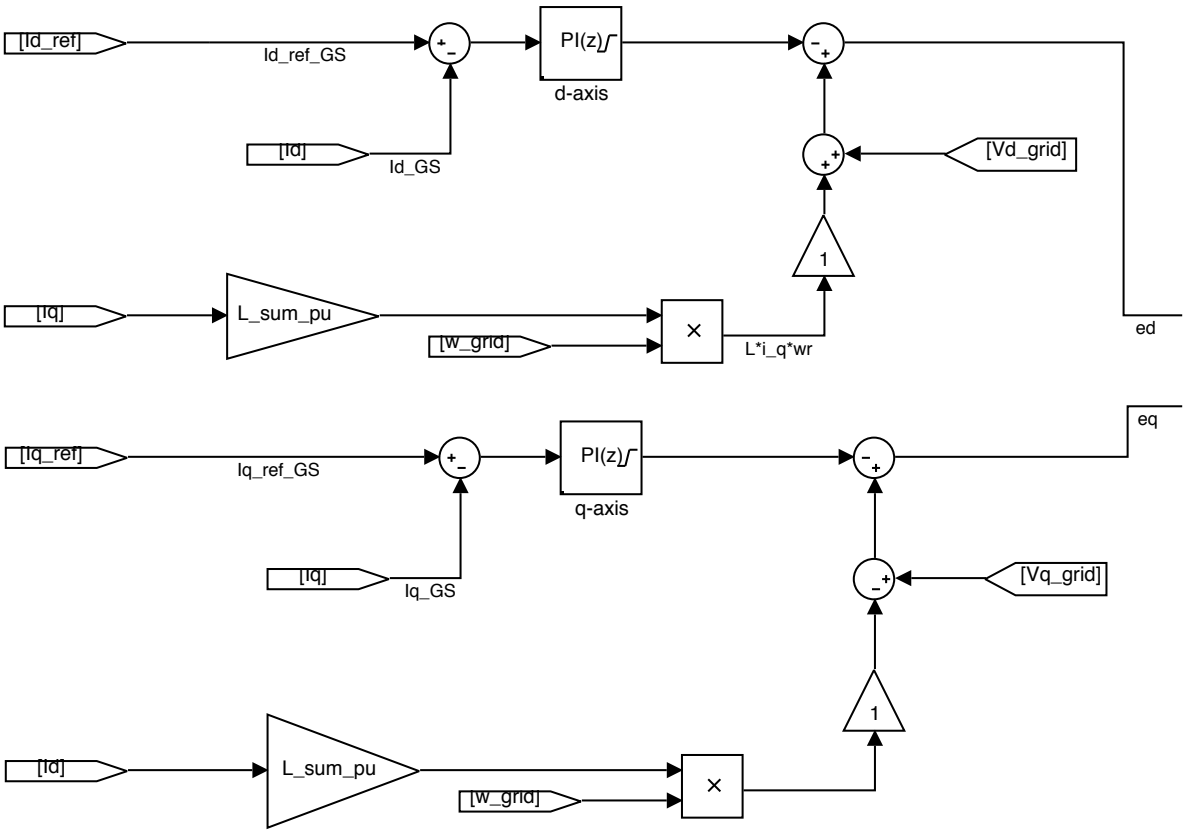

Figure C.12: Inner loop: current control

C.1.2 GSC: VSM Control

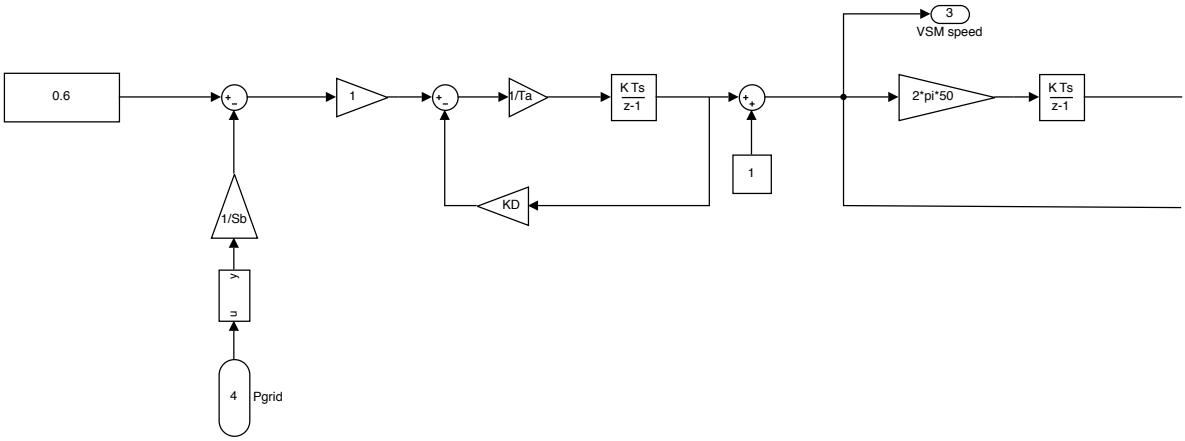

Figure C.13: Swing equation to regulate VSM angle and speed based on power balance

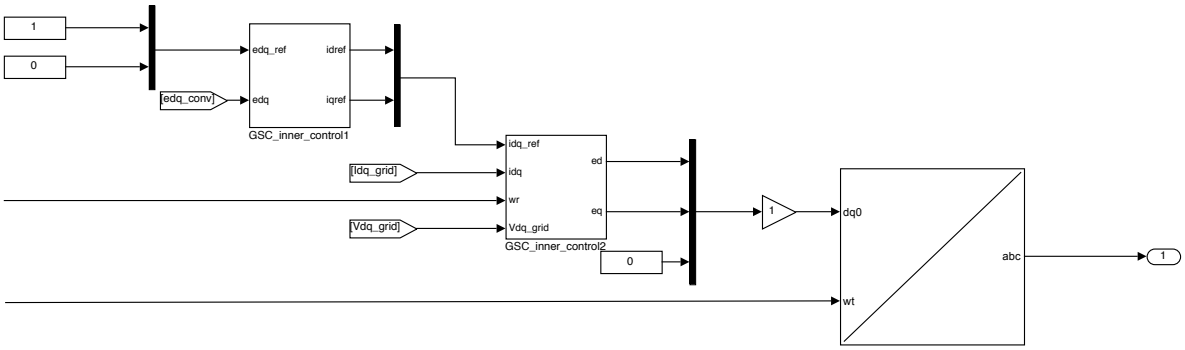

Figure C.14: Overview of SRF voltage and current controller

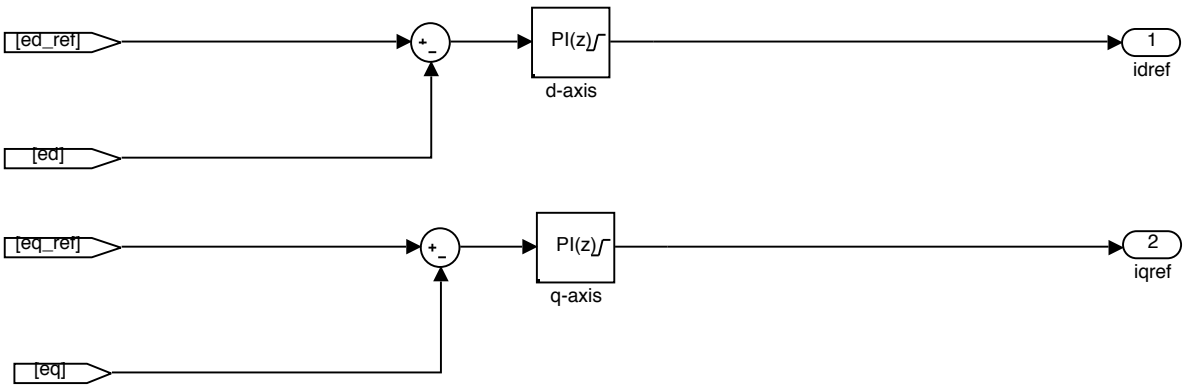

Figure C.15: Inside the SRF voltage controller

C.1.3 MSC: Classical Torque Control

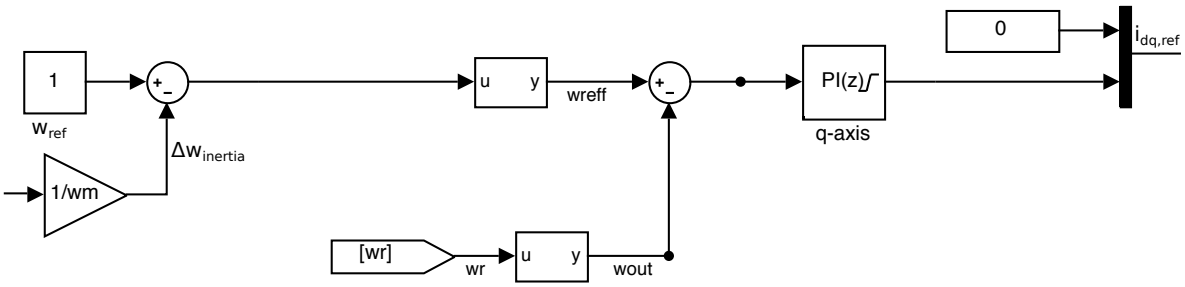

Figure C.16: Outer loop: speed control

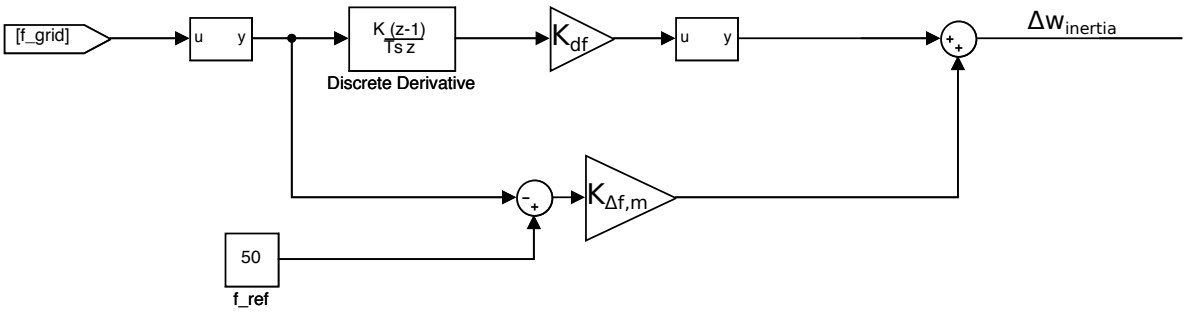

Figure C.17: Supplementary inertia control

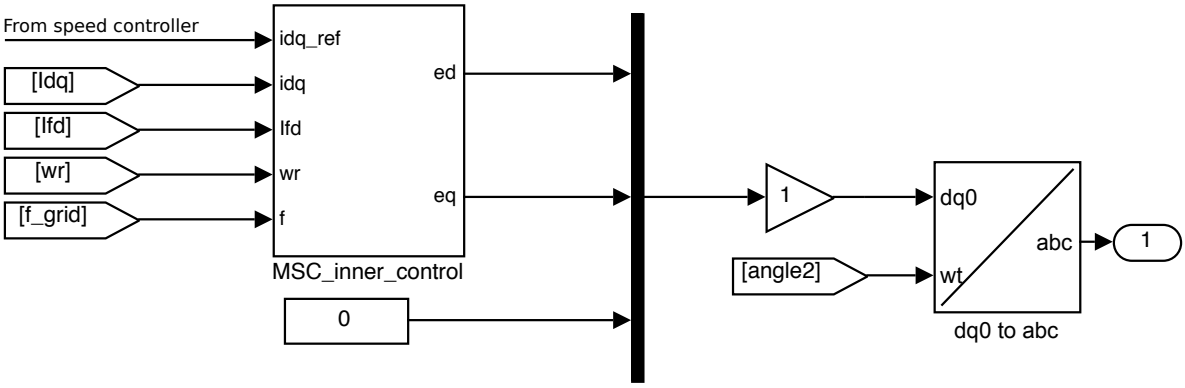

Figure C.18: Current control block with transformation

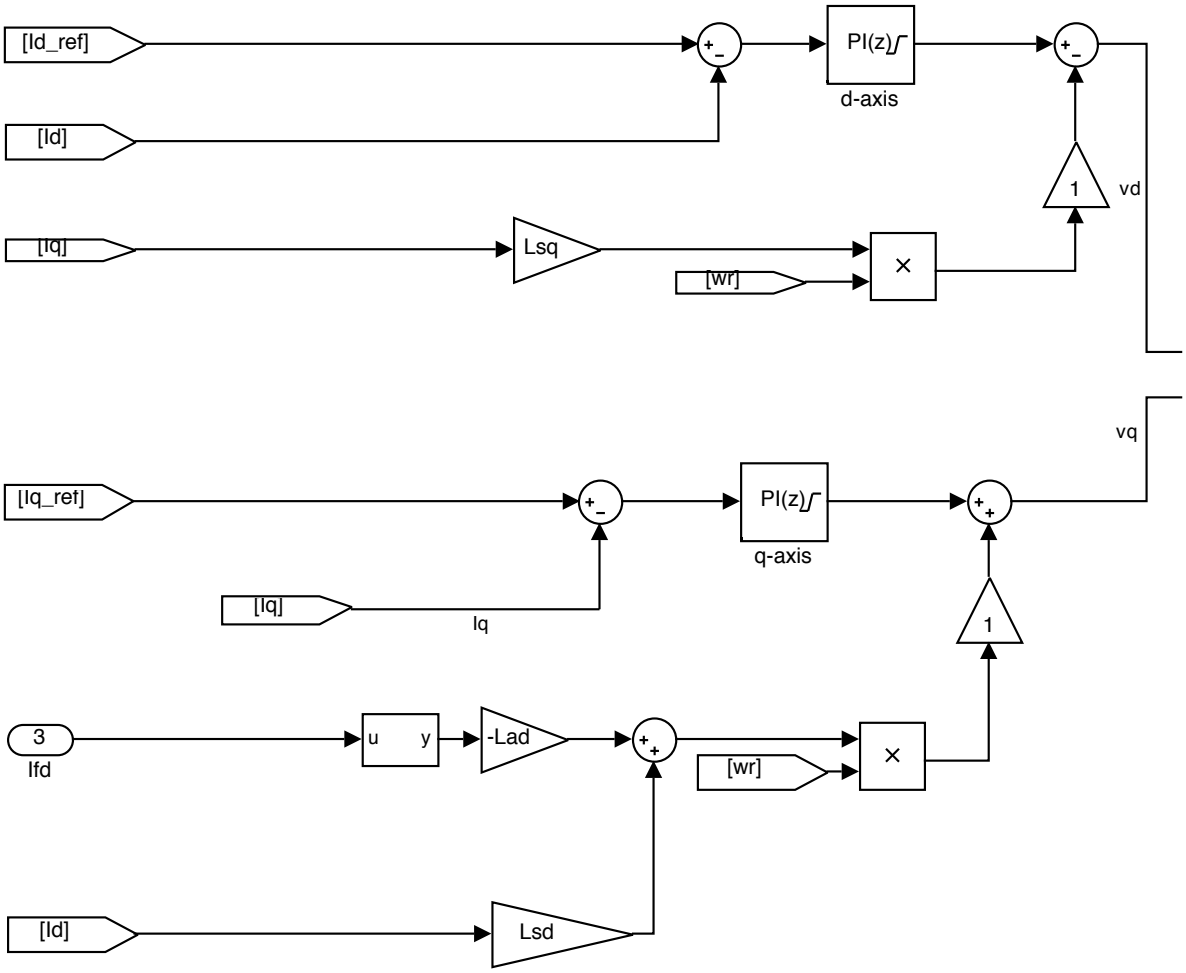

Figure C.19: Inner loop: current control

C.1.4 MSC: VSM Control

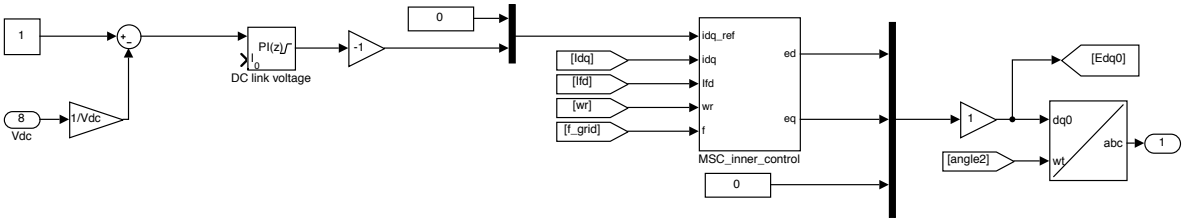

Figure C.20: Overview of the DC link voltage controller and SRF current controller

C.2 Grid

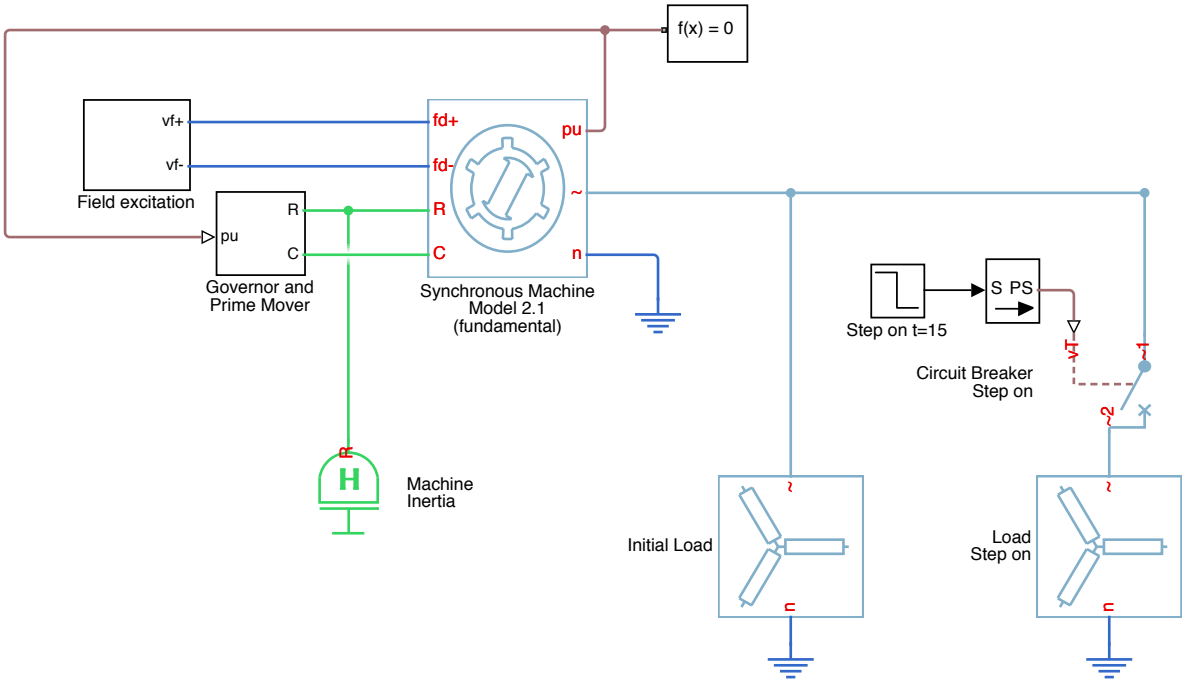

Figure C.21: Grid represented as a synchronous machine and loads